Extremely Low Cycle Fatigue Assessment of Thick-Walled Steel Piers

A dissertation submitted to the Graduate School of Engineering of
Nagoya University
in partial fulfillment of the requirements for
the Degree of Doctor of Engineering

By
Tao CHEN
July 2007

ACKNOWLEDGEMENTS

I would like to express my sincere gratitude to my advisor, Professor Kazuo Tateishi, for his tireless supports, encouragement and inspiration through my study. His invaluable support and care made possible the completion of this study. I am also grateful to Professor Hanbin Ge for the many valuable suggestions and enjoyable discussions. I further extend my appreciations to Prof. Kentaro Yamada for his help.

I am grateful to Prof. Obata Makoto of Nagoya Institute of Technology for providing constructive comments and valuable time serving as my advisory committee.

The laboratory assistance provided by Prof. Akira Kasai is gratefully acknowledged.

I would like to extend my sincere appreciation to Dr. Takeshi Hanji for his valuable help.

I am indebted to many of my colleagues in the laboratories, for their invaluable contributions throughout all phases of research.

Many thanks also go to all my friends and colleagues who made my life so full and happy by their warm friendship and understanding during those past years.

The scholarship provided by Ministry of Education, Culture, Sports, Science and Technology (MEXT) of Japan is gratefully acknowledged.

My special thanks go to my parents for their loving support and encouragement.

ABSTRACT

This dissertation investigates the extremely low cycle fatigue failure of thick-walled steel piers through numerical analysis with complementary tests, and then proposes a strain approach assessment methodology. Extremely low cycle fatigue problem often arises in earthquake engineering. Seismic induced several cyclic strain reversals in thick-walled steel pier, resulting in low cycle fatigue failure instead of local buckling.

In the first part of the work, T-shaped welded joint was analyzed by FEM with fine and coarse model. It was found parameters, such as main plate thickness, weld leg length, constitutive model, yield stress and loading pattern, have negligible influence to the relationship between local strain range and element strain range. Whereas the effect of weld toe radius is dominant. Then a simple approach was proposed after systematic analysis. Furthermore, the validity of the proposed methods is examined by constant and random amplitude loading tests using T-shaped welded joint.

As the second part of the work, thick-walled steel pier was investigated with shell-solid and beam model. The nominal strain, which is the average value of strain along effective failure length, was correlated to local strain at weld toe. Taking into account the geometrical parameters of width thickness ratio and slenderness ratio, the conservative relationship was established. Then extremely low cycle fatigue methodology for thick-walled steel pier was brought out based on beam element model, which is practicable in engineering application. Subsequently four tests were conducted on thick-walled steel pier subjected to incremental or constant amplitude loading. Test results of crack initiation life were used to verify the proposed method and good correlation was observed.

The extension of this methodology was carried out to thick-walled steel pier excited by strong ground motions. Dynamic analysis was performed. Then cumulative damage index versus maximum nominal strain and ductility ratio were plotted respectively. Finally, conservative threshold values of maximum nominal strain and ductility ratio are given, which can be employed in engineering practice to predict crack initiation life.

TABLE OF CONTENTS

LIST OF TABLES

LIST OF FIGURES

Chapter 1

INTRODUCTION

1.1 Background

Steel piers are usually used for elevated highway bridges mainly in metropolitan areas, because of their small cross-sectional areas and the excellence in seismic resistance. However, site investigations following the 1995 great Hanshin-Awaji earthquake demonstrated the vulnerability of steel pier. Two types of failure mode, which are local buckling and low cycle fatigue (Usami, 2006), were observed. For local buckling, many researches have been conducted and guidelines have been established (Usami, 2005). It is characterized by large deformation and obvious decrement in loading capacity. But low cycle fatigue is brittle and cannot be easily discerned before crack has grown considerably. Photographs shown in **Fig. 1.1** are typical brittle failure due to low cycle fatigue. Similar phenomenon was also observed in steel frame structures in the 1994 Northridge earthquake. This type of failure mode poses challenges to researchers. However, researches on the low cycle fatigue of civil structures in extremely large strain region, corresponding to a strain magnitude of more than 10% and a fatigue life of less than tens of cycles, are limited and design guidelines have not been established in civil engineering.

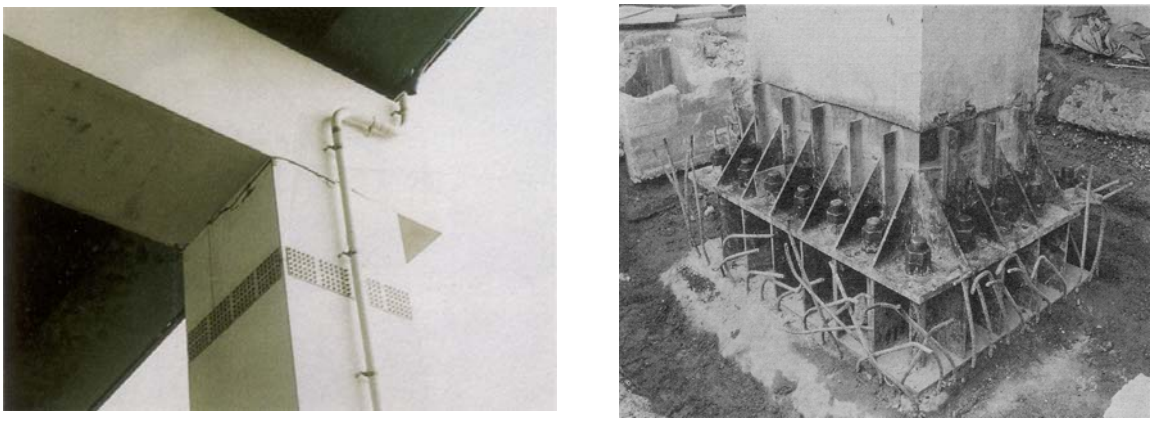

Fig. 1.1 Fracture triggered by low cycle fatigue in steel bridge piers in the Great Hanshin-Awaji Earthquake

Some previous studies have been carried out from material and structural component level for different purposes. Unfortunately, consensus hasn't been reached on it and cumbersome procedures is certainly not applicable to most engineering applications. That will be addressed in detail in the following section. For these reasons, this dissertation is focused on a systematic investigation on extremely low cycle fatigue (ELCF) due to seismic action.

1.2 Previous research

1.2.1 General remarks on fatigue

Fatigue problem was firstly noticed during industry revolution in 19^{th} century. In 1829, a German mining administrator Albert, W. A. J. observed, studied and reported the failure of iron mine-hoist chains arising from repeated small loadings (Albert 1838). This is the first recorded observation of metal fatigue. After that, many researchers have been investigated high cycle fatigue and developed sophisticated methodology (Schütz 1996).

Generally, fatigue problems are classified into three gross categories according to the number of cycles to failure, just as **Fig. 1.2** shows. Historically, high cycle fatigue is defined as situations that require more than 10^4 cycles to failure where stress is low and deformation primarily elastic. Whereas, we call failure occurs after less than 10^4 cycles, in which stress ranges surpass yield stress, as low cycle fatigue failure. In a seismic event, steel piers may undergo large strain fluctuations of typically one to tens of cycles. To distinguish it from other low cycle fatigue phenomena, we call it as extremely low cycle fatigue in current study. (Shimada, K. et al. 1987; Dufailly and Lemaitre 1995; Kanvinde, A.M. and Deierlein, G.G. 2004). Damage accumulation is taking place inside the materials during earthquake, which is irreversible.

Specifications and codes for high cycle fatigue are normally portrayed by the S-N curves illustrated in **Fig.1.2**. These curves are log-log plots of stress range as a function of the number of stress cycles. A series of S-N curves (categories A-H) are required for fatigue design according to fatigue design recommendations by Japanese society of steel construction (JSSC 1995). Besides the stress-life method, another two available methods are strain-life method and the linear-elastic fracture mechanics method.

Low-cycle fatigue due to thermal and high stress is usually characterized by the Coffin-Manson relation, which was proposed independently by S. S. Manson (1953) and L. F. Coffin (1954):

$$\frac{\Delta\varepsilon_p}{2} = \varepsilon_f^{'}(2N)^c \tag{1-1}$$

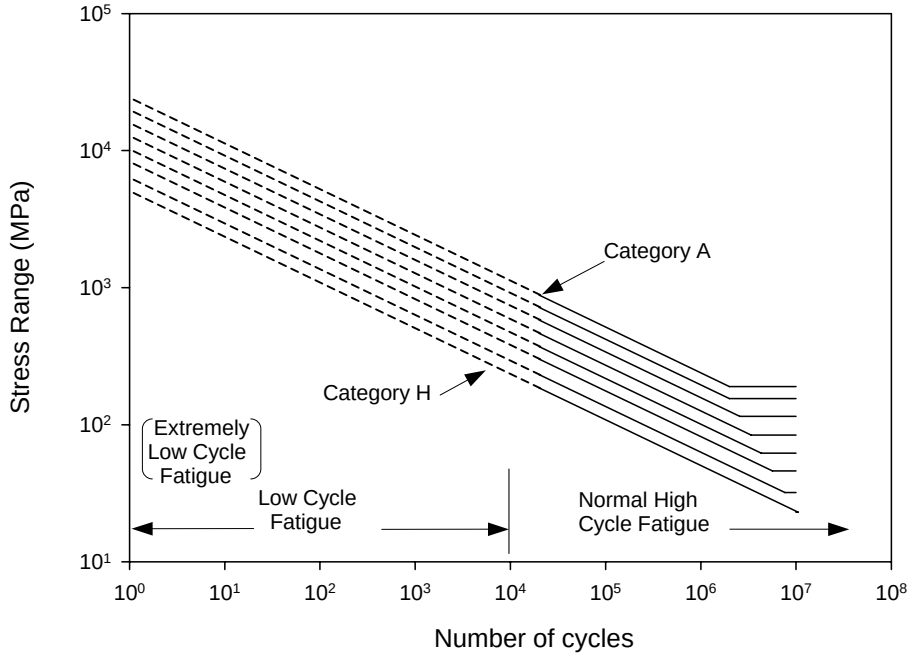

Fig. 1.2 Fatigue classification and S-N curves

where: $\Delta\varepsilon_p/2$ is the plastic strain amplitude; ε_f' is an empirical constant known as the fatigue ductility coefficient, the failure strain for a single reversal; $2N$ is the number of reversals to failure (N cycles); c is an empirical constant known as the fatigue ductility exponent, commonly ranging from -0.5 to -0.7 for metals.

The original Coffin-Manson equation relates plastic strain amplitude with fatigue life. Instead of plastic strain amplitude, which can be somewhat difficult to obtain and inconvenient for practical use, the total strain amplitude was used as one variant of the relationship by Mander et al. (1994), Liu et al. (2005a, 2005b) and Tateishi et al. (2005, 2007).

1.2.2 Low cycle fatigue of steel structure in civil engineering

Recently observed fracture of steel structures in earthquakes is usually initiated from welded joint. This may owe to the presence of strain raiser of local geometry shape, residual stress and welding flaws et al. To understand the causes of fracture and establish design guideline, researchers set out from various approaches. And the research objects also vary for different purposes. The specimens are usually hourglass shaped or panel shaped coupon, small scale welded joint, and beam or column models.

Intensive studies have been conducted on coupon test of different steel materials. And most of steel coupons are hourglass shape and subjected to axial loading (Nishimura and Miki 1978,

Shimada, K. et al. 1987, Komotori, J. and Shimizu, M. 1991, Nakajima, N. and Yamada, M. 2000, Masatoshi K. 2001). Most of them employed empirical equation of Coffin-Manson. Mander et al. (1994) investigated low cycle fatigue behavior of unmachined rebar. And they used total strain amplitude instead of plastic strain during fitting curve.

Liu et al. (2005a, 2005b) once conducted a series of tests to investigate the behaviors of low-cycle bending-fatigue on A36 square and rectangular steel bars. And they found that using the test results of constant cyclic loading to predict the strength of low-cycle bending fatigue under random loadings might introduce large error.

Low cycle fatigue failure of civil structures mainly occurred in the region of weld. But few tests have been conducted on weld deposit or heat affected zone (HAZ) for its difficulty to conduct. Usually butt weldments are tested (Seto, A. et al. 1999). And Madi et al. (2004) extracted weldment fatigue specimen of hourglass shape from butt-welded pipe connection to determine reduction life coefficient for the design and construction of fast breeder reactors.

Tateishi and Hanji (2004 and 2007) developed an image-based system to investigate large strain bending deformation of welded panel and obtained extremely low cycle fatigue strength curves of base metal, heat affected zone and weld deposit. They also carried out low cycle fatigue test on T-shaped welded joint to validate local strain approach based on the curves. Good correlation was observed for the results (Hanji et al. 2006).

Besides low cycle fatigue researches at material level, other investigations were also conducted to structural components. But they were mainly focused on the general behavior.

Some researchers (Ballio et al. 1997, Ballio and Castiglioni 1995, and Ferreira et al. 1998) use a similar experimental approach for low cycle fatigue as for high cycle fatigue. These past studies focus on the S-N curves specified by European code and correlate global displacement parameters with strain. They suggest that the high cycle fatigue curves can be extrapolated for low cycle fatigue if strain range is substituted for stress range.

Krawinkler and Zohhrei (1983) carried out very comprehensive experiments to investigate two potential types of failure with cantilever I-shaped beam, one due to local buckling of flanges and the other due to weld fracture of the connection. They proposed a relationship between the fatigue endurance and the plastic portion of the generalized displacement component, which is expressed by Coffin-Manson type equation. The conclusion drawn from this study was that simple cumulative damage models could be used to assess deterioration and failure in structural components under arbitrary loading histories.

For structural steel component, many researchers employed general deformation parameters, it can either be a strain, a distortion angle, a rotation, a displacement or other deformation quantity, according to the type of failure to be analyzed (Calado and Azevedo 1989). While these approaches represent important advances in the low cycle fatigue life

prediction methodology, they are typically geometry dependent and do not directly incorporate localized effects or the stress and strain histories that triggered crack initiation.

Recently, with the development of numerical analysis technique, some strain-based methodologies have been proposed since cracks naturally initiate and propagate in regions where the strain is most severe. For welded joints, fatigue crack usually stems from weld toe.

Sakano et al. (1995, 1997, 1998 and 2001) carried out a series of low cycle fatigue tests on steel beam-column joint and pier base joint subjected to constant amplitude loading, and assessed fatigue life by the strain near the weld toe. The effect of triangular ribs was also investigated.

According to Kuwamura's research, the low cycle fatigue fracture modes comprise three sequential phases: (1) the initiation of a ductile crack in the local area of high stress and strain concentration of welded joint, (2) stable propagation of this crack, (3) the suddenly propagation of the crack in a brittle manner (Kuwamura 1997). As reported by many researchers, the fracture in the steel piers most often occurs at the corner of the column base welded joint where stress and strain concentrations provide a ductile trigger to a brittle fracture. Kuwamura conducted experiments of ductile crack initiation of round bar with a notch subjected to monotonic loading. Four grades of steels were studied (Kuwamura and Yamamoto 1997).

However, seismic excitation is cyclic and can result in repeated loading for steel structure. The monotonic test did not represent the real behavior of steel. For cyclic loading on brittle fracture, Kuwamura et al. proposed Similitude Law of Pre-fracture Hysteresis (Kuwamura and Takagi 2004), which established the relationships between amplitude and cycles to fracture. The law states that the relationships are given by an invariant equation, which is not influenced by any of material, welding and connection. The following is the simplest equation proposed as an example of the invariant function:

$$\log N_f = A - k \cdot \log \mu_p \tag{1-2}$$

where A and k are constants, μ_p is ductility amplitude and N_f is number of cycles to fracture.

Obviously, the equation is similar to the Manson-Coffin equation of low cycle fatigue although he states it's not a fatigue problem.

A micro mechanics-based stress modified critical strain (SMCS) model has been presented to evaluate conditions for ductile fracture initiation by Chi et al. (2006). Validation has been conducted to three-point bending and compact tension with sharp or blunt notch specimens (Chi et al. 2006). A further step research was also conducted to develop cyclic void growth model (Kanvinde and Deierlein 2004).

Ge et al. (2005, Matsui and Ge 2006) employed Gurson's micro void model to investigate ductile crack initiation for structural steel and applied it to thick-walled steel piers under incremental cyclic loading. And Ge et al. (2007) carried out experimental test on thick-walled steel pier. But they didn't consider the effect of local geometry shape of weld toe during modeling .

During the study of crack propagation of low cycle fatigue, some researchers use J-integral introduced from high cycle fatigue (Yamashita et al. 2003). But others states that it is questionable to apply conventional fracture mechanics to model fracture under large-scale yielding excited by seismic action (Kanvinde and Deierlein 2004).

1.2.3 Discussions

Endeavor has been exerted to low cycle fatigue studies of structural steel and steel structures. However, there are still many important questions that need further investigation. Followings are some comments and discussions.

Firstly, fatigue fracture of welded joints is influenced by the welding details. Generally, weld toe radius and flank angle are basic geometry parameters for weld bead. Large plastic strain occurs at weld toe and that the local strain concentration can be one of the main factors contributing to crack initiation and propagation, which result in fracture during earthquake. Some researchers assess low cycle fatigue life using local strain approach. That means very fine mesh size is necessary to simulate local shape. Unfortunately, modeling the whole structure with weld toe local profile is impracticable and beyond the capacity of computers in engineering practice. Structural zooming technique is also capable of strain analysis by refinement of local model. But it wasn't used in steel pier analysis for the laborious meshing during modeling weld toe profile around corners and determining boundary conditions of local model.

Secondly, studies of low cycle fatigue at steel material level are well established. On the other hand, investigations of steel structural component mainly focus on general deformation parameters and empirical equations have been proposed case by case. There is a discrepancy of researches between material and structural component level. How to bridge up the gap is still a formidable problem.

Thirdly, cumulative damage model should be used during assessment since several reversals experienced due to strong ground motion. In the past seismic design, general parameter such as certain ductility ratio before failure is the main index. However, cumulative damage is essential to the assessment and rehabilitation. Several cumulative damage rules have been proposed during researches of high cycle fatigue. But Miner's rule is still the most used one for its simplicity and efficiency in low cycle fatigue region(Miner, M.A. 1945). The

rule is usually employed with rain flow algorithm since it seems the best counting methods (Maddox 1991).

Lastly, most of existing low cycle fatigue tests on steel components, such as column-beam and pier base welded joint, are I-shaped or H-shaped cross section. Whereas, box section steel pier is very popular in Japan (Ge et al. 2000). Researches on low cycle fatigue for thick-walled steel pier with box section are rarely found.

1.3 Objectives

Based on the aforementioned discussions, the ultimate purpose of this research is to develop a strain approach to extremely low cycle fatigue assessment methodology, which is applicable to seismic assessment for thick-walled steel pier in engineering practice. **Fig. 1.3** shows the flowchart of extremely low cycle fatigue assessment. Once established, it will contribute to a better understanding of the fracture in thick-walled steel pier excited by strong ground motions.

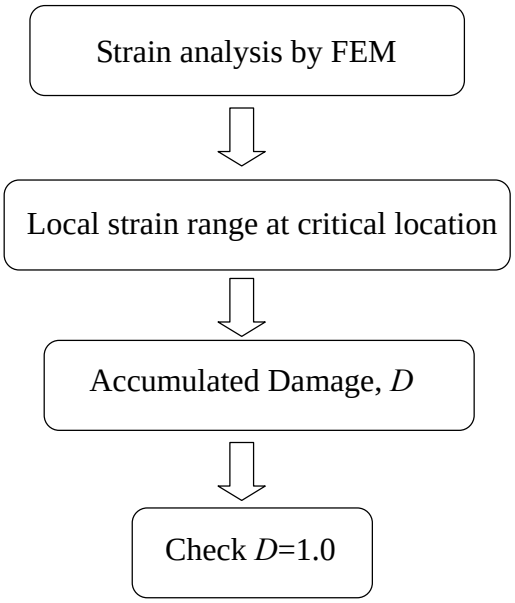

Fig. 1.3 Flowchart of ELCF assessment

The objectives of this study are:

- To bridge the gap between the burdensome modeling of weld toe profile and the modeling that ignores it, which are based on T-shaped welded joint. Endeavors should be

made to correlate the strain range relationship between fine and coarse model. Validation tests are also necessary.

- To establish a simple strain approach to extremely low cycle fatigue assessment for thick-walled steel piers with box section. Three-dimensional FE analysis and simple beam element model will be conducted on steel piers subjected to incremental cyclic loading. Several parameters should be considered. Then the relationship between the nominal strain range, which is obtained by averaging strain along effective failure length, and the local strain range at weld toe is investigated. The objective is to correlate nominal strain with local strain and propose one applicable method. Moreover, cyclic test on steel pier is required to validate the proposed method.
- To study the behavior of extremely low cycle fatigue failure of thick walled steel pier excited by accelerogram through dynamic analysis. Cumulative damage indexes should be calculated and related to maximum nominal strain and ductility ratio for engineering application. Then some practical parameters maybe proposed for application in civil engineering.

1.4 Structure of dissertation

This dissertation consists of seven chapters, including the introduction and summary (Chapter 1 and 7). The main part (Chapter 2~6) is arranged to fulfill the aforementioned objectives. Firstly a simple local strain approach was proposed after finite element analysis of T-shaped welded joint considering several parameters (Chapter 2). To further verify the simple approach, T-shaped welded joint subjected to random amplitude loading was performed. The results, together with results of constant amplitude test, are used to validate the proposed approach (Chapter 3). After that an extensive finite element analysis was executed to thick-walled steel piers, and a conservative method was proposed to correlate nominal strain range and local strain range for extremely low cycle fatigue assessment (Chapter 4). Incremental or constant amplitude loading tests were carried out on thick-walled steel piers and the results validated the methodology (Chapter 5). Finally, dynamic analysis, which is steel piers excited by strong ground motions, was presented to find some parameters that can be used for guidance of design.

Followings are brief contents of chapters:

Chapter 1 provides important background, previous research, objectives and organization of the dissertation.

Chapter 2 establishes a simple local strain approach to T-shaped welded joint by comprehensive numerical analysis based on strain range of fine and coarse models. Several

parameters are considered, such as main plate thickness, weld leg length, strain hardening ratio, yield stress, loading pattern and weld toe radius. This approach makes it possible to assess extremely low cycle fatigue by coarse model.

Chapter 3 validates the local strain approach proposed in the previous chapter by carrying out random loading test on T-shaped welded joint. Results of constant amplitude loading test are also used to verify the approach.

Chapter 4 examines thick-walled steel piers with shell-solid and beam model. Geometry parameters of width thickness ratio and slenderness ratio are considered. Nominal strain is correlated to local strain at weld toe. Then extremely low cycle fatigue assessment methodology is established based on beam element model. It becomes applicable for engineering problems.

Chapter 5 describes the cyclic test and analysis of thick-walled steel pier. It consists of one incremental and three constant amplitude cyclic loading tests. Crack initiation life, propagation pattern and life are recorded. And the methodology brought out in previous chapter is employed to assess crack initiation life comparing to test results. Good correlation is observed.

Chapter 6 performs dynamic analysis for thick-walled steel pier to investigate possible extremely low cycle fatigue failure. Excitations are strong ground motions recorded at different sites in Great Hanshin-Awaji Earthquake. Then damage cumulative index is plotted with maximum nominal strain and ductility ratio respectively. Some parameters are suggested to guide future design in prevent of crack initiation.

Chapter 7 presents the summary and conclusions of this study. Some suggestions for future study are also presented.

Chapter 2

A SIMPLE LOCAL STRAIN APPROACH TO WELDED JOINT

2.1 General remarks

Numerous methods have been developed to assess the fatigue resistance of welded structures (Rudolph et al. 2003; Marquis and Samuelsson 2005). Several types based on nominal stress, structural hot spot, effective notch stress (strain) and fracture mechanics are used in codes and standards (JSSC 1995; Hobbacher 2003). **Fig. 2.1** illustrates the available methods for welded components.

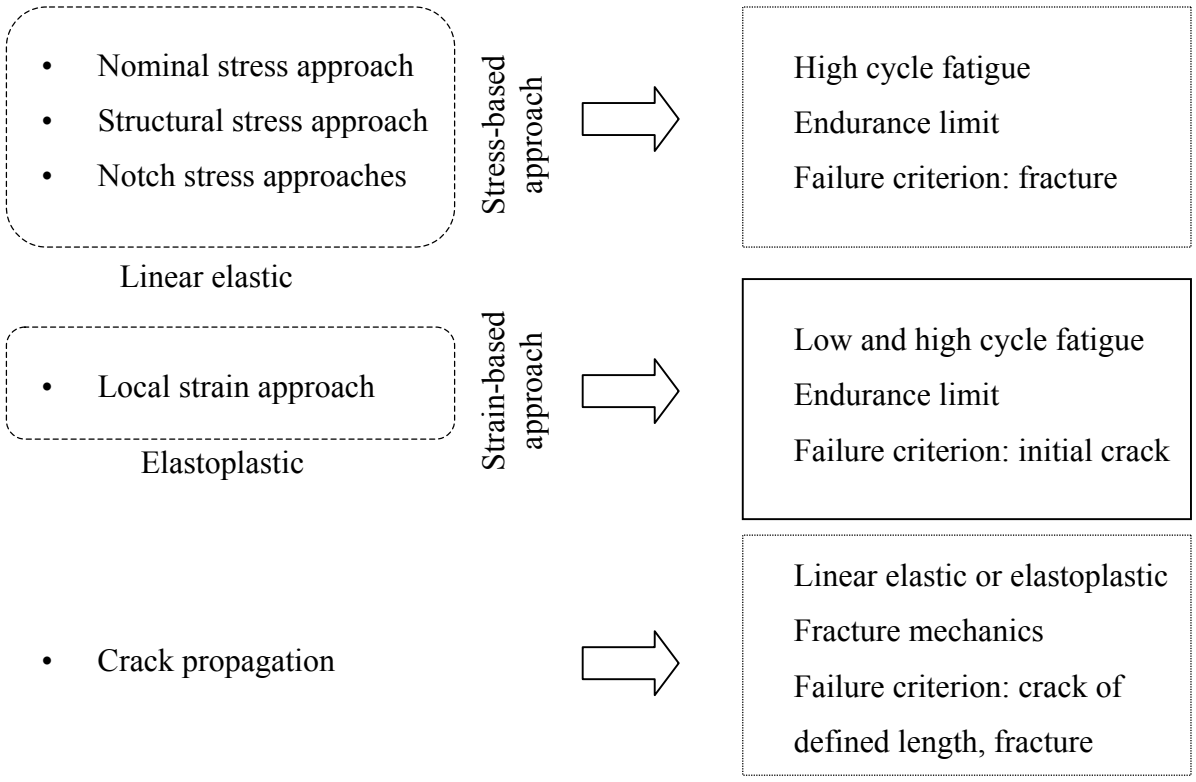

Fig. 2.1 Fatigue of welded components (Rudolph et al. 2003)

The nominal stress method, which is calculated on the basis of the net cross section without taking into account the effect of geometric discontinuities such as holes, grooves, fillets, etc., but are included in the corresponding detail class and S-N curve.

But for complex welded details, it may be difficult to evaluate what is "nominal stress" and apply it to S-N curves. Several papers in the recent literature suggest kinds of structural stress values for fatigue strength predictions. The most popular is hot spot stress, which is based on extrapolated values at the weld toe of the structural distribution (Nihei et al. 1996; Hobbacher 2003). Others are robust structural stress method proposed by Dong (2005), 1mm geometrical stress developed by Xiao and Yamada (2004). The local properties, such as weld toe geometry, are still included in the master S-N curve that independent of joint category.

The effect of local weld toe geometry can be included in the analysis using notch stress or strain methods. Conception of local stress (strain) approach is that the mechanical behavior of the material at the notch root is similar to the behaviour of axially loaded coupon test. This method can give good predictions, but a major shortcoming is an extensive FE-modeling of weld geometries for determining the local stress or strain.

Fracture mechanics approach to fatigue crack propagation has been demonstrated in the past for crack propagation (Anderson, 2005). For welded structure, the actual weld toe geometry is considered and an initial crack is assumed. Guidelines and successful application of the fracture mechanics in welded structures is well established (Maddox, 1991).

2.2 Incentive and procedure

Local strain approach is employed for low cycle fatigue assessment of welded components since it is not nominal or hot spot stresses (strains) that are responsible for damage but local strain at the weld toe. This approach is presented by Radaj et al. (1996, 1998) and Rudolph et al. (2003). Usually, weld toe geometries are characterized by weld toe radius r and flank angle θ as shown in **Fig 2.2**.

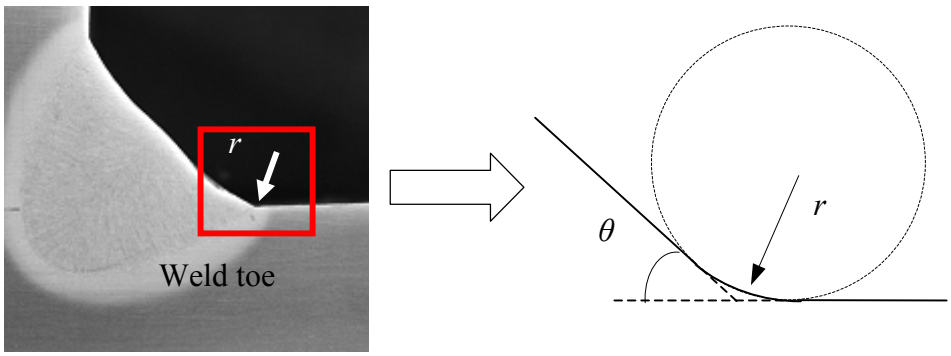

Fig. 2.2 Weld toe geometries

To calculate local strain, finite element method is adopted as a powerful numerical tool for the local strain analysis. The weld toe geometries have to be modeled precisely in order to obtain reliable results for the notch strain. Then problem arises during modeling, especially for real welded component. In engineering practice, real structures are in large size whereas mesh size should be as fine as 0.1mm in order to catch weld toe profile (Rudolph et al. 2003; Hanji et al. 2006). It's not practicable to include weld toe profile during structure modeling in engineering practice and this beyond the capacity of commonly used computers. Trade-off should be made between precision and calculating efficiency.

Some researchers analyzed FE models of actually structures without consideration of weld toe profile (Xiao and Yamata, 2004). And the mesh size is commonly several millimeters. It also demonstrates that the strain in weld toe region is influenced by the mesh size, so mesh size should be fixed as reference model. In this paper, the model with 1mm mesh size, which doesn't model weld toe profile, is named coarse model. Correspondingly, the model taking into account the weld toe profile is called fine model.

The objective of this study is to bridge the gap between the burdensome modeling of weld toe profile and the modeling that ignores it. Strains of both models are investigated. In the elasto-plastic region, there isn't proportional relationship between the stress and strain. And because of that, there is an essentially difference in the strain time histories (Jankovie, 2001). That means the local strain cannot be obtained by strain concentration factor as in the elastic region. At the same time, it is known that the amplitudes of the cyclic stress and strain components at the weld toe primarily determine the cyclic initiation of the technical incipient crack. So efforts are made to correlate the strain range relationship between fine model and coarse model.

In this work, T-shaped welded joint is employed. Then 2D elasto-plastic finite element models of the joints are analyzed using plane strain element to evaluate local strain range near weld toe under random loading blocks. Several parameters are taken into account, such as main geometrical parameters, material properties, and weld toe profile. Loading pattern is considered as well. Which parameter is the most influential to the relationship is discussed. Finally, a simple approach is proposed.

2.3 Numerical procedure

2.3.1 FE models and geometry parameters

T-shaped joint was introduced to the numerical analysis. **Fig. 2.3** and **Table 2.1** show the geometry configurations. The dimensions of T-shaped joints are that main plate thickness is 12, 24 and 36mm respectively while the transverse plate thickness remains 12mm. For

specimens with various main plate thicknesses, the ratio of support distance to main plate thickness remains constant. The radius of curvature at the weld toe *r* is highly variable and scattering (Tagaki et al. 1982; Radaj 1996). In the current research, several radiuses were considered from 0.2mm to 2mm, as shown in last column of **Table 2.1**. T-shaped joint subjected to vertical loading through transverse plate can be assumed as bending loading mode for main plate.

Half symmetry finite element model was built for the 2-D plain strain analysis, as shown in **Fig. 2.4 a)**. These FE models can be generally classified as fine model and coarse model. Fine models were those include weld toe profile and the minimum mesh size is around 0.02 ~ 0.05mm, about one tenth of toe radiuses as shown in **Fig. 2.4 b)**. Coarse models were used which minimum mesh size was fixed as 1mm and it didn't take account of weld toe profile as shown in **Fig. 2.4 c)**. The choice of mesh size is decided after considering available computer capability and referring to former researches (Xiao and Yamada, 2004; Rudolph, J et al. 2003). The boundary conditions are supports at the main plate ends, symmetry condition and cyclic loading. In numerical analysis, the radius is set to zero in coarse model. But for fine model, radius value has to be determined. Radaj and Sonsino (1998) proposed a fictitious radius that is generally assumed as 1mm in the worst case. Here, four different radiuses were modeled which are 0.2, 0.5, 1 and 2mm respectively. The flank angle remains constant that is assumed as 45^{o} since its effect on local strain is negligible (Hanji et al. 2006).

MSC.Marc package was employed to 2-D plain strain FE analysis, using full integration 4-noded elements and 3-noded triangle elements.

2.3.2 Material parameters

During the modeling, the character of the weldment are required to be considered. They consist different portions (base metal, weld deposit and HAZ), welding residual stresses and geometrical characteristics. In general, the material characteristic values of the base material are used (Radaj 1996). But in a previous investigation, it was also confirmed that different materials' constitutive models had little influence on the local strain at weld toe (Hanji et al. 2006). It is known that some factors, such as surface roughness, surface damage and surface treatments etc., are important for high cycle fatigue and the fatigue limit, but they are generally overruled during low cycle fatigue where plastic deformations at the material surface will occur anyway.

In the current numerical analysis, if not explicitly denoted, bilinear constitutive model of base metal was adopted for weldment. Yield strength, Young's modulus and Poisson's ratio of the base metal are 407MPa, 2.00×10^{5}MPa and 0.3. The strain hardening ratio, which is the

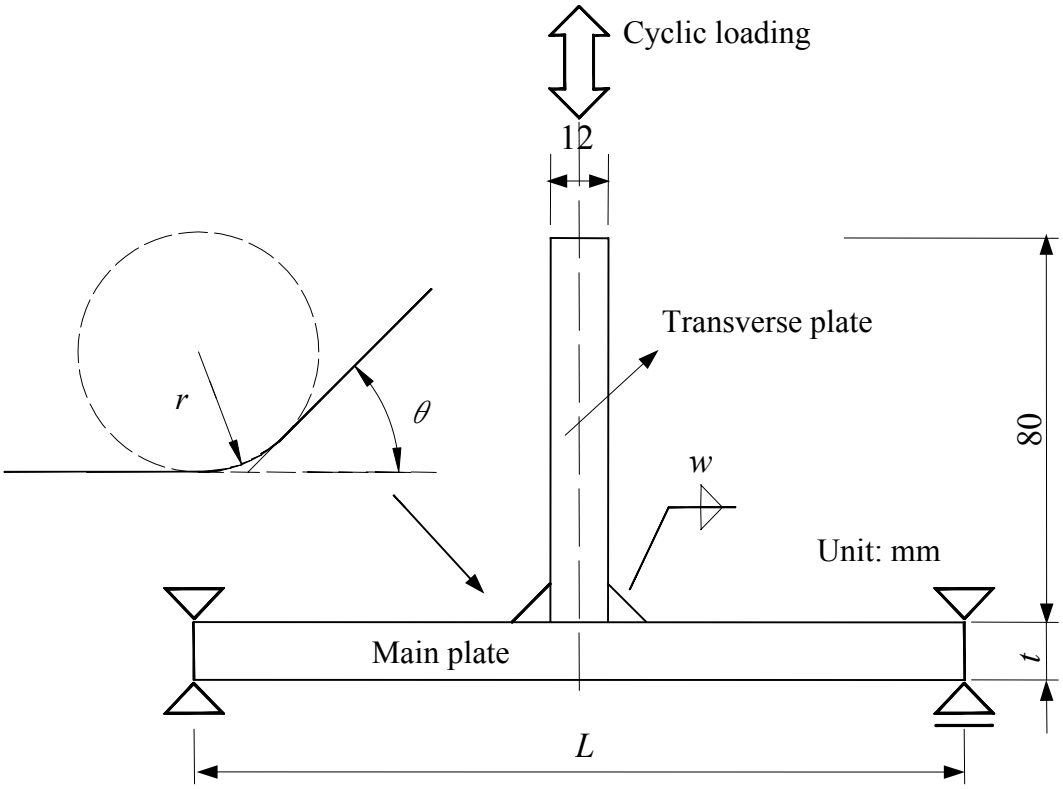

Fig. 2.3 Geometry configurations of T-shaped welded joint

Table 2.1 Cases for FE analysis

Thickness t (mm)	Span L (mm)	Weld leg length w (mm)	Weld toe radius r(mm)
12	160	6, 8, 10	0.2, 0.5, 1.0 2.0
24	320		
36	480		

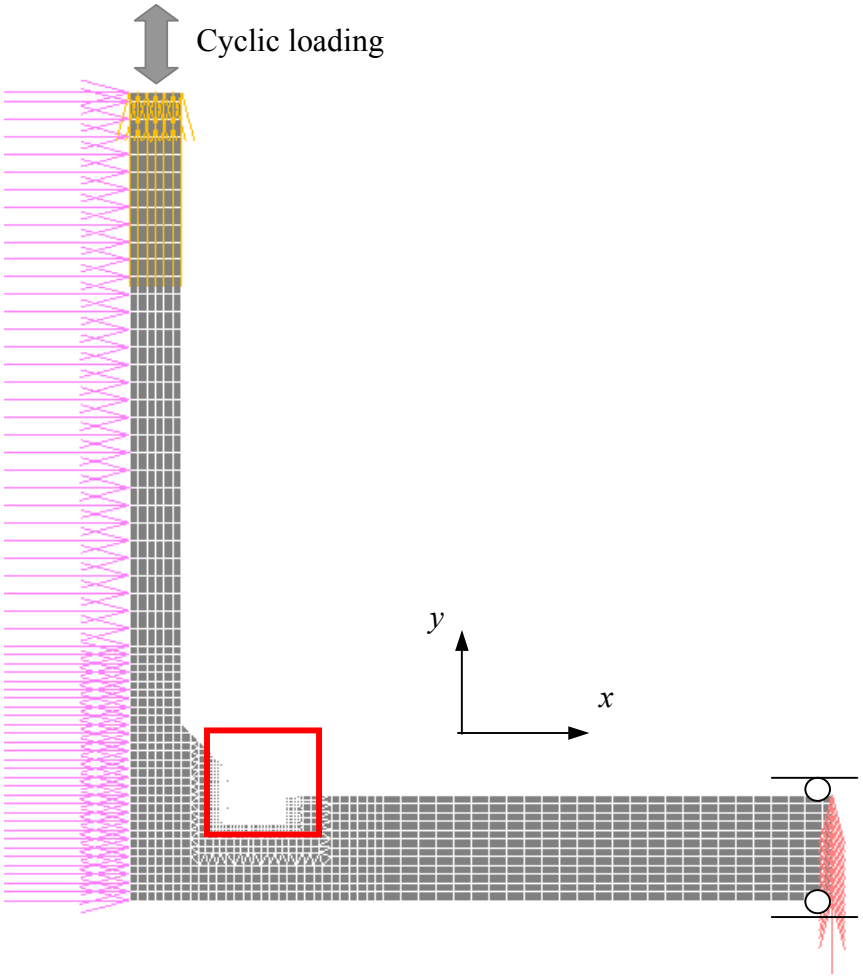

a) Half FE model

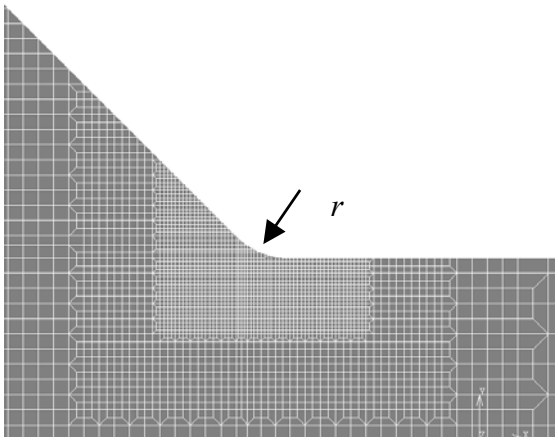

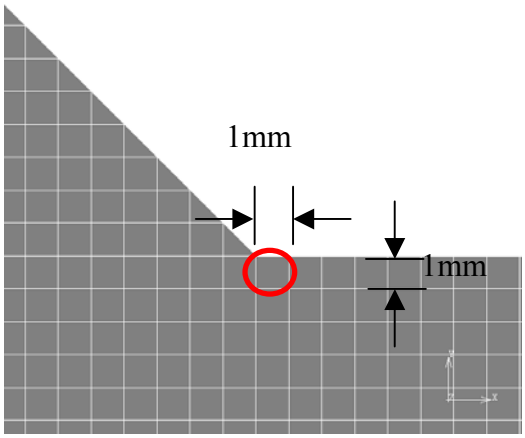

b) Fine FE model near weld toe c) Coarse model near weld toe

Fig. 2.4 FE models and FE model near weld toe

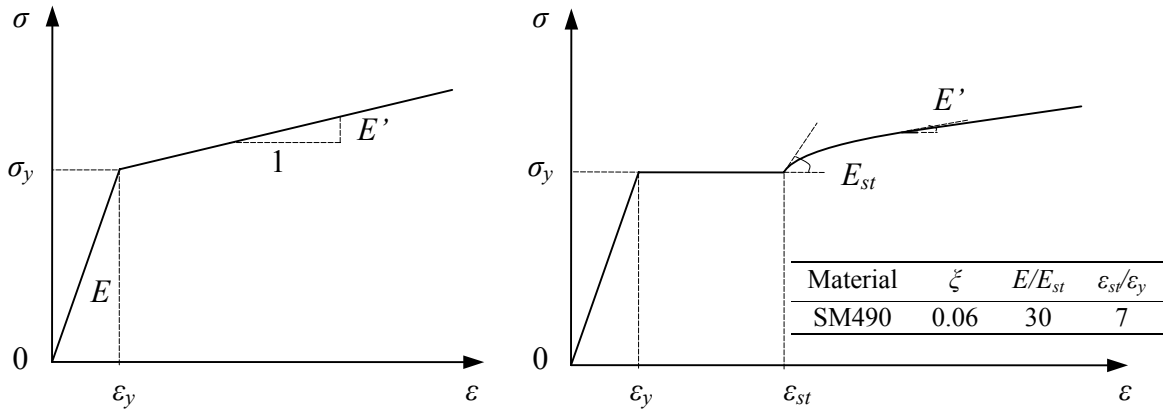

a) Model I and II b) Model III

Fig. 2.5 Constitutive model

ratio between post-yield tangent and initial elastic tangent, was assumed as 1/100 and kinematic model was adopted during analysis. This constitutive model is named as model I, as shown in **Fig. 2.5 a)**.

To investigate the effect of constitutive models. Another two models were also investigated. Model II is similar to model I, but the strain hardening ratio was assumed as 1/200. Besides bilinear constitutive model was employed during analysis, another constitutive model III shown in **Fig. 2.5 b)** was also employed,. The stress strain relationship can be expressed as follows (Usami 2006).

$$\frac{\sigma}{\sigma_y} = \frac{1}{\xi}\frac{E_{st}}{E}\left(1 - e^{-\xi\left(\frac{\varepsilon}{\varepsilon_y} - \frac{\varepsilon_{st}}{\varepsilon_y}\right)}\right) + 1 \qquad (\varepsilon \geq \varepsilon_{st}) \qquad (2\text{-}1)$$

2.3.3 Loading histories

Fig. 2.6 illustrates random displacements versus time that were obtained by random function. Five blocks were used in the current study. Abscissa represents nominal time while ordinate denotes normalized displacement. Random amplitude blocks were applied to specimens under displacement controlled loading. For T-shaped welded joint, this caused bending in the main plate and fatigue initiated at the weld toe.

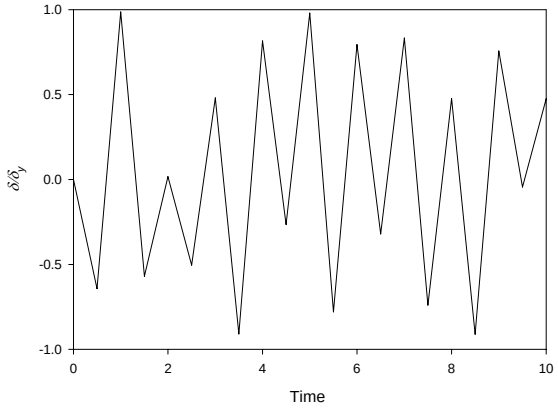

a) [$-\delta_y$, δ_y]

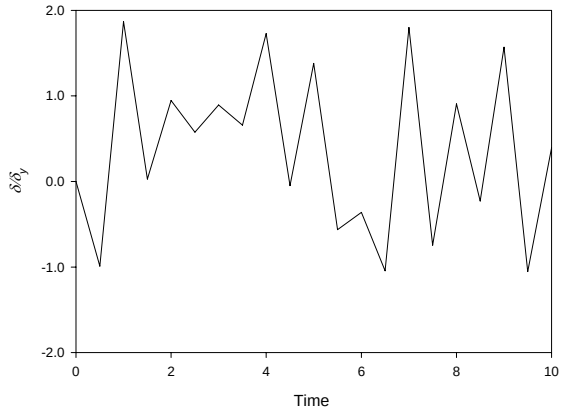

b) [$-2\delta_y$, $2\delta_y$]

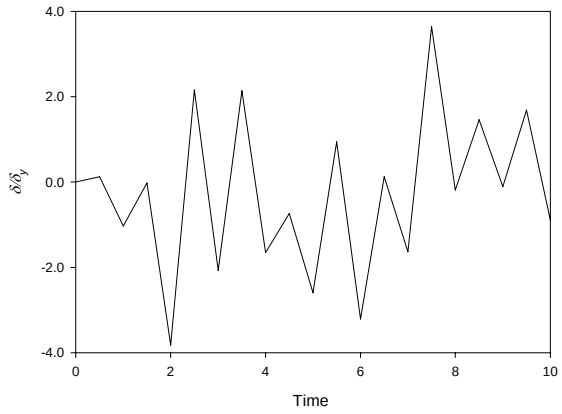

c) [$-4\delta_y$, $4\delta_y$]

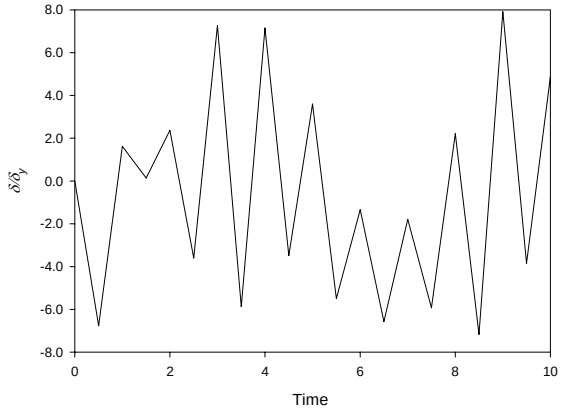

d) [$-8\delta_y$, $8\delta_y$]

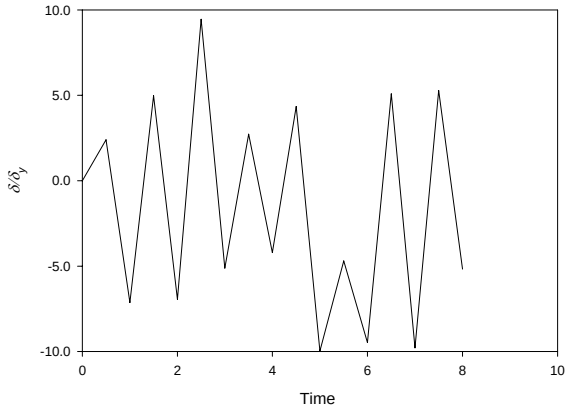

e) [$-10\delta_y$, $10\delta_y$]

Fig. 2.6 Random loading displacement

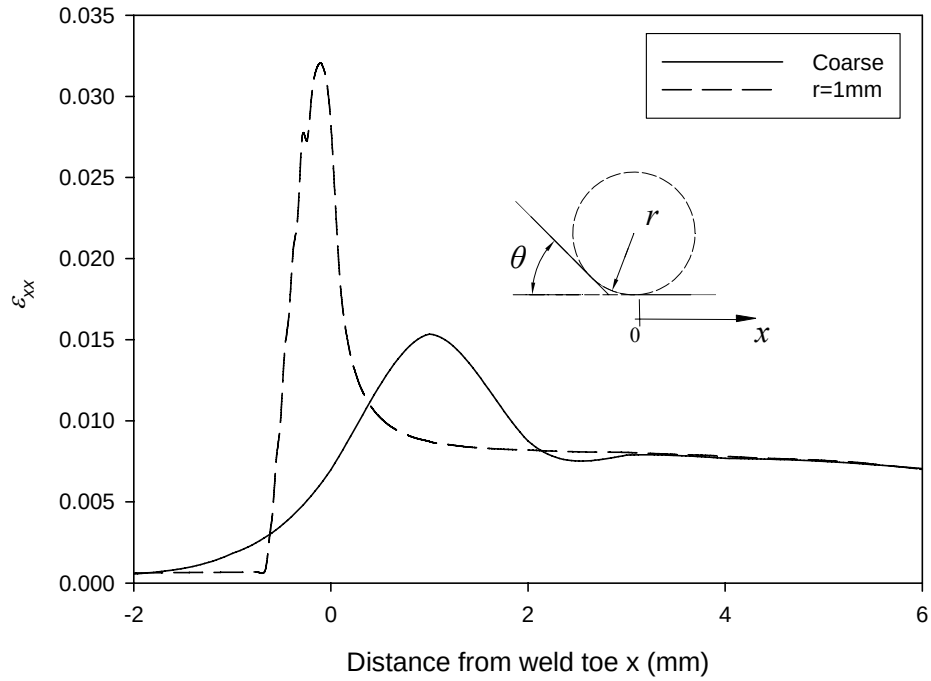

Fig. 2.7 Distribution of strain

2.4 Numerical analysis results

Several FE models were analyzed by MSC.Marc package, then the strain distribution near the weld toe and strain time history were obtained. For coarse model, the average strain of element ε_e in x direction, which is near the weld toe circled in **Fig. 2.4 c)**, was calculated. For fine models, the strain tangent to the surface with maximum absolute value was acquired. **Fig. 2.7** illustrates an example of the strain distribution along the surface when main plate thickness is 12mm and loading displacement is 1.76mm. For other loading levels, similar phenomena were observed.

In this study, rain flow counting method was employed for counting strain time history when estimating fatigue life (Jonge, J.B. 1982; Maddox 2001). Values of strain range that are less than 2 times of yielding strain were ignored during plotting since strain range of low cycle fatigue is generally larger than it.

During the analysis, several parameters were taken into account such as main plate thickness, weld leg length, yield stress of material, constitutive model, loading pattern and weld toe radius. They will be discussed in detail in the following section.

2.4.1 Effect of main plate thickness

Weld toe radius is fixed but the thickness varied. Three kinds of thickness were considered, which are 12, 24 and 36mm. Typical results of 1mm weld toe radius are presented in **Fig. 2.8**. Abscissa represents the strain range of coarse model, whereas the ordinate indicates the strain range of fine models. It shows that the data points of thick plate are above the data points of thin plate but the data scatter in a narrow band. In other cases, similar phenomenon was also observed. Dispersion decreases with the increasing of weld toe radius.

2.4.2 Effect of weld leg length

Fig. 2.9 shows the strain ranges obtained from coarse and fine models with respect to weld leg length, where main plate thickness remains 12mm and weld toe radius is 1mm. The weld leg length is 6, 8 and 10mm respectively. Little scatter was observed in the graph. Same phenomena were also observed for other radiuses. Then it can be stated that influence of weld leg length on the strain range relationship is negligible.

2.4.3 Effect of constitutive model

In total, three kinds of constitutive models described beforehand are adopted during engineering analysis. Yield stress remains 407MPa and the main plate thickness is 12mm.

Comparison of results obtained with different constitutive models were plotted in **Fig. 2.10**. Little scatter of the data was observed. Then we can say the bilinear constitutive model is appropriate to use.

2.4.4 Effect of yield stress

To investigate the influence of yield stress, three kinds of yield stress were considered, which are 300, 407 and 500MPa respectively. The strain hardening ratio remains constant as 1/100 and main plate thickness is 12mm. The results were plotted in **Fig. 2.11** for comparison. As it can be seen in graphs, there exists little scattered of dots. So the influence of yield stress is also negligible.

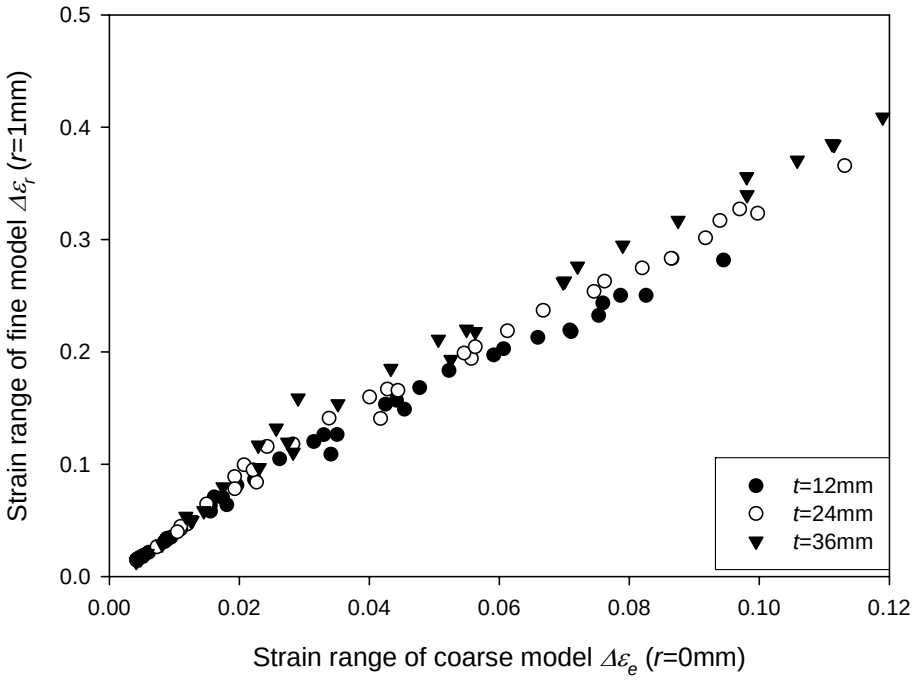

Fig. 2.8 Strain range relationship with respect to thickness

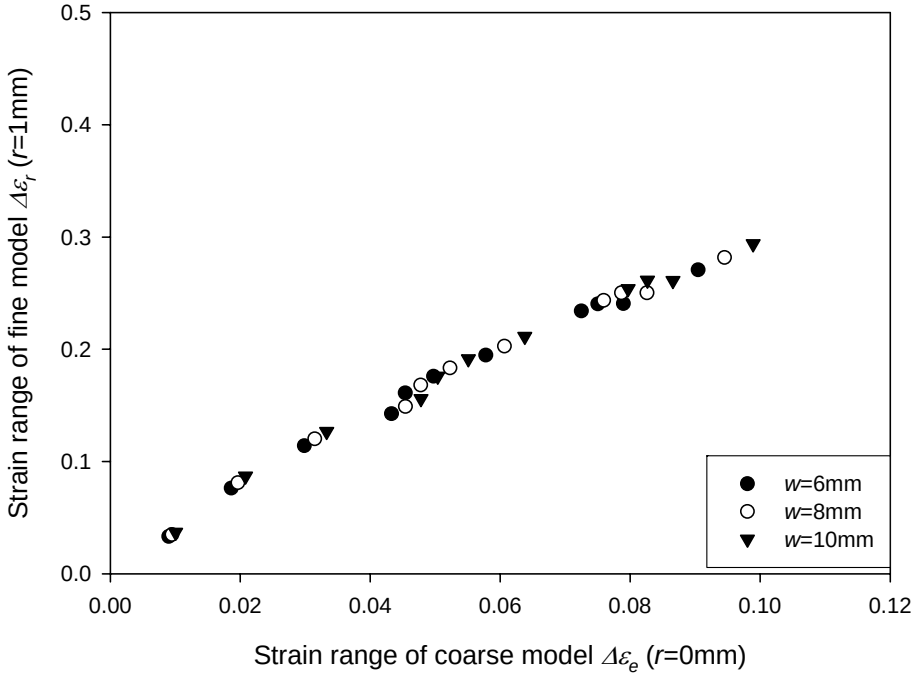

Fig. 2.9 Strain range relationship with respect to weld leg length

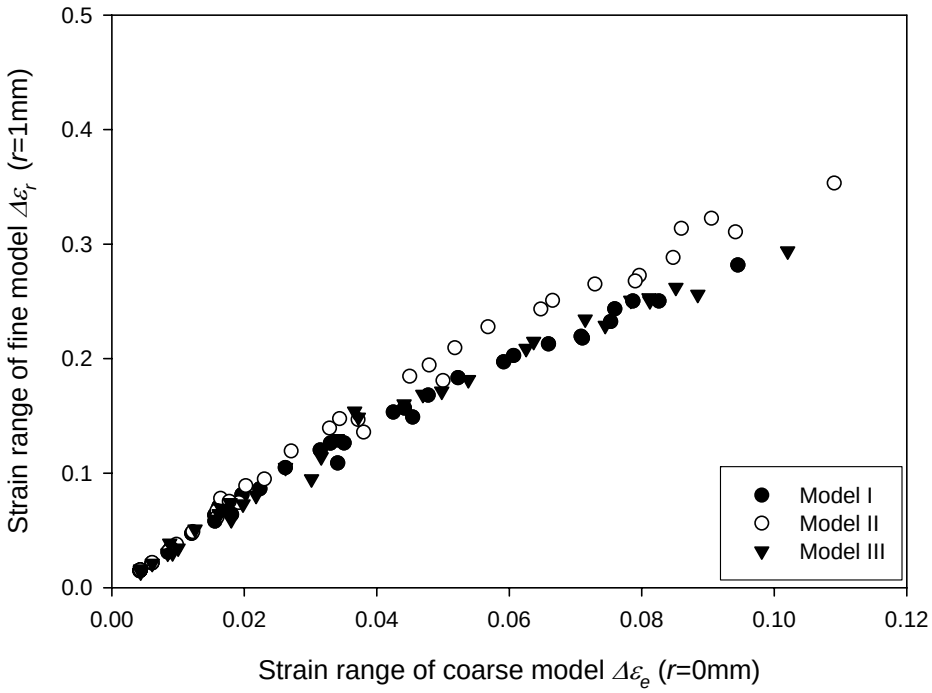

Fig. 2.10 Strain range relationship with respect to constitutive model

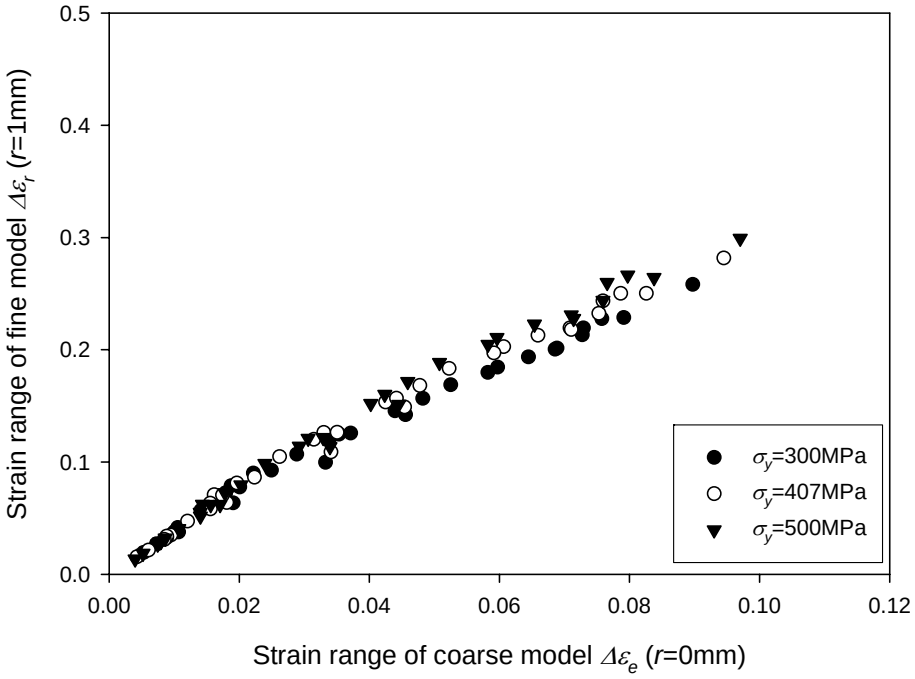

Fig. 2.11 Strain range relationship with respect to yield stress

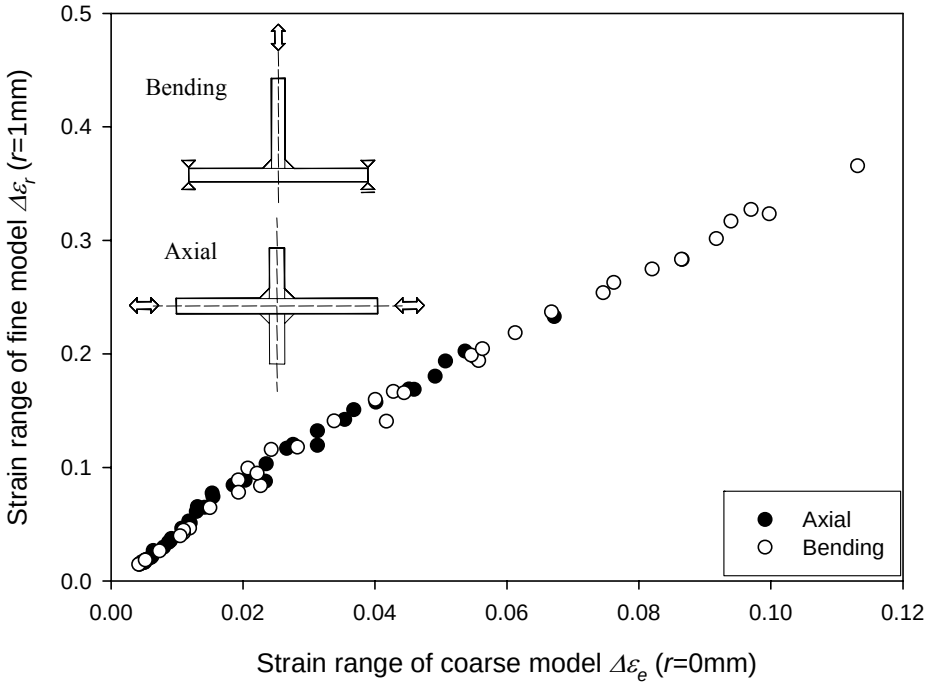

Fig. 2.12 Strain range relationship with respect to loading pattern

2.4.5 Effect of loading pattern

Aforementioned discussions were limited to the bending pattern. In order to compare the results with axial loading pattern, cruciform joint was introduced. It was subjected to cyclic axial loading through main plate. The results were graphed and contrasted in **Fig. 2.12**, where main plate thickness is 24mm and weld toe radius is 1mm. Axial loading pattern data points and bending pattern data points are little scattered.

2.4.6 Effect of weld toe radius

Strain range results were illustrated in **Fig. 2.13**. It was discovered that data points scattered with variation of weld toe radius. This is not a surprise, since notch radius is influential to the strain concentration. It should be noted that the weld local profile would change with varying loading level when large plastic strain is introduced. The effect was considered implicitly during analysis since updated Lagrange additive decomposition was adopted. That's partly contributes to the data scatter and nonlinearity in **Fig. 2.13**. During data processing the initial weld toe radius was adopted as main parameter during analysis for simplicity. Plate thickness of steel piers is typically around 24mm in Japan. So T-shaped models, whose main plate

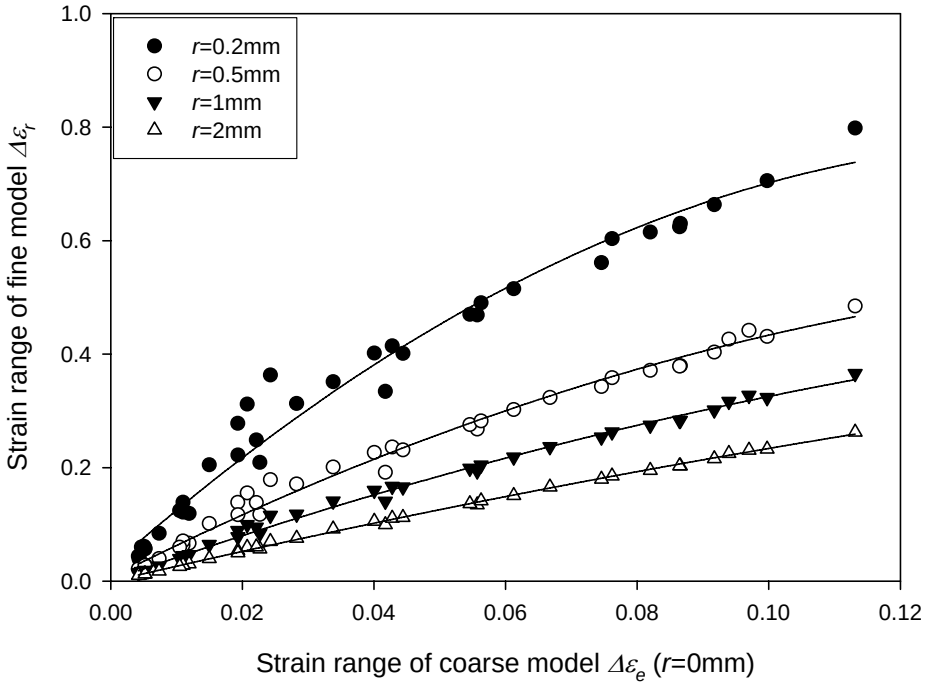

Fig. 2.13 Strain range relationship with respect to radius

thickness is 24mm and weld leg length is 8mm, were investigated after subjected to random amplitude loading blocks.

From the engineering point of view, the radius is the most influential parameter to the strain range relationship while others' effects can be ignored. If the relationship between coarse model and fine model can be established, then the general used local strain approach of weld toe which requires high expenditure in its modeling weld toe profile, can be simplified to only by coarse model for application.

Quadratic regression was applied for fitting the data with respect to weld toe radius. Fitting curves were also plotted in **Fig. 2.13**. The equations are listed in **Table 2.2**.

Table 2.2 Equations for strain range

Equation	$\Delta\varepsilon_r = a\Delta\varepsilon_e^2 + b\Delta\varepsilon_e$	
Weld toe radius (mm)	a	b
0.2	-44.6	11.4
0.5	-17.9	6.1
1.0	-9.2	4.2
2.0	-3.5	2.7

* $\Delta\varepsilon_e / \varepsilon_y \leq 57$

where $\Delta\varepsilon_e$ is strain range of coarse model that radius is 0mm. $\Delta\varepsilon_r$ is strain range of the fine models that radiuses are 0.2, 0.5, 1 and 2mm respectively.

2.5 Summary and conclusions

Local strain at weld toe, from where cracks may start and eventually result in fracture, is crucial to the low cycle fatigue assessment of welded joint. To calculate local strain, laborious work is inevitable during modeling weld toe profile. And it becomes unable to be realized when establishing large dimension model that includes weld toe profile. So a new local strain based approach has been developed as a solution to eliminate cumbersome modeling weld toe profile.

Several two-dimensional FE models of T-shaped welded joints with various weld toe radiuses were built and analyzed when they were subjected to random loading blocks. Parameters such as main plate thickness, weld leg length, constitutive model, yield stress and weld toe radius were discussed in this paper. Besides these, bending and axial loading pattern's effects were also studied. It turns out that weld toe radius is the most influential parameter while others are trivial. Then an approach based on strain range relationship was established for low cycle fatigue assessment from the engineering viewpoint. The strain range relationships between coarse model and fine model were obtained by regression.

The aim of this chapter is an attempt to establish a simple approach to low cycle fatigue assessment for welded joint and the loading pattern is mainly bending. However, test is necessary to validate the proposed method.

Chapter 3

TEST OF T-SHAPED WELDED JOINT

3.1 General remarks

The preceding chapter has provided a simple local strain approach to extremely low cycle fatigue assessment with coarse model. In the past, researchers conducted test on T-shaped welded joint with constant amplitude loading (Hanji et al. 2006).

However, seismic induced strain fluctuations are random instead of constant. To validate the proposed method, random loading test were carried out and the results were presented in this chapter. Three pairs of T-shaped welded joint specimens were subjected to random loading. The objective is to verify the proposed local strain approach based on coarse element model. Results of test with constant amplitude were also used for validation.

3.2 Test program

3.2.1 Specimen configuration

Geometry configuration of specimen is shown in **Fig. 3.1**. A single weldment was made consisting of 300mm×70mm main plate and 150mm transverse plate welded to it with 8 mm double fillet. Specimens are made from commercial SM490YA steel plate of 12mm thickness. They were assembled as T shape and welded by submerged arc welding. The mechanical properties and chemical compositions are tabulated in **Table 3.1**.

Since weld toe profile is vital to the local strain concentration when it is subjected to loading. Local profiles, which are weld toe radius r and flank angle θ, were measured by silicone-based impression material. Firstly, a string of silicone was applied at the toes before testing, and then slices were cut out of the silicone strings and photographed. The pictures were processed in a computer program where a circle was fitted at the weld toe. Measured results were shown in **Fig. 3.2**. Ninety measurements were made and the weld toe radius fluctuated between 0.4898 and 2.01 mm; flank angel varied between 27.44 and 61.65 degree. Average values of radius and angle are 0.9643mm and 46.29 degree.

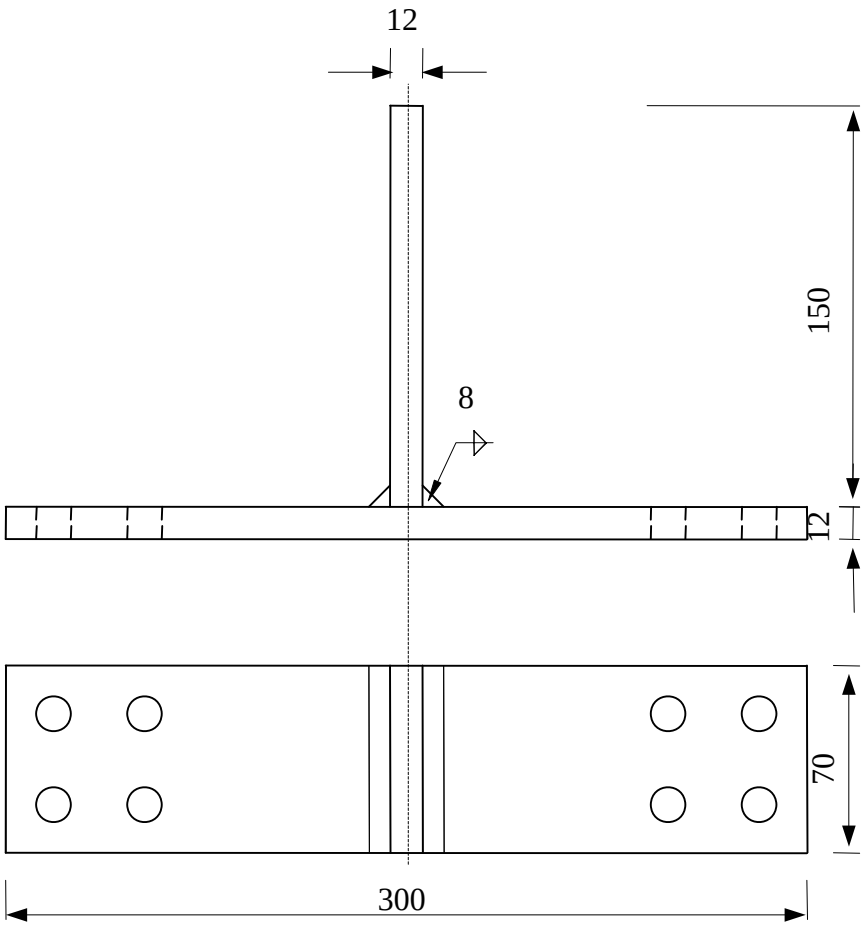

Fig. 3.1 Geometry dimensions of test specimen

Table 3.1 Mechanical properties and chemical compositions

	Yield Stress (MPa)	Tensile Strength (MPa)	Elongation (%)	Chemical compositions (%)				
SM490YA				C	Si	Mn	P	S
	393	545	27	0.17	0.35	1.46	0.023	0.006

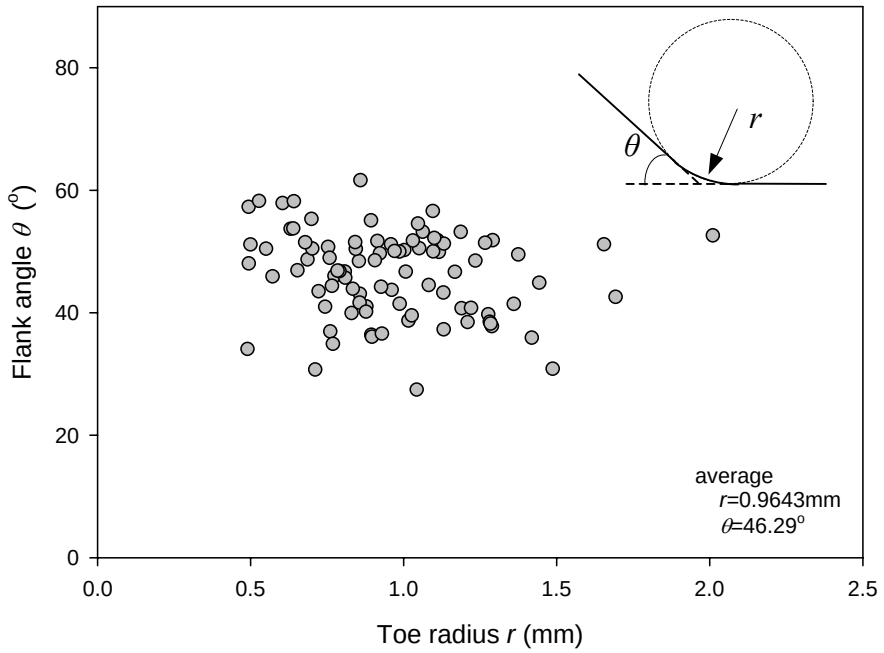

Fig. 3.2 Weld toe radius r and flank angle θ

3.2.2 Test setup

A fatigue test machine, which type is EHF-UB300KN-40L, was employed to test the specimens under cyclic loading as shown in **Fig. 3.3**. The testing machine consists of a load frame, actuator, upper and lower grips. And a constant pressure hydraulic pump provides the power for the system. A pair of specimens was tested by fatigue test machine each time. Two specimens are bolted by four bolts at the both main plate ends. At the same time two transverse plates' ends are gripped by upper and lower clips respectively. Then random loading blocks were applied to the transverse plate end through upper clip while lower clip is fixed. The loading is under displacement control. This will cause bending in the main plate with fatigue initiating at the edge of the weld toe where it interacts with the main plate.

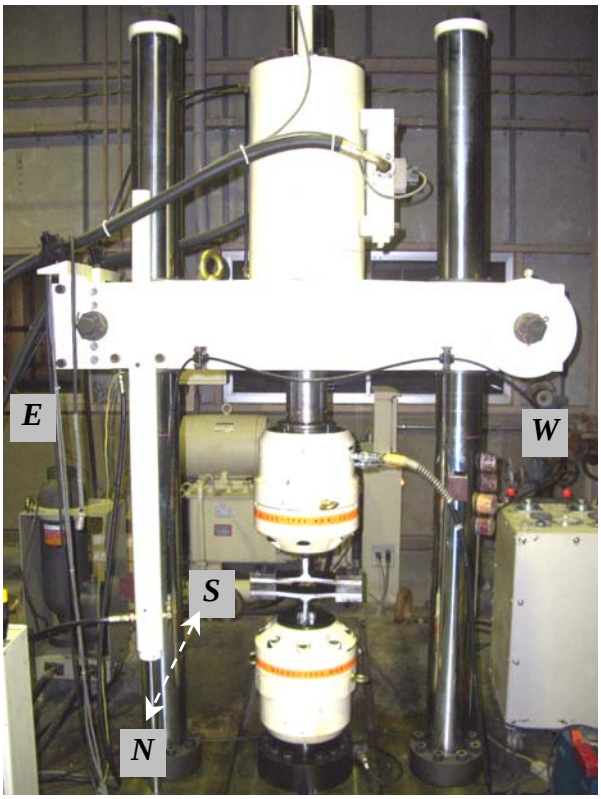

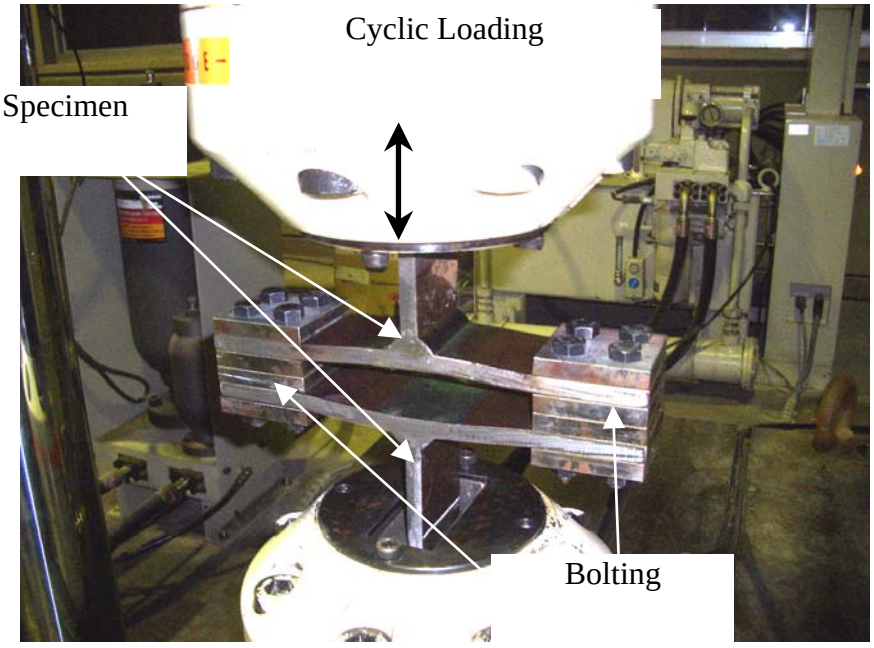

Fig. 3.3 View of test setup

3.2.3 Loading history

Random displacement loading is adopted as simulation of extremely low cycle fatigue applied to specimens.

The yield displacement of T-shaped specimen can be calculated. Then three blocks of variation amplitude that were created by random function can be defined as **Fig. 3.4** shows (recorded displacement history). Considering the symmetry of pair specimens, the displacement is 2 times of single specimen.

Quasi-static loading is applied to test specimens. Loading velocity is 0.05mm per second. Loading history was applied according to predefined values until cracks propagated through the whole section along width on surfaces for all weld toes. After that, constant zero mean amplitude loading was applied to specimens until rupture.

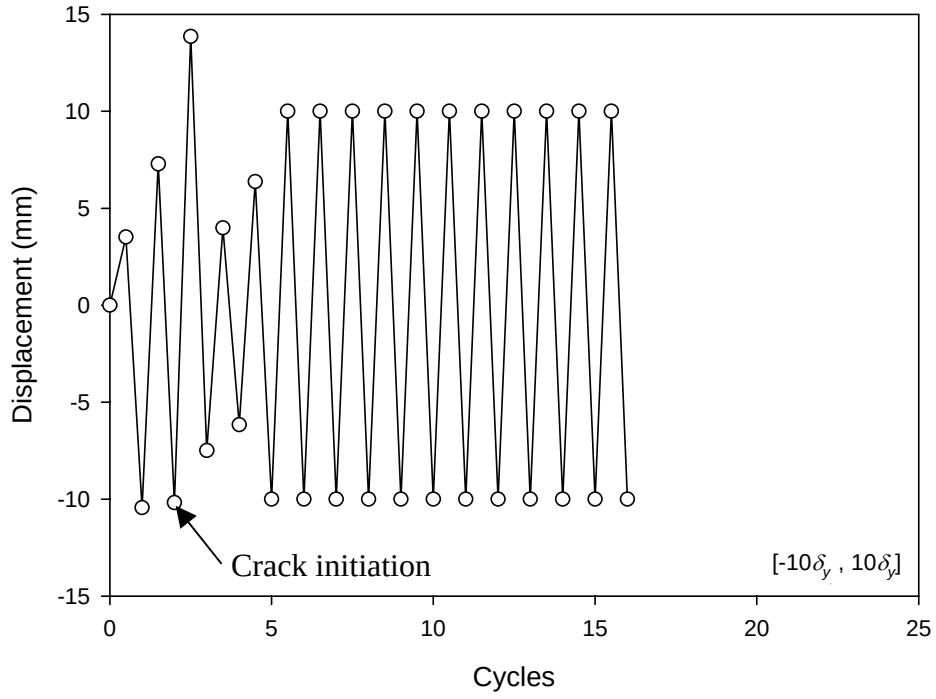

a) [-10δ_y, 10δ_y]

Fig. 3.4 Random displacement loading

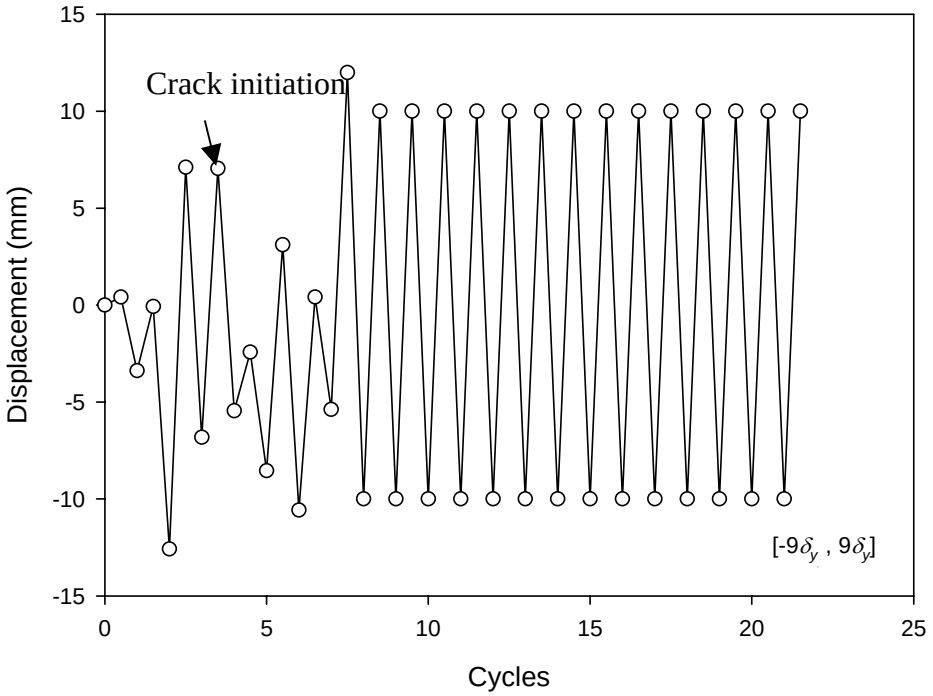

b) [-9δ_y, 9δ_y]

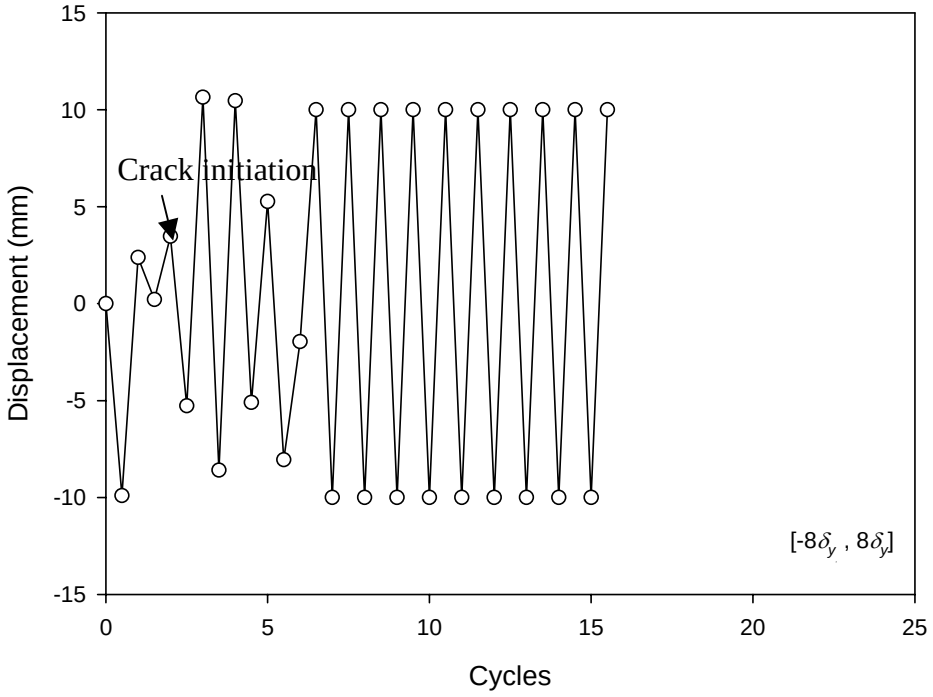

c) [-8δ_y, 8δ_y]

Fig. 3.4 Random displacement loading

3.3 Test results and observations

Crack observation was executed during test. It was fulfilled by black light illuminating the weld after spraying magnet powder (MT). The sequence and pattern of crack initiation and propagation were recorded during test at every half cycle.

Theoretically the crack should initiate at all weld toes simultaneously. But weld imperfections and fabrication errors existed for specimens. It was observed that first crack initiated from the imperfection of weld or the overlapping of the welds. Cracks already reached several millimeters when they were firstly identified. The initiation point was in the weld deposit as shown in **Fig. 3.5.** All cracks were at weld toe and parallel to the fillet weld direction. With progressive loading, cracks propagated from the initiation points until crack joined into one long crack through whole width.

After cracks propagated through whole width, specimens were subjected to zero mean constant amplitude displacement loading. With increasing number of cycles, crack deepened into thickness direction from surface to inner. At last one of the welds ruptured. Photographs of failure modes and rupture sections were shown in **Fig. 3.6**.

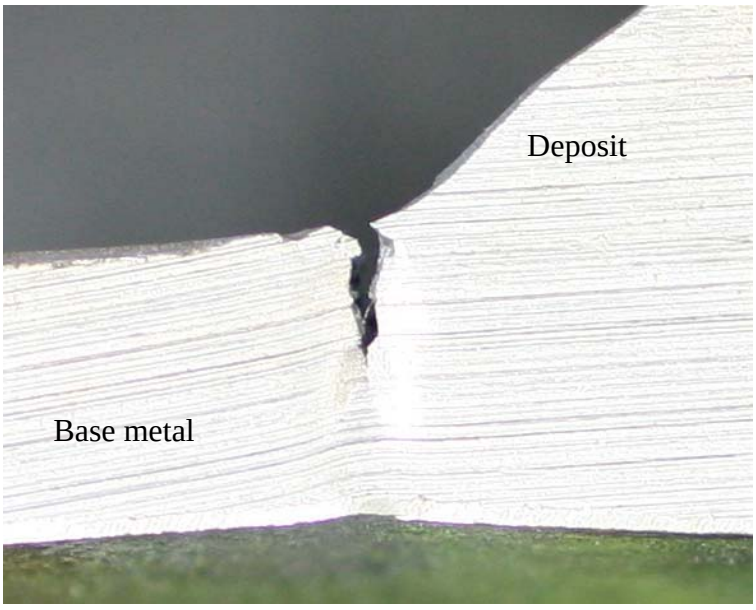

Fig. 3.5 Crack initiation

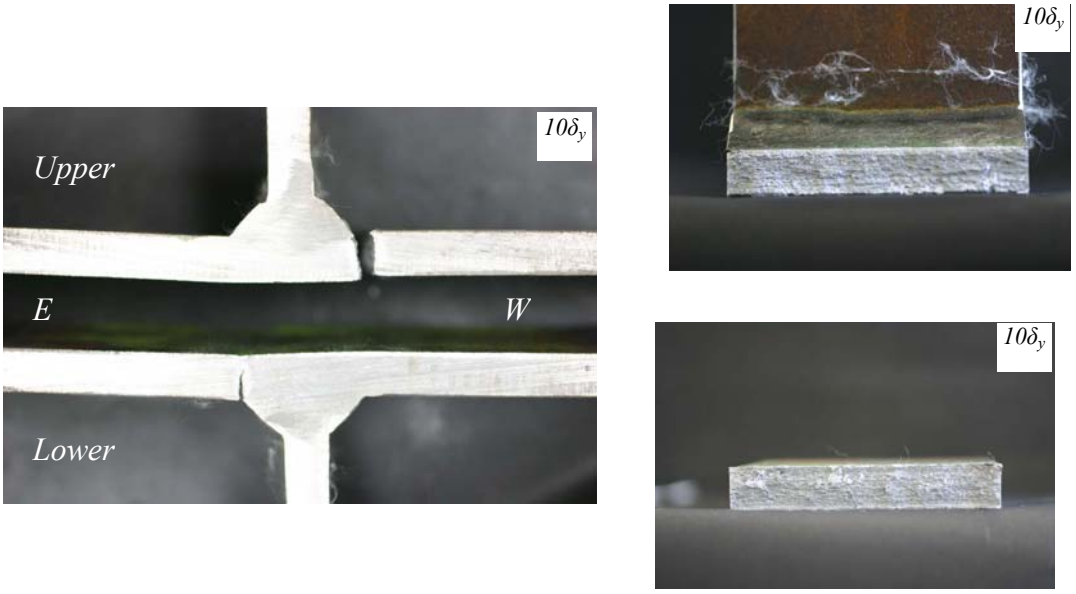

a) [-10δ_y, 10δ_y]

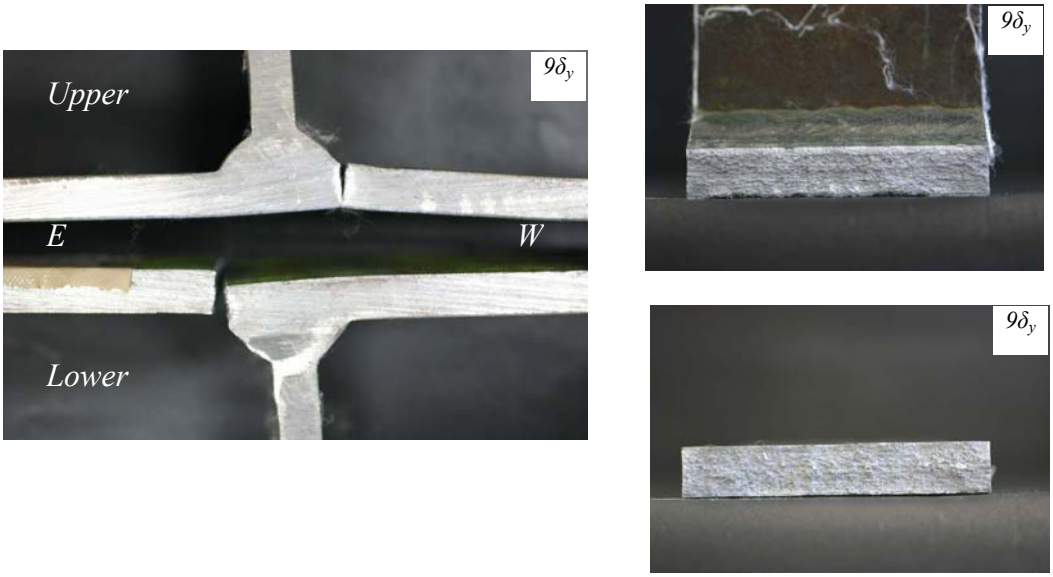

b) [-9δ_y, 9δ_y]

Fig. 3.6 Failure modes of specimens and ruptured cross section

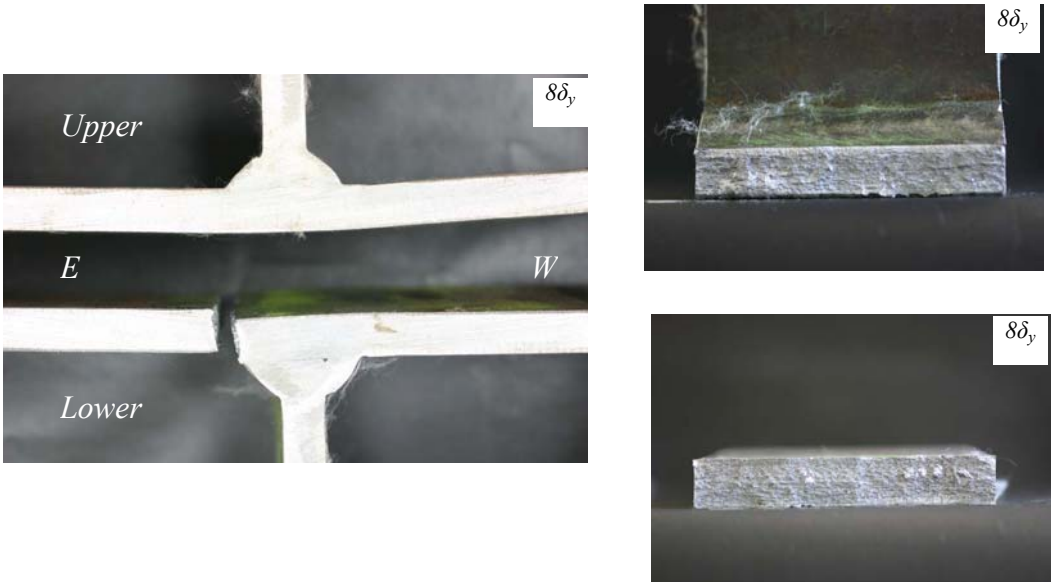

c) [-8δ_y, 8δ_y]

Fig. 3.6 Failure modes of specimens and ruptured cross section

3.4 Application of the proposed method

3.4.1 Extremely low cycle fatigue life model and cumulative damage rule

Extremely low cycle fatigue strength curves were obtained by a newly developed image testing system especially for large strain field (Teteishi et al. 2004; 2007). The results are expressed by Coffin -Manson equation,

$$\varepsilon_{ta} \cdot N^k = C \tag{3-1}$$

where ε_{ta} is the total strain amplitude; N is number of cycles to crack initiation; k and C are empirical constant listed in **Table 3.2.** This criterion is developed based on the crack initiation life when the crack length attains 0.5mm.

Researchers have found that cumulative damage due to low cycle fatigue is closely related to the number of strain cycles that structural elements suffer during earthquake excitation (Cosenza et al. 1993). In practice, structures are usually subjected to variable amplitude loadings. To evaluate the cumulative damage, a linear cumulative damage rule is brought out by Miner (1945):

Table 3.2 Material parameters

	k	C
Base metal	0.587	0.392
Deposited metal	0.587	0.261
Heat affected zone	0.587	0.203

$$D = \sum_{i=1}^{k} \frac{n_i}{N_i} \tag{3-2}$$

where D is the damage index, n_i and N_i are the number of cycles under the constant amplitude loading and the fatigue life under the same loading, respectively. In engineering practice, damage index is equal to zero when there is no damage and is equal to unity when failure occurs.

3.4.2 Constant amplitude loading

Constant amplitude loading test to T-shaped welded joint was conducted by Hanji et al. (2006) during former researches. And very detailed FE models were analyzed to get local strain at weld toe to assess low cycle fatigue life. Detailed information can be referred to relating papers.

Here, only coarse model was created and then element strains were acquired. Weld toe radius is 0.73mm after statistical analysis according to reference. Then equation was obtained by interpolation from **Table 2.2**. Element strain range can be converted to local strain range. The local strain amplitudes versus number of cycles to crack initiation were plotted in **Fig. 3.7**. In the graph, marks represents test results whereas lines are fatigue strength curved obtained by former researches for large strain field (Tateishi 2005, 2007). Solid line represents fatigue strength of plain material. Dotted line and dashed line are reflections of weld deposit and HAZ respectively. It can be found that dots of test results are close to the strength curve of deposited metal. This is consistent with the observed phenomenon of crack initiation, which initiated from weld deposit. It is observed that the correlation between the analysis and the experiment is good enough for constant amplitude loading.

This validates that the proposed method is applicable to extremely low cycle fatigue assessment for welded joint with constant amplitude loading.

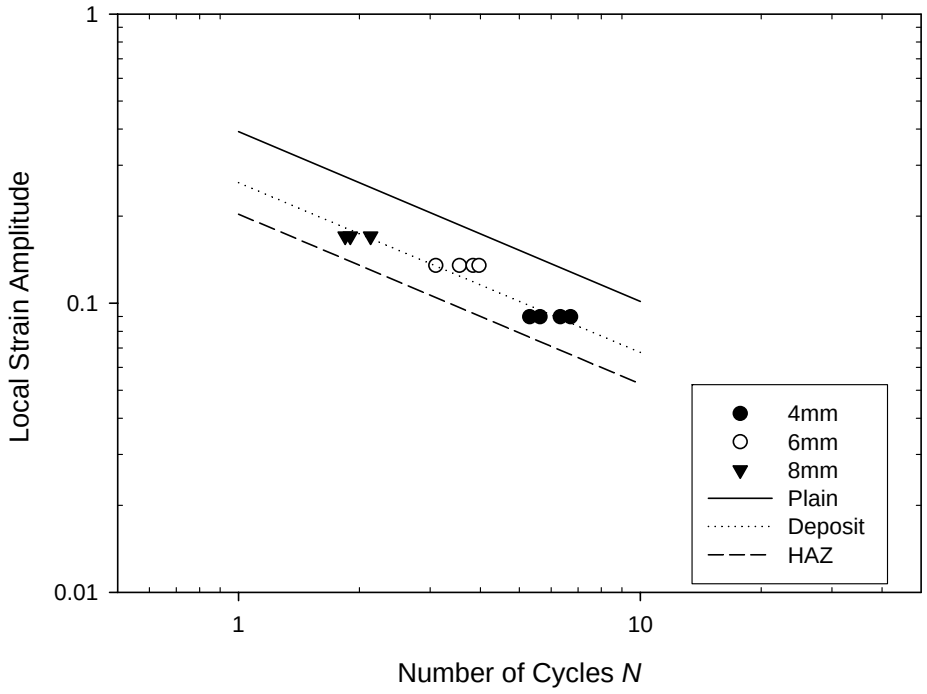

Fig. 3.7 Number of cycles to crack initiation versus local strain amplitude—constant

3.4.3 Random loading

Results of random loading test described beforehand were used. Before the test, weld toe radius and flank angle were measured by silicone-base impression materials. Statistical analysis was employed to process measured data. It is well known that the mean minus two times of standard deviation is the lower bound of a 95% confidence interval. So the weld toe radius was obtained as 0.3939mm. Flank angle was set as 45^{o} for its influence on local strain distribution is negligible (Hanji 2006). Strain range relationship for 0.3939mm radius can be linearly interpolated between the equations of 0.2mm and 0.5mm radius. Then a coarse model with a minimum mesh size of 1mm is adequate to calculate the local strain range at weld toe.

The equivalent strain amplitude versus number of cycles to crack initiation observed during test was plotted in **Fig. 3.8** together with extremely low cycle fatigue strength curves. Based on the graph, data points are above the line of weld deposit. Considering the phenomenon that observed crack initiation locations are near weld toe and in the weld deposit, it seems the proposed approach yielded out conservative results. In fact, the outcome is reasonable. Firstly, cracks reached several millimeters instead of 0.5mm when they were observed during test for the first time (Tateishi 2004). Secondly, small radius was adopted. Thirdly, the relationship of

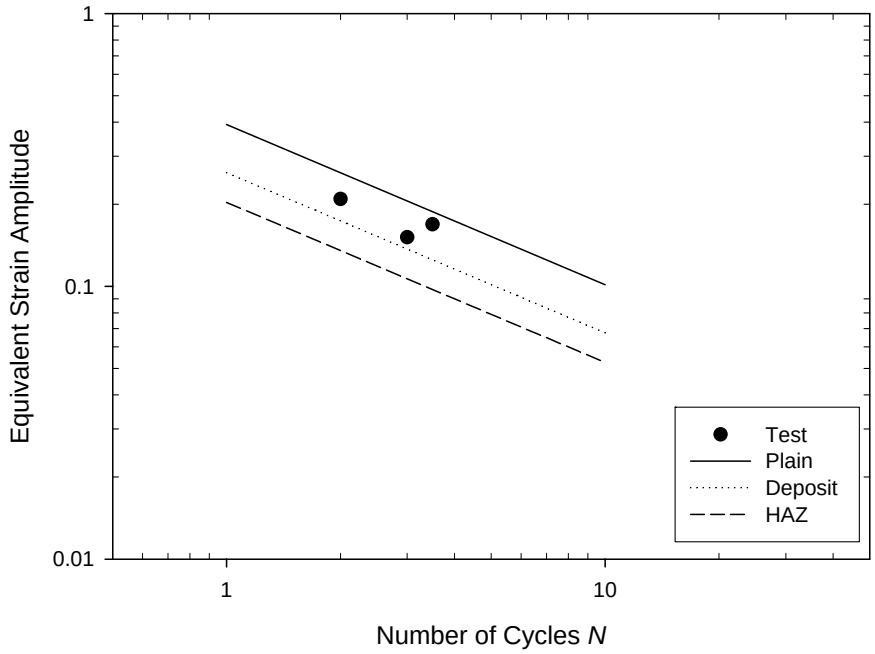

Fig. 3.8 Number of cycles to crack initiation versus local strain amplitude—random

strain range is based on plate thickness of 24mm instead of 12mm, which gives conservative results.

3.5 Summary and conclusions

In this chapter, random amplitude loading test on T-shaped weld joint was conducted. The test was conducted to verify the simple local strain approach proposed in the Chapter 2. Results of constant amplitude loading test was also used for validation. It was found that the proposed strain range relationship equations could yield out reasonable estimation of extremely low cycle fatigue life. The validation and applicability of the approach were confirmed.

Chapter 4

STUDY ON ELCF ASSESSMENT OF THICK-WALLED STEEL PIER

4.1 General remarks

Steel pier failed due to low cycle fatigue was firstly observed in the Great Hanshin-Awaji Earthquake. After that, researches have focused on it and several approaches have been proposed. But the methods vary in their applicability and degree of sophistication; and consensus has not been reached.

In this chapter, thick walled un-stiffened steel piers with box section are investigated as a fundamental research. The objective of the research is to find a simple way to extremely low cycle fatigue assessment by strain approach, which relates local strain at weld toe to nominal strain. Three-dimensional FE analysis by MSC.Marc is conducted on steel piers subjected to incremental cyclic loading in order to investigate local strain behavior at cracking point. On the other hand, analysis with beam element is also introduced to obtain nominal strain near fixed end. Then the relationship between the nominal strain range and the local strain range at weld toe is investigated. Finally, a simple approach to get conservative assessment of extremely low cycle fatigue is proposed.

4.2 Steel piers

Steel pier fixed at one end is subjected to incremental cyclic lateral loading H with constant axial loading P, as shown in **Fig. 4.1**. The dimensions of analyzed models are listed in **Table 4.1** referring to the researches by Sakano et al. (1995) and Ge et al. (2007). The geometrical parameters are represented by width-thickness ratio parameter (R_f) of flange plate and slenderness ratio parameter ($\bar{\lambda}$) given as follows,

$$R_f = \frac{b}{t}\sqrt{\frac{12(1-\nu^2)}{\pi^2\kappa}}\sqrt{\frac{\sigma_y}{E}} \tag{4-1}$$

$$\bar{\lambda} = \frac{Kh}{R}\frac{1}{\pi}\sqrt{\frac{\sigma_y}{E}} \tag{4-2}$$

where b: flange width, t: plate thickness, σ_y: yield stress, E: young's modulus, v: Poisson's ratio, κ: buckling coefficient of a plate, h: column height, K: effective length factor (K=2.0 for a fixed-free column), R: radius of gyration of steel section, P/P_y: axial load ratio, P_y: product of yield stress and cross-section area.

In this study, three kinds of width thickness ratio R_f were designed and they are relatively small. So we called them thick-walled steel pier to distinguish them from thin-walled steel pier, which are prone to fail with local buckling. It should be noted that the plate thickness is 12mm that is thin steel plate in practice.

A bilinear constitutive model, which has yield stress of 400MPa and young's modulus of 2.0×10^5MPa, was adopted. Poisson's ratio was 0.3 and strain-hardening ratio, which is the ratio between post-yield tangent and initial elastic tangent, was assumed as 1/100. The kinematic hardening was used with von Mises yield criterion.

Incremental cyclic loading shown in **Fig. 4.2** was applied under displacement control. The displacement increment was δ_{y0}, obtained from the following equation:

$$\delta_{y0} = \frac{H_{y0}h^3}{3EI} \tag{4-3}$$

where

$$H_{y0} = \frac{M_y}{h} \tag{4-4}$$

M_y: yield moment, and I: moment of inertia.

The analysis continued until the displacement attains 10 times of δ_{y0}.

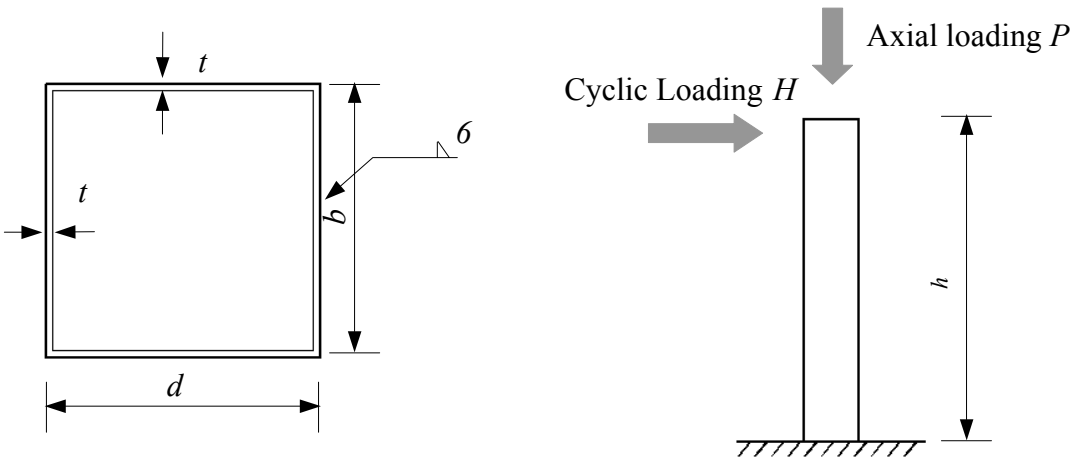

Fig. 4.1 Geometry configuration of un-stiffened box section steel pier

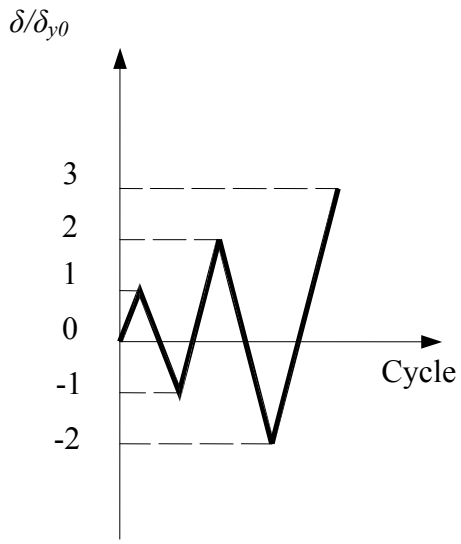

Fig. 4.2 Cyclic loading pattern

Table 4.1 Parameters of models

No.	R_f	$\bar{\lambda}$	h *	b*	d*	t*	P/P_y
U1	0.2118	0.5369	700	108	88	12	0
U2	0.2118	0.3835	500	108	88	12	0
U3	0.2118	0.3068	400	108	88	12	0
U4	0.2451	0.5556	1000	125	125	12	0
U5	0.2451	0.4306	775	125	125	12	0
U6	0.2451	0.3056	550	125	125	12	0
U7	0.3268	0.5568	1000	125	125	9	0
U8	0.3268	0.4287	770	125	125	9	0
U9	0.3268	0.3062	550	125	125	9	0
U10	0.3268	0.3062	550	125	125	9	0.1
U11	0.3268	0.3062	550	125	125	9	0.2

*Unit: mm

4.3 FE modeling

In this study, weld bead, flange and web at corner were modeled by fine solid element mesh with 1mm×1mm×1mm size. Relative coarse fine mesh was assigned in the further part. But the mesh dimension along width remains 1mm. Solid element type is eight-node, isoparametric, and arbitrary hexahedral elements. For computational efficiency, only the lower part of the columns was represented by the solid element. The upper part of the column was represented by shell elements that are four-node, thick-shell elements. They were linked by rigid elements. The height of solid part, which is 1.5 times of flange width, was decided by trial analyses and referred to other researches (Ge et al. 2000; Matsui 2006). Only half of the pier was discretized by virtue of the symmetry of the geometry and the boundary conditions. Weld leg length was assumed as 6mm. An example of FE model is shown in **Fig. 4.3 a)**.

For engineering design, it is not practical to use fine mesh of solid element and to accurately obtain the strain field in the vicinity of the weld toe. As an alternative, the fiber element model, shown in **Fig. 4.3 b)**, was also created and analyzed. It was fulfilled by two-node 3D type beam element incorporated in MSC.Marc. For box section, 28 integration points are specified. In the figure, l_e denotes the effective failure length of steel pier, which is the smaller value of 0.7b and diaphragm space (Zheng et al. 2003). Here, five elements are assigned along l_e. It was determined after comparing the results of models with 5, 10,15 and 20 partitions along l_e.

In the present analysis, initial imperfections such as initial deflections and residual stresses are not considered, because the large amplitudes of alternating loads that results in large plastic strain will reduce the effects of initial imperfections and residual stresses.

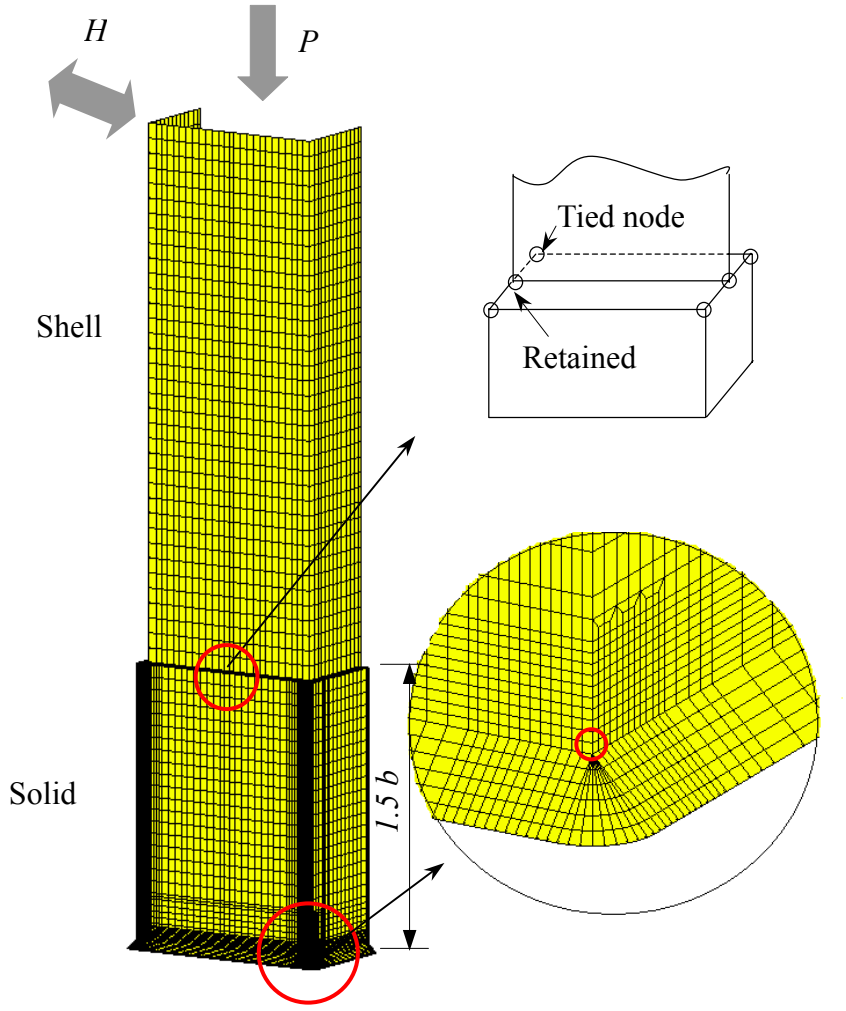

a) Solid-shell element model

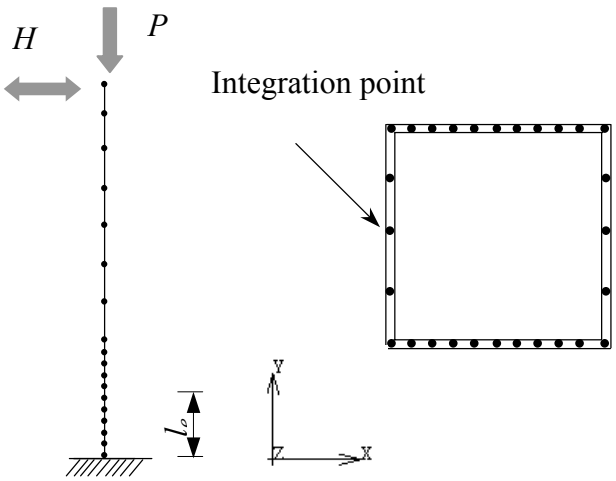

b) Beam element model

Fig. 4.3 Illustrations of FE models

4.4 Analysis results

Fig. 4.4 illustrates typical horizontal load-displacement curves at the top of piers obtained by finite element analysis. The horizontal load H and the horizontal displacement δ were normalized by H_{y0} and δ_{y0}, respectively. Solid line indicates the analytical results of thick walled pier U9 in this study. And dashed line shows the results of thin walled pier B2 cited from Usami et al.'s research (2000). It should be noted that envelope line for thick walled pier is different from thin walled piers owing to different failure modes. For thin walled pier, the envelope line attains maximum value then descends with local buckling. But for thick walled pier, the envelope line continuously ascends with increment of horizontal displacement, which means extremely low cycle fatigue than local buckling can be a dominant failure mode.

Fig. 4.5 shows the strain distribution along the flange width with the increment of loading displacement applied to pier U9. Significant strain concentration can be observed and it develops very fast in the initial several displacement levels then increases slowly. The analysis results also indicate the maximum strain exists at the corner. This conforms to the fact that cracks initiated from the corner during test (Sakano et al. 1995; Ge et al. 2007).

4.4.1 Strain range relationship

The history of strain component in height direction of the element at the corner, circled in **Fig. 4.3 a)**, was acquired by solid-shell model. The strain history was processed into strain ranges with the employment of rainflow counting method (Maddox 1991). After that, the strain range of element was converted to the local strain range $\Delta\varepsilon_r$ with respect to weld toe radius by equations in **Table 2.2**. According to the measurement of weld toe radius (Tagaki et al. 1982; Radaj 1996), 0.2, 0.5, 1 and 2mm weld toe radiuses were assumed. Meanwhile, nominal strain, which is the average strain along effective failure length in the flange, can be calculated by beam element model. Then the nominal stain range $\Delta\varepsilon_a$ was obtained by rain flow counting.

Fig. 4.6 illustrates the comparison of strain range of pier U9 when weld toe radius is 1mm. Judging from the figure, the line is almost linear for nominal strain range, but obvious nonlinear is observed for local strain range at weld toe. In this study, the ratio between both strain ranges, $\Delta\varepsilon_r / \Delta\varepsilon_a$, is called strain range ratio.

Several parametric studies were conducted using the solid-shell model and the beam model. They are axial compression loading, slenderness ratio, and width-thickness ratio. Typical results of weld toe radius with 1mm are illustrated here for discussion. Similar phenomenon was observed for other radiuses, and the results were summarized in Appendix.

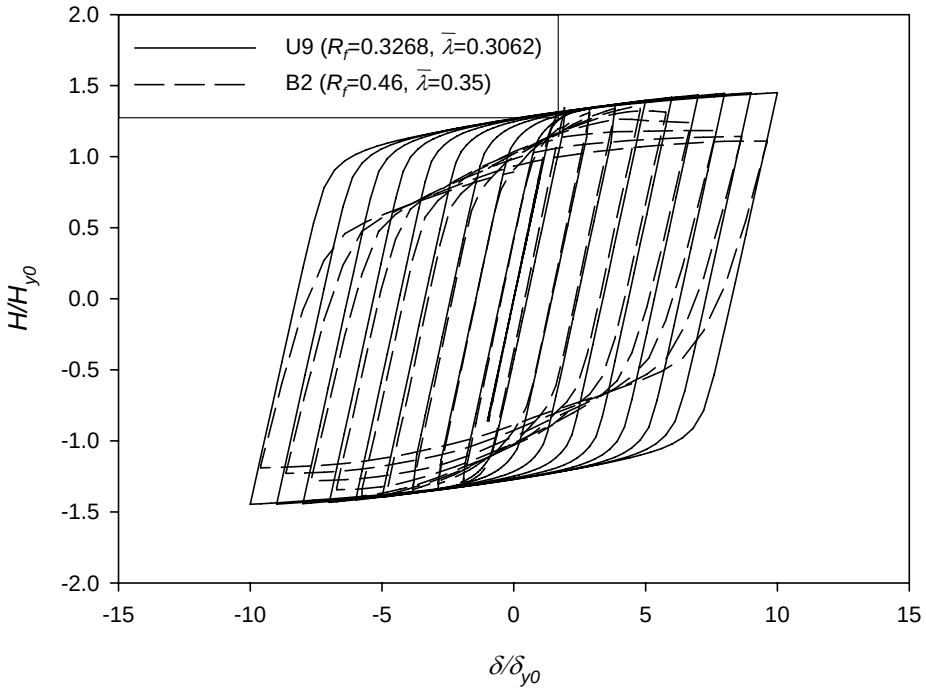

Fig. 4.4 Horizontal load-displacement hysteresis curves

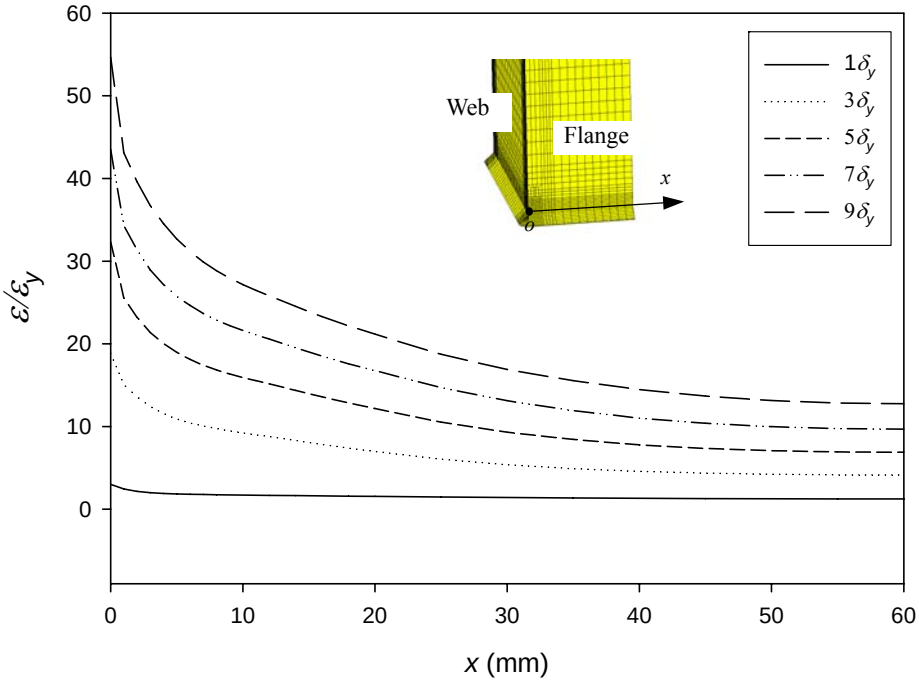

Fig. 4.5 Strain distribution near pier base (U9)

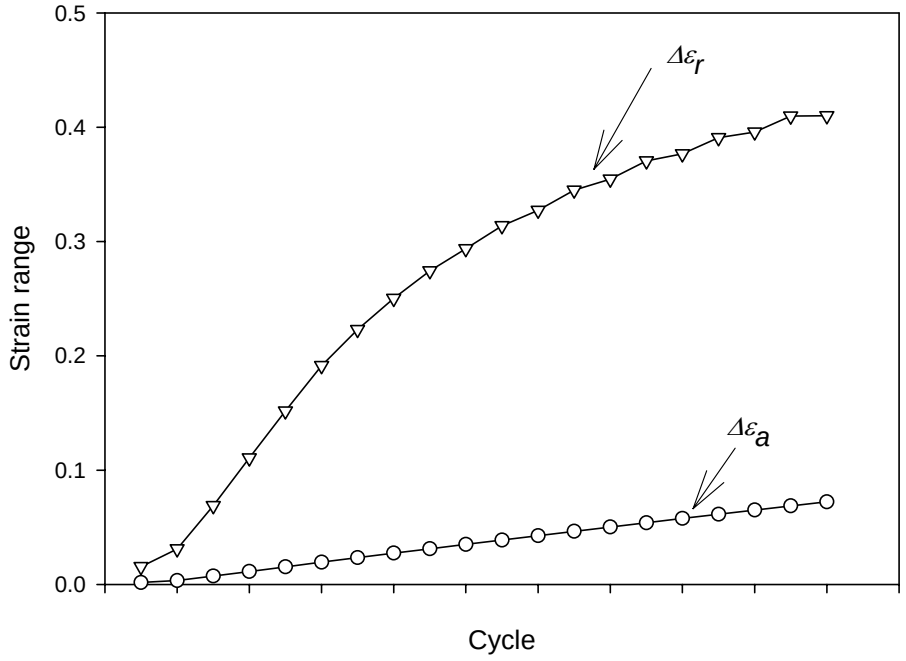

Fig. 4.6 Nominal strain range and local strain range (U9)

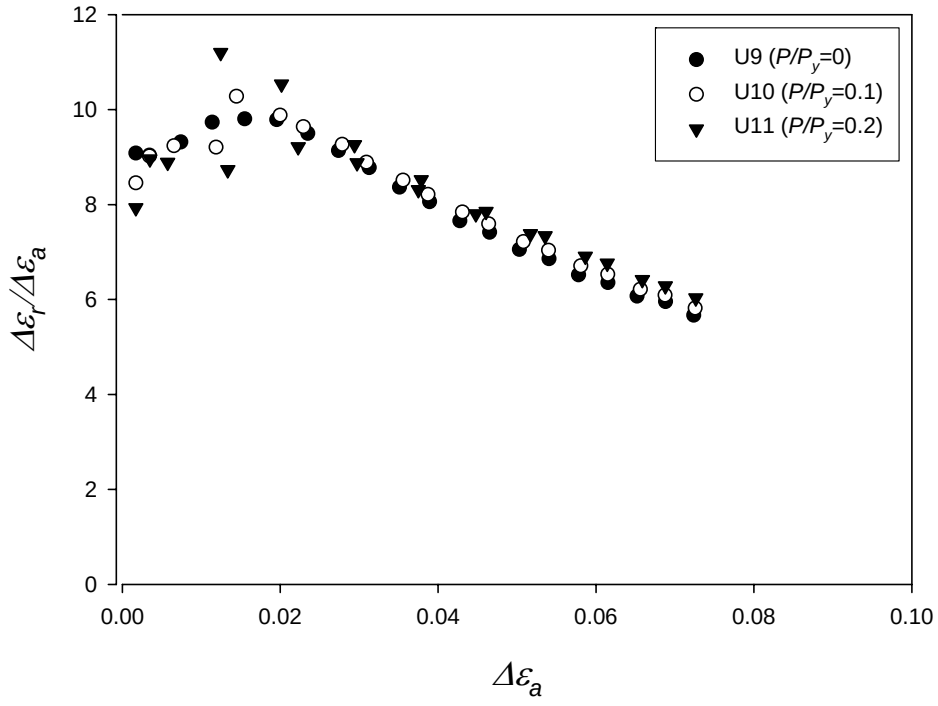

Fig. 4.7 Relationship with respect to axial loading

(R_f=0.3268, $\bar{\lambda}$ =0.3062)

Firstly, effect of axial compression load was investigated as shown in **Fig. 4.7**. In the graph, the strain range ratios versus the nominal strain range were plotted with respect to axial load ratio. The strain ratios locate in the range around 6 to 10. The strain range ratio has a peak when nominal strain range is around 0.02, and then decreases with the increment of the nominal strain range. In small average strain range around 0.02, some scatter can be observed. The cause of the scatter is not clear at present. But in most part the relationship between the nominal strain range and the strain range ratio is almost same regardless of the axial loading level.

Secondly, effect of slenderness ratio is shown in **Fig. 4.8**. It is observed that for large slenderness ratio, strain ratio decreases with the increment of nominal strain range continuously. This is different from the result of small slenderness ratio, which has an acme around 0.02. For three different width thickness ratios, the results of small slenderness ratio are above those of large slenderness ratio.

Lastly, effect of width-thickness ratio is shown in **Fig. 4.9**. The slenderness ratios remain almost constant for three different models. The relationships coincide with each other and the effect of width-thickness ratio is negligible.

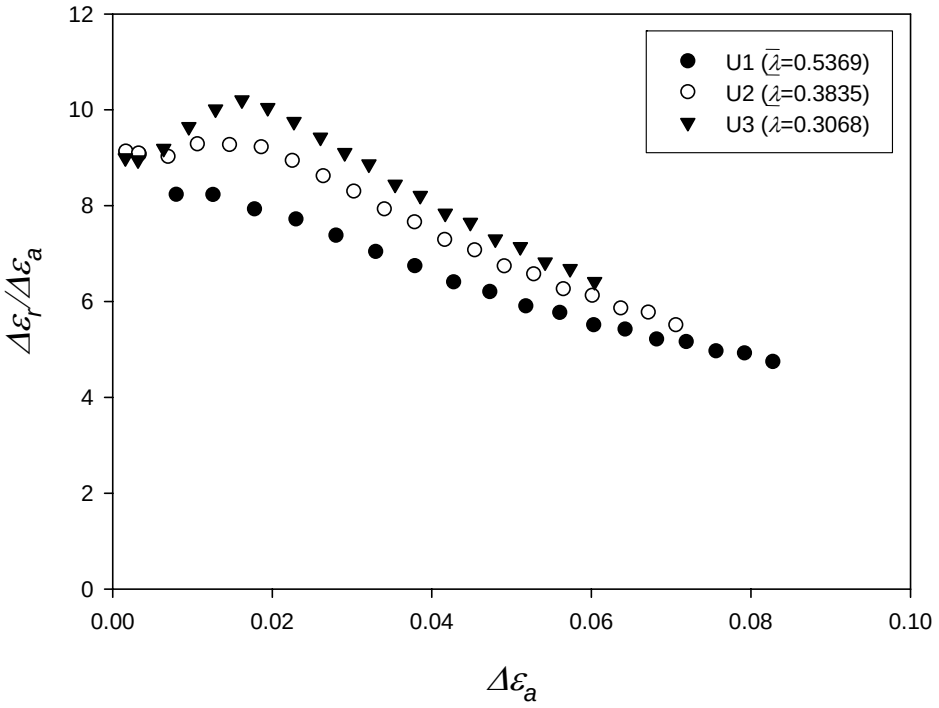

a) R_f=0.2118, P/P_y=0

Fig. 4.8 Relationship with respect to slenderness ratio

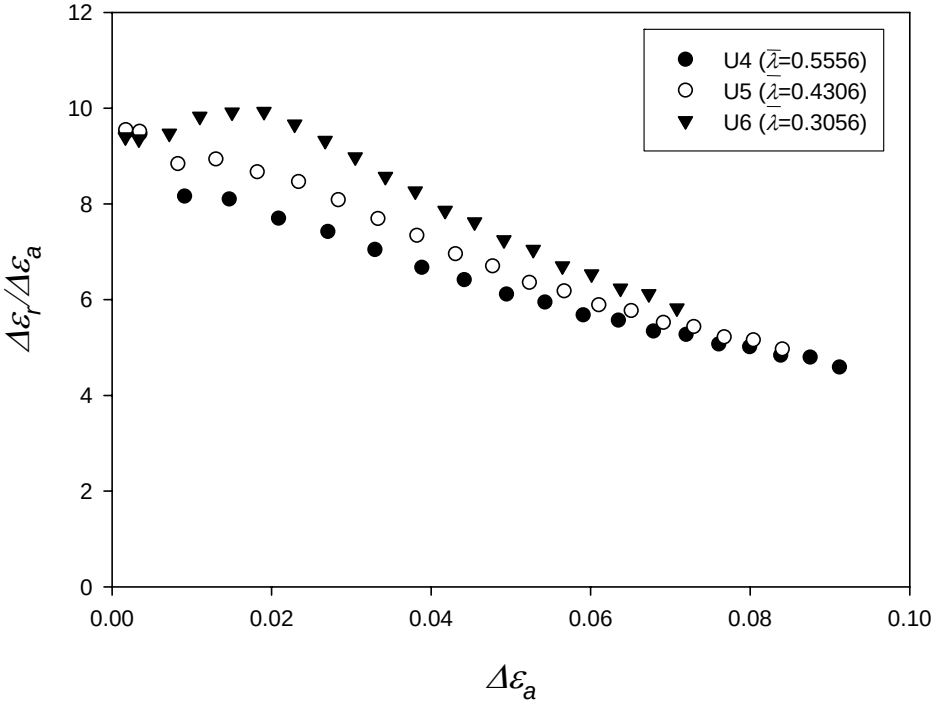

b) R_f=0.2451, P/P_y =0

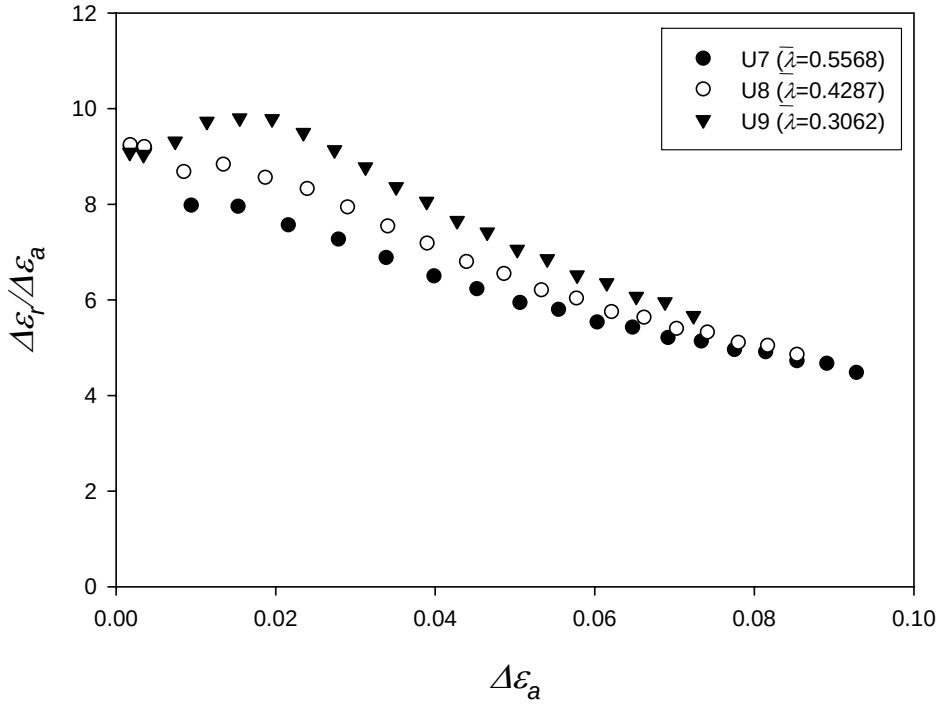

c) R_f=0.3268, P/P_y =0

Fig. 4.8 Relationship with respect to slenderness ratio

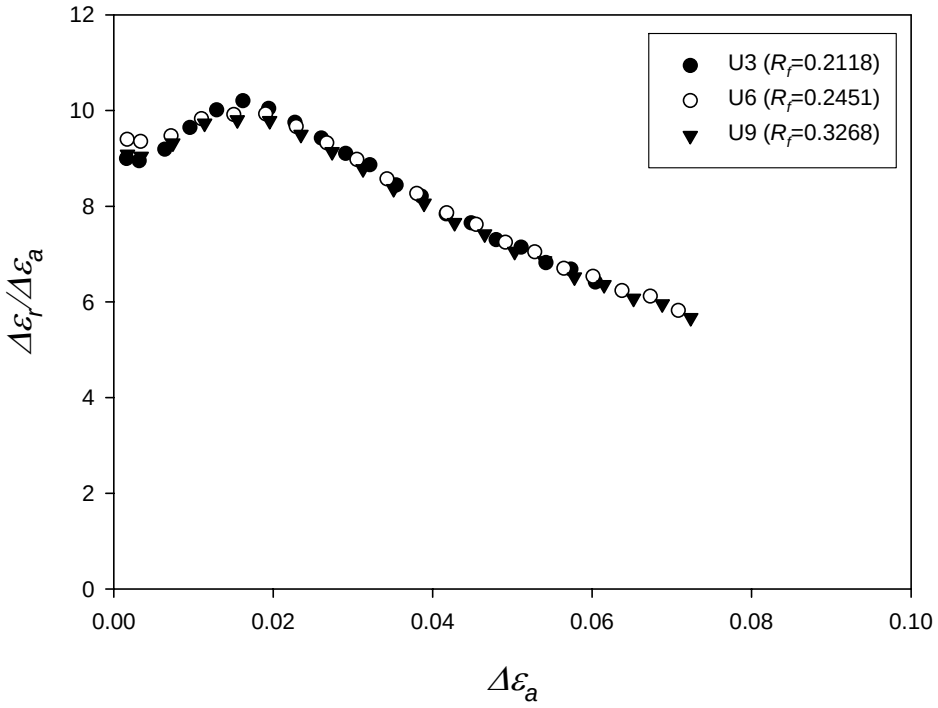

Fig. 4.9 Relationship with respect to width thickness ratio

($\bar{\lambda}$ ≈0.3062, P/P_y =0)

4.4.2 Simple approach to extremely low cycle fatigue assessment

All results for the weld toe radius of 1mm were summarized in **Fig. 4.10**. From the data in the figure, the conservative upper bound regression line was determined. For other weld toe radiuses, the same procedure was performed and the results were shown in **Fig. 4.11** and **Table 4.2**. The strain range ratio isn't constant but declined with the increment of strain range. The reason may lie in the fact that strain concentration exists for shell-solid model along flange, while uniform strain distribution along flange is assumed in beam element model. With the increment of loading cycles, strain redistributes along the flange and strain concentration is reduced due to large scale yielding. That will result in lessening of the strain range ratio.

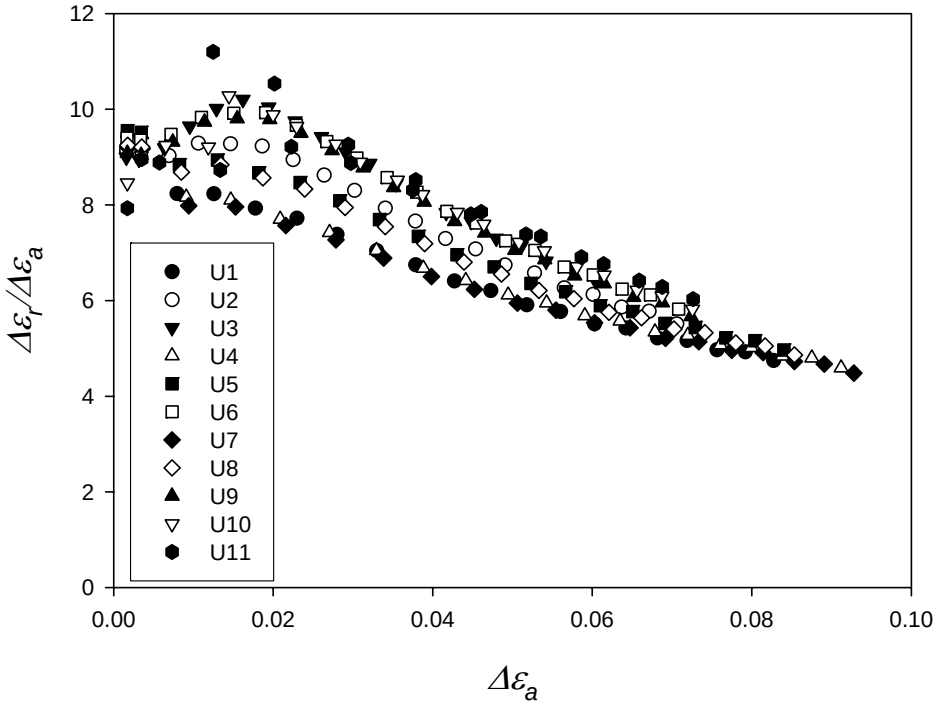

Fig. 4.10 Summary of results

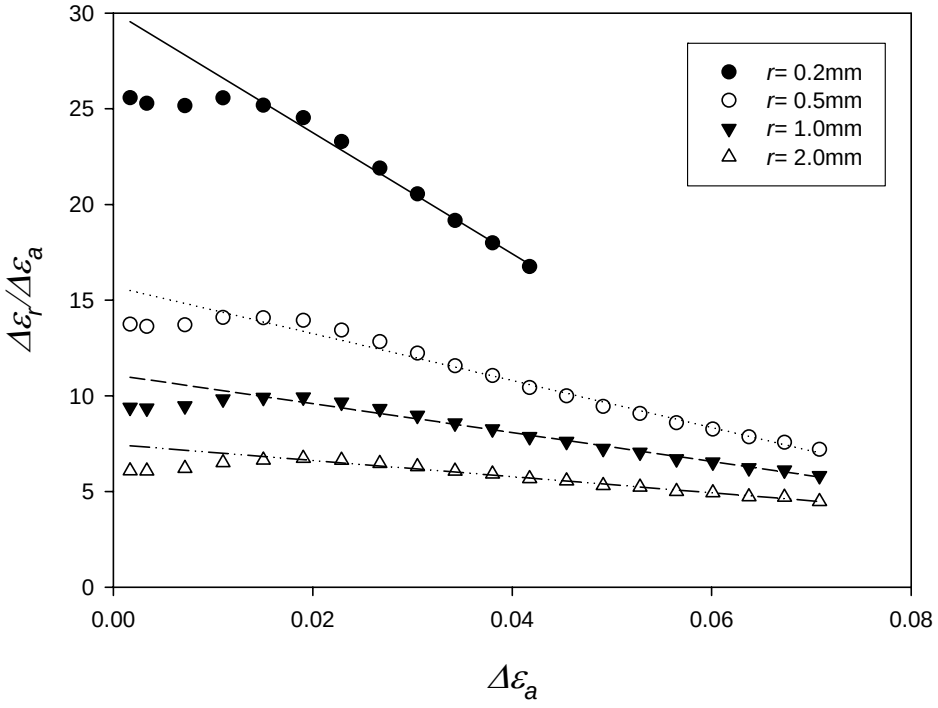

Fig. 4.11 Relationship with respect to radius

Table 4.2 Equations for strain range ratio between local strain range and nominal strain range

Equation	$\Delta\varepsilon_r/\Delta\varepsilon_a = a\Delta\varepsilon_a + b$	
Weld toe radius (mm)	*a*	*b*
0.2	-316.6	30.1
0.5	-122.8	15.7
1.0	-75.5	11.1
2.0	-42.1	7.5

* $\Delta\varepsilon_a/\varepsilon_y \le 35$

4.4.3 Extremely low cycle fatigue assessment

Now, we have two ways to estimate the local strain range at the weld toe as shown in **Fig. 4.12**. One is based on the solid-shell model analysis and the relationships in **Table 3.2**. Another is on the beam model analysis and the relationships in **Table 4.2**. The former will give more accurate estimation, but unpractical in design. Conversely, the latter is practical, but will give a conservative estimation, since the upper bound was taken when deriving the relationships in **Table 4.2**. Extremely low cycle fatigue life was predicted with local strain range estimated by these two ways, and the results were illustrated in **Fig. 4.13**. It is observed that the predicted life is strongly related to the weld toe radius. And the results based on beam model are always in conservative side. **Fig. 4.14** presents a comparison of fatigue lives obtained by these two methods. In the current loading pattern, the variant is small and only around half cycle and one cycle. The extremely low cycle fatigue assessment with the local strain range obtained by the combination of beam model analysis and **Table 4.2** gives moderately conservative side results.

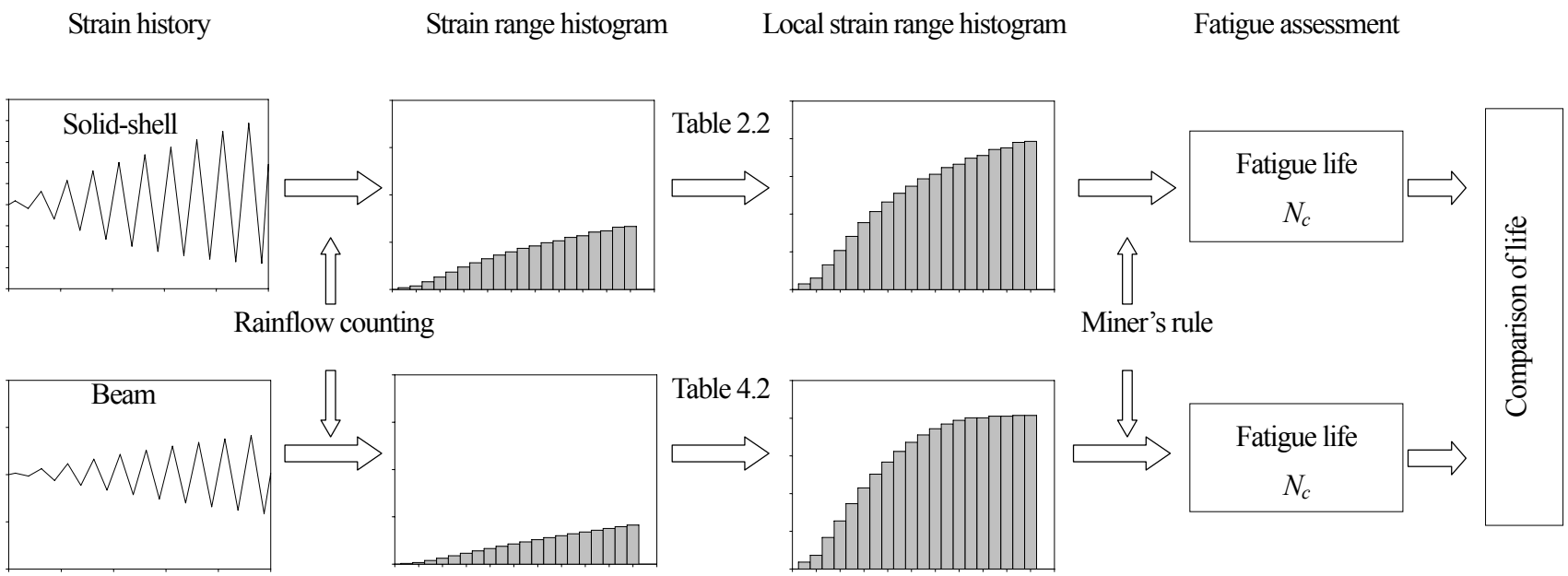

Fig. 4.12 Two ways of ELCF assessment for steel pier

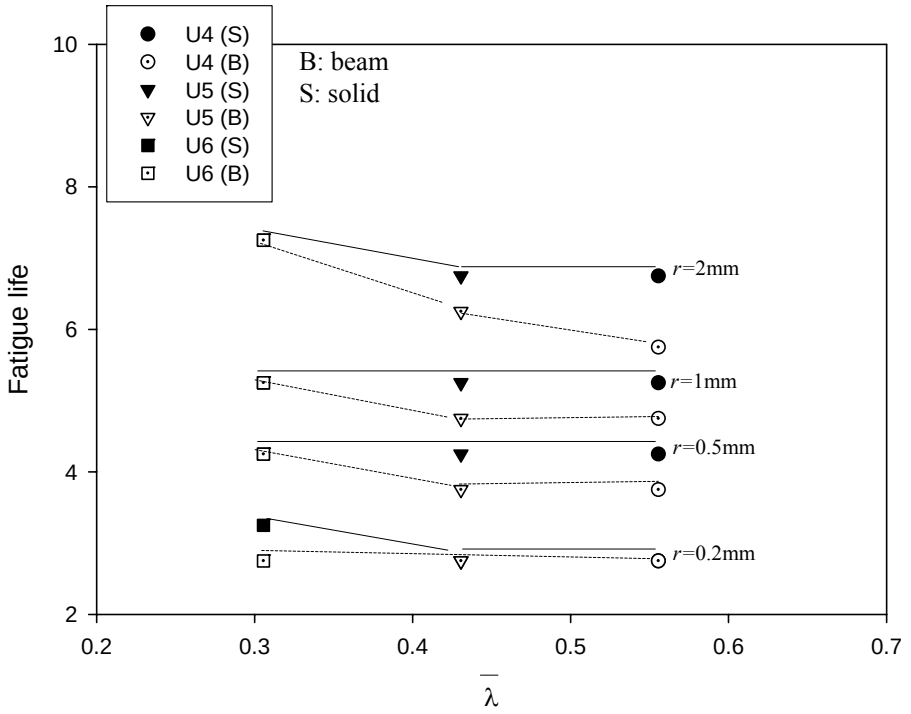

a) R_f=0.2451, P=0

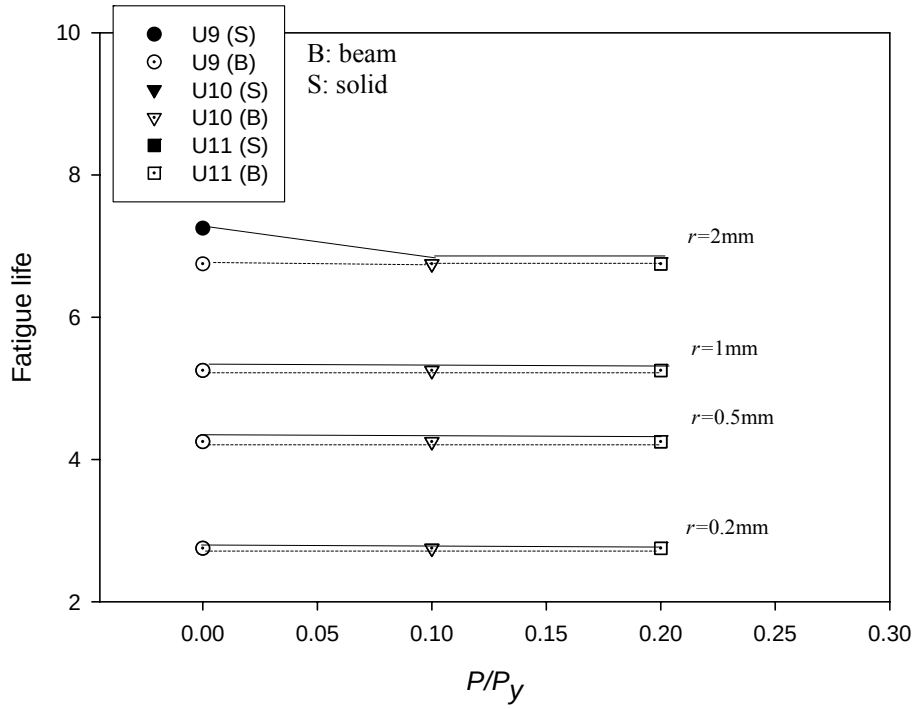

b) R_f=0.3268, $\bar{\lambda}$=0.3062

Fig. 4.13 Predicted ELCF life

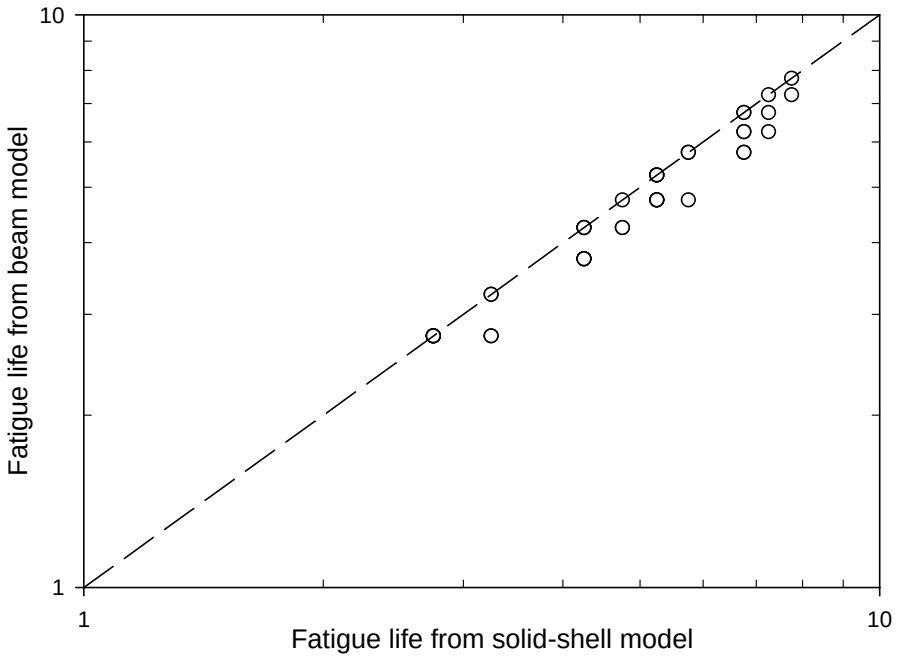

Fig. 4.14 Comparison of ELCF life

4.5 Summary and conclusions

This chapter presents a strain based approach for the extremely low cycle fatigue assessment of thick-walled steel piers subjected to incremental cyclic loading. The numerical investigation for both solid-shell element model and beam element model were carried out. Based on the analytical results, the following conclusions are reached.

1) The relationships between strain range ratio and nominal strain range are not influenced by axial loading and width-thickness ratio. Whereas slenderness ratio and weld toe radius are principal parameters.

2) A simple approach to assess ELCF of steel piers based on beam model analysis was proposed, which gives conservative prediction.

The strain based damage assessment method will provide the researchers and structural engineers with valuable tool for the design; retrofit and post-earthquake damage evaluation of steel piers. However, further experimental study is still required.

Chapter 5

TEST OF THICK-WALLED STEEL PIER

5.1 General remarks

The preceding chapter has provided the strain approach to thick-walled steel pier based on beam model. To validate the proposed approach, experimental test is necessary. But available tests of steel piers are limited and geometry parameters of weld toe are usually neglected in earlier researches. So we carried out extremely low cycle fatigue test on thick-walled steel pier.

In this chapter, we present the results of thick-walled steel piers subjected to incremental or constant amplitude cyclic loading. The objectives of this study are to investigate the extremely low cycle fatigue life of steel pier and verify the proposed strain approach. During the test, fatigue cracks initiated from weld toe at the corner and propagated along the weld toe. Finally, the piers ruptured without local buckling. The failure of low cycle fatigue induced by large cyclic deformation has been elucidated. In a further step, the crack initiation life was estimated based on local strain range by proposed simple approach. It is indicated that correlation between the test result and the estimated fatigue life is good enough.

5.2 Test program

5.2.1 Specimen configuration

Fig. 5.1 and **Table 5.1** show the configurations and dimensions of specimens. They are un-stiffened thick-walled steel piers with box section. Plate thickness is 12mm. Flange width and web breadth is 125mm. The width thickness ratio R_f and slenderness ratio $\bar{\lambda}$ are defined as equation (4-1) and (4-2).

In this study, width thickness ratio R_f of specimens is 0.2389, which is relatively small to avoid local buckling by referring to other researches (Sakano et al. 1995; Ge et al. 2007). So specimens were named as thick-walled steel pier for small R_f irrespective of plate thickness. Two slenderness ratios $\bar{\lambda}$ are considered, which are 0.4179 and 0.2979.

Horizontal yield load H_y and yield displacement δ_y in **Table 5.1** is calculated based on Timoshenko beam theory. All specimens are made from SM490YA. The mechanical

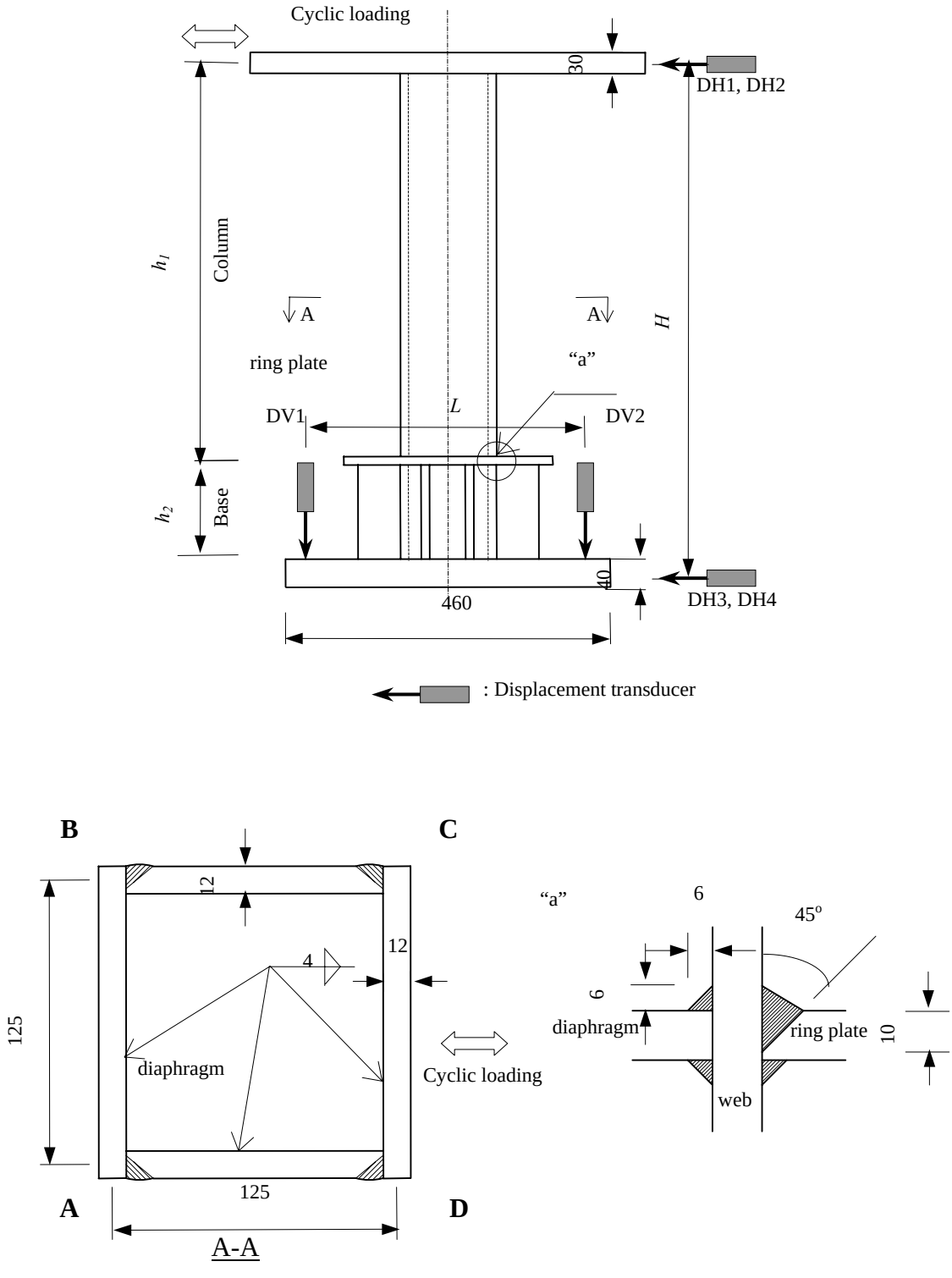

Fig. 5.1 Configuration of test specimen

Table 5.1 Geometry configuration and parameters of specimen

Specimen	h_1 (mm)	h_2 (mm)	I_1 ($\times 10^7$mm^4)	I_2 ($\times 10^7$mm^4)	R_f	$\bar{\lambda}$	δ_y (mm)	H_y (kN)
U6	550	133	1.5769	4.7289	0.2389	0.2979	4.12	159.05
U5	775	208	1.5769	4.7289	0.2389	0.4197	7.96	112.87

Table 5.2 Mechanical properties and chemical compositions

SM490YA	Yield Stress (MPa)	Tensile Strength (MPa)	Elongation (%)	Chemical compositions (%)				
				C	Si	Mn	P	S
	380	531	25	0.16	0.35	1.47	0.015	0.009

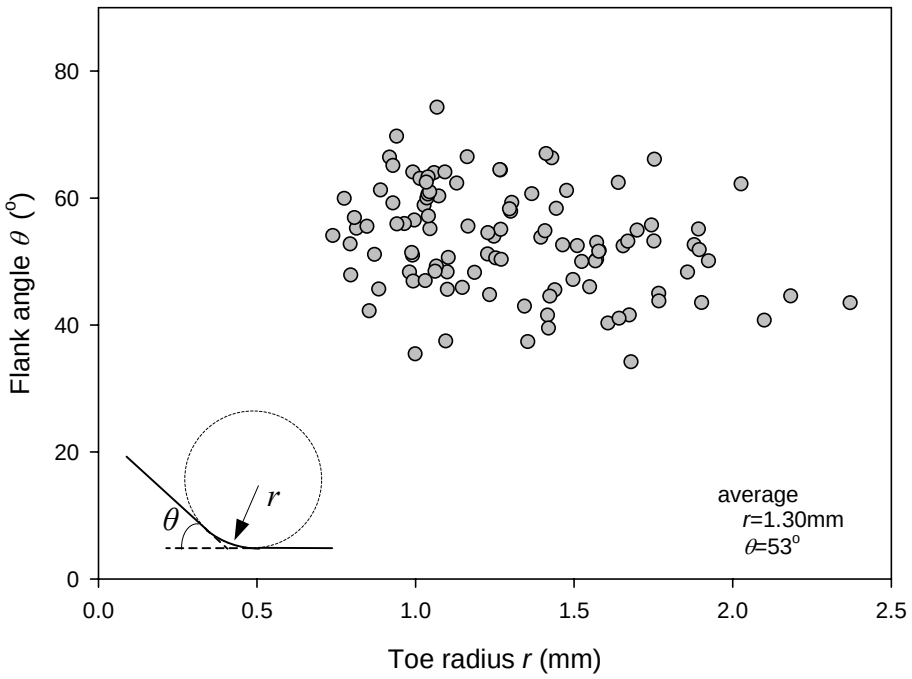

Fig. 5.2 Measured toe radius r and flank angle θ

properties and chemical compositions are tabulated in **Table 5.2**. The welding method was CO_2 gas shielded semi-automatic welding with filler metal of 1.2 mm in diameter. The specimens are in as-welded state. Plate assembly of the base joint is similar to that commonly used in actual steel piers.

Weld toe profile is essential to the local strain concentration. Basic geometry parameters of weld bead, which are weld toe radius r and flank angle θ, were measured by silicon based impression material. The results are plotted in **Fig. 5.2**. They are corresponding to corners of crack initiation observed during test. For all results, average toe radius is 1.30mm and flank angle is 53^o.

5.2.2 Test setup

Fig. 5.3 illustrates the test set up. Each specimen was bolted to the base and loaded at the top. Lateral quasi-static cyclic load is applied by an actuator. In the current study, axial loading wasn't applied to specimens because its effect to strain range is trivial according the numerical analysis results in Chapter 4. Six displacement transducers were placed on the test pier, as shown in **Fig. 5.1**. Four of them were used to acquire the horizontal displacements and two of them were placed vertically on the base plate to calculate rotation. Then top lateral displacement can be calibrated by subtraction of base deformations.

The arrangement of strain gauges is shown in **Fig. 5.4**, which were installed along flange and 5mm away from weld toe on two sides.

For convenience of identification during crack observation, corners are marked as A~D as shown in **Fig. 5.1**.

5.2.3 Loading pattern

The tests were conducted under displacement control for horizontal direction. Positive direction was defined as when corner C and D were initially under tension. Commonly used incremental cyclic loading procedure was employed for one specimen, as shown in **Fig. 5.5 a)**, which was named U6-I. Constant amplitude loading, as shown in **Fig. 5.5 b)**, was applied to other three specimens. The amplitude was 3 (U6-C3) or 6 (U6-C6 and U5-C6) times of yield displacement. Totally, four specimens were tested under different loading patterns.

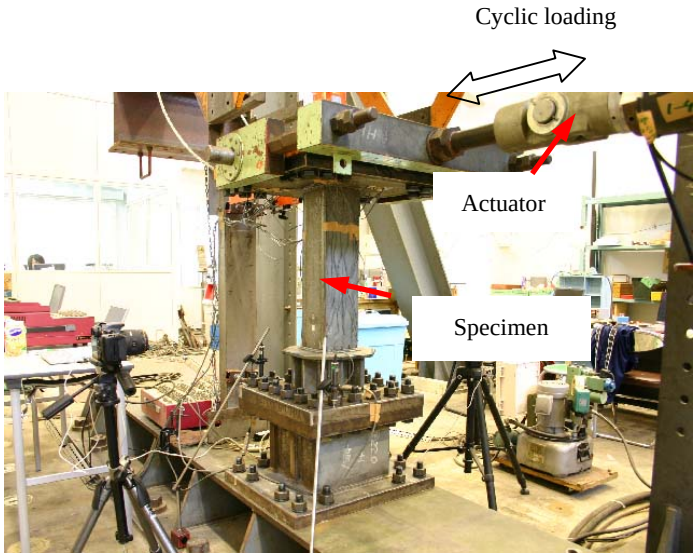

Fig. 5.3 Test setup

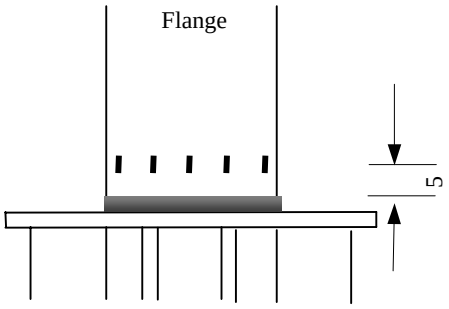

Fig. 5.4 Arrangement of strain gauges

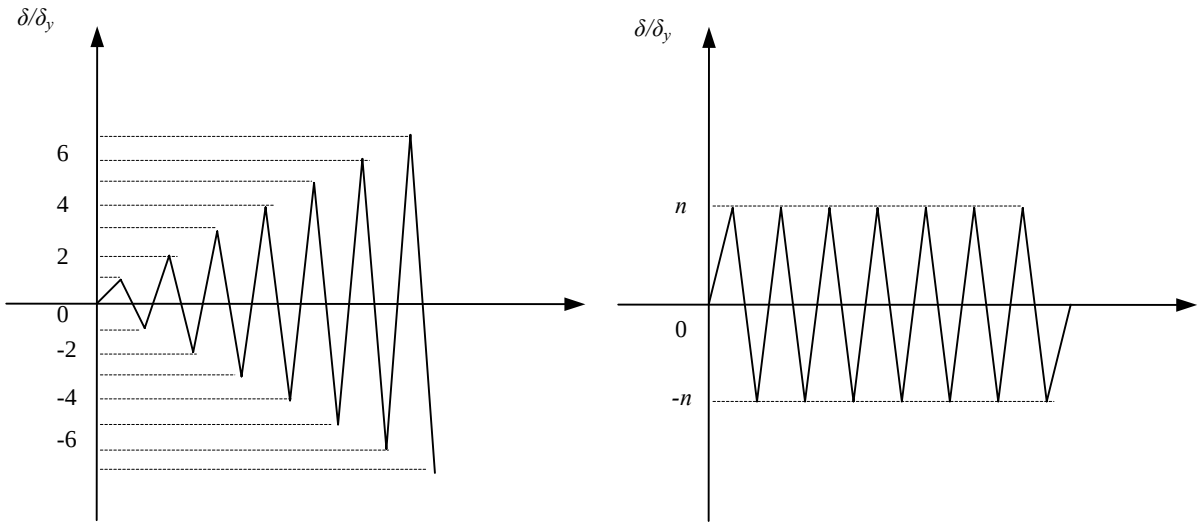

a) Incremental cyclic loading b) Constant amplitude loading

Fig. 5.5 Loading pattern

5.3 Test results and observations

5.3.1 Hysteretic curves

Fig. 5.6 shows the load-displacement hysteretic curves of specimens. Abscissa represents normalized horizontal displacement at top δ/δ_y, whereas the ordinate indicates normalized load of actuator H/H_y. Because of the limitation of testing devices, only initial several loops were measured and recorded.

Specimens failed by stable crack growth instead of brittle fracture and no local buckling was observed through the test. This is consistent with the expectation before test. In the figure, N_i and N_f denote number of cycles to crack initiation and failure observed during test.

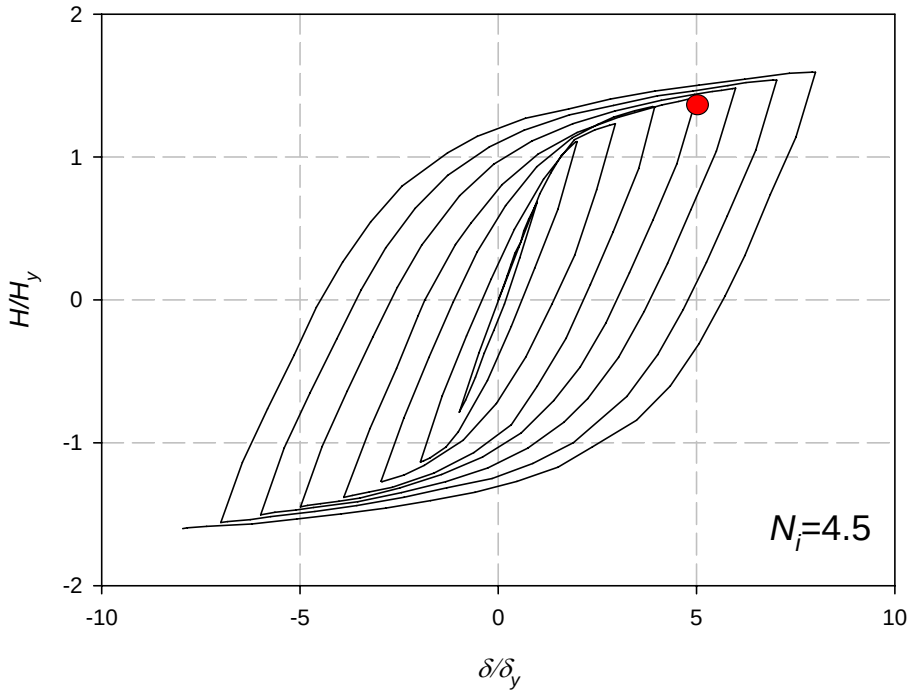

a) U6-I

Fig. 5.6 Load-displacement hysteretic curves

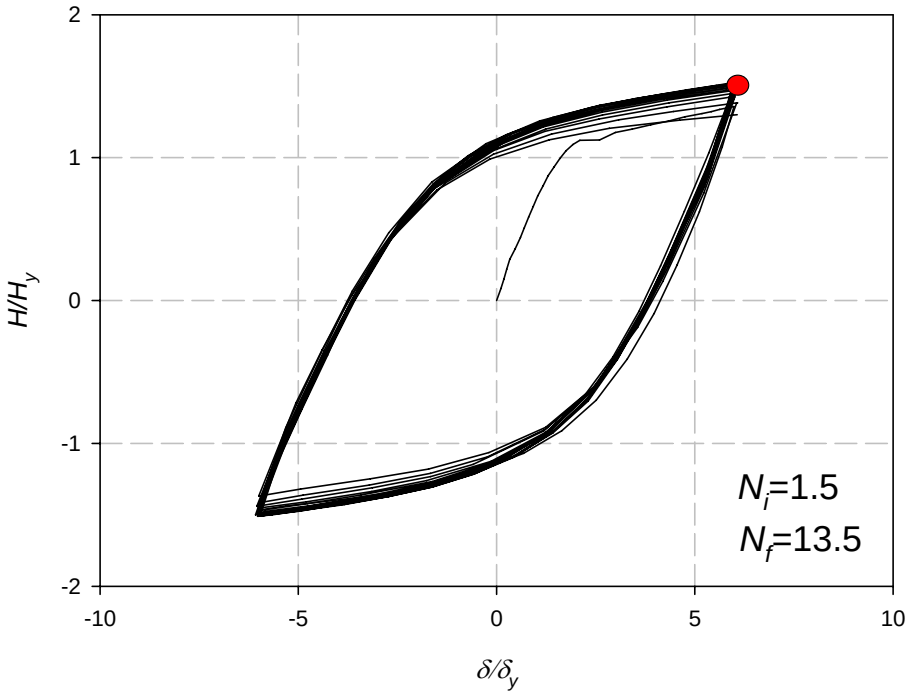

b) U6-C6

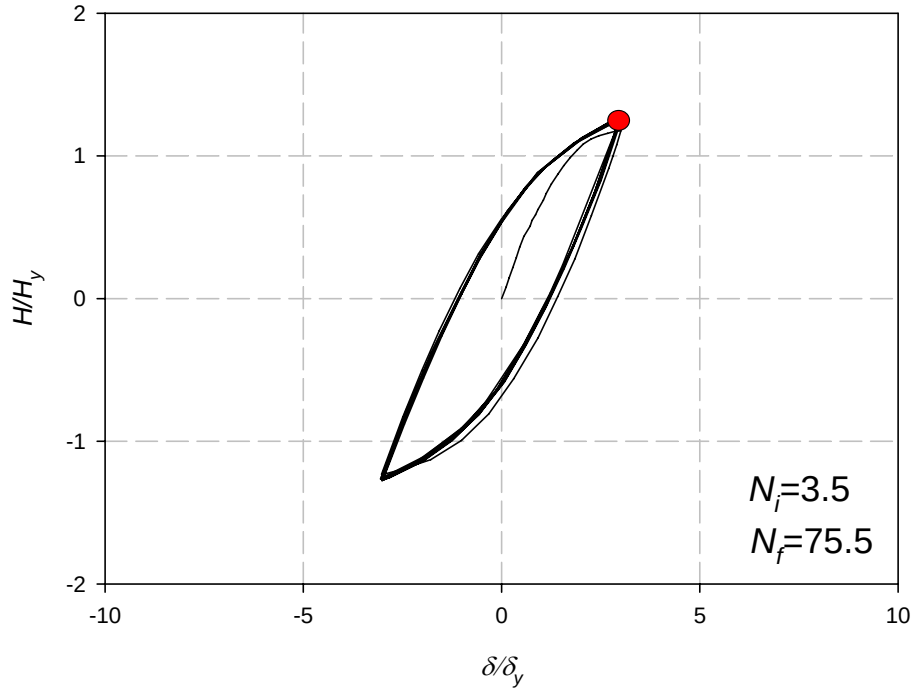

c) U6-C3

Fig. 5.6 Load-displacement hysteretic curves

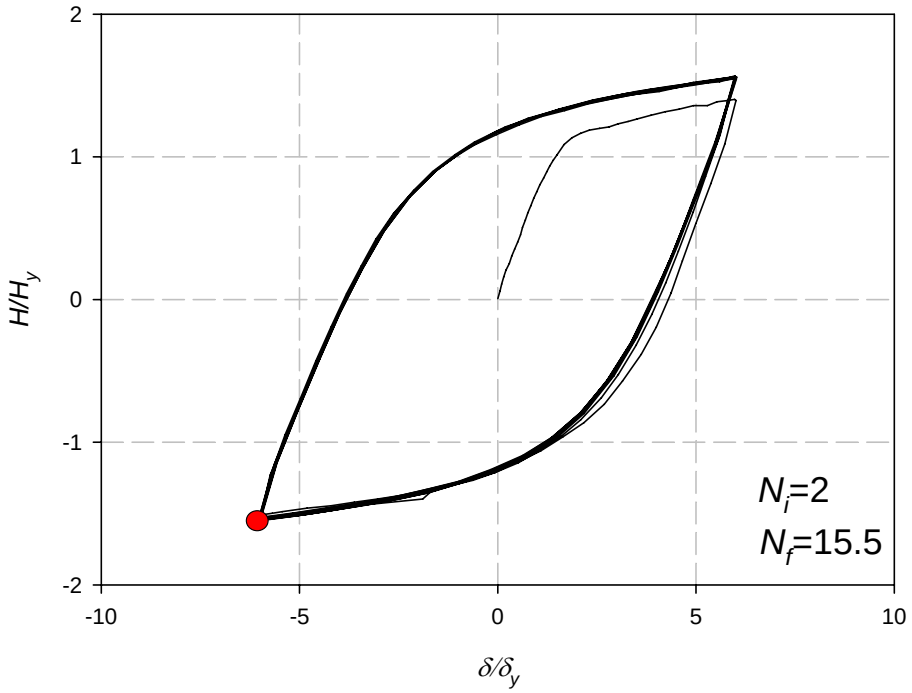

d) U5-C6

Fig. 5.6 Load-displacement hysteretic curves

5.3.2 Strain distribution and history

Fig. 5.7 shows typical strain distributions along flange, which were recorded by gauges 5mm away from weld toe. Although these values cannot be directly used to assess crack initiation life, they illustrate the general distribution of strains at high loading level. The loading displacement was $6\delta_y$ except for U6-C3, which was $3\delta_y$. It can be seen that strains near corner are larger than those of inner part. This is consistent with the numerical analysis results (Matsui and Ge 2006). The distribution was similar regardless of loading type and configuration.

Fig. 5.8 illustrates typical strain histories recorded by strain gauges at corners on both flanges, which were results of incremental cyclic loading to specimen U6-I and constant amplitude loading to specimen U6-C6 respectively. The strain attained as large as 4% that is far beyond yield strain. Strain hardening effect was also observed from the graphs. However, strain range is almost constant.

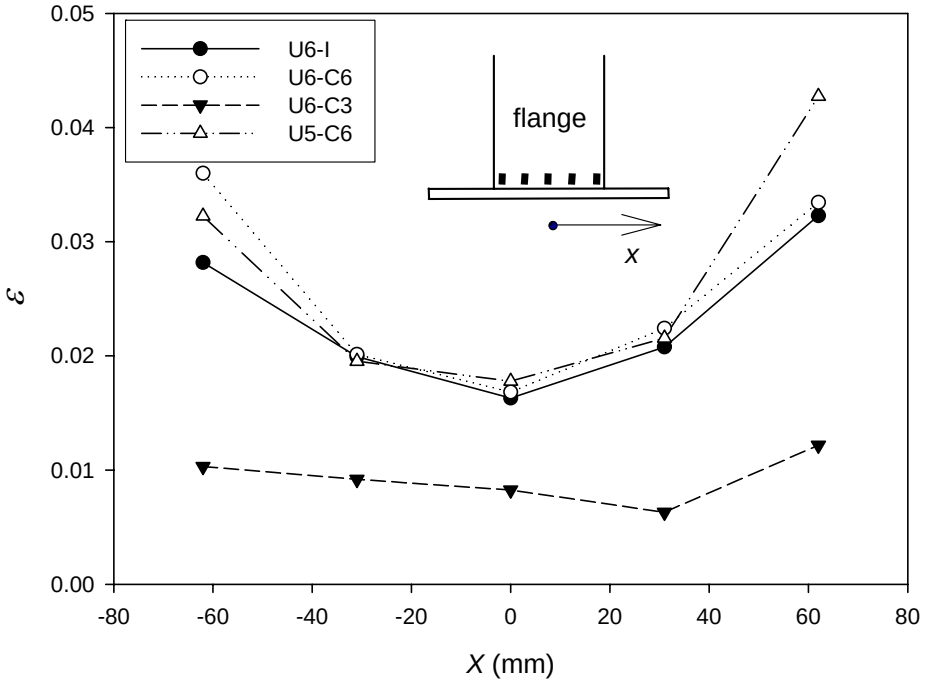

Fig. 5.7 Strain distribution along flange

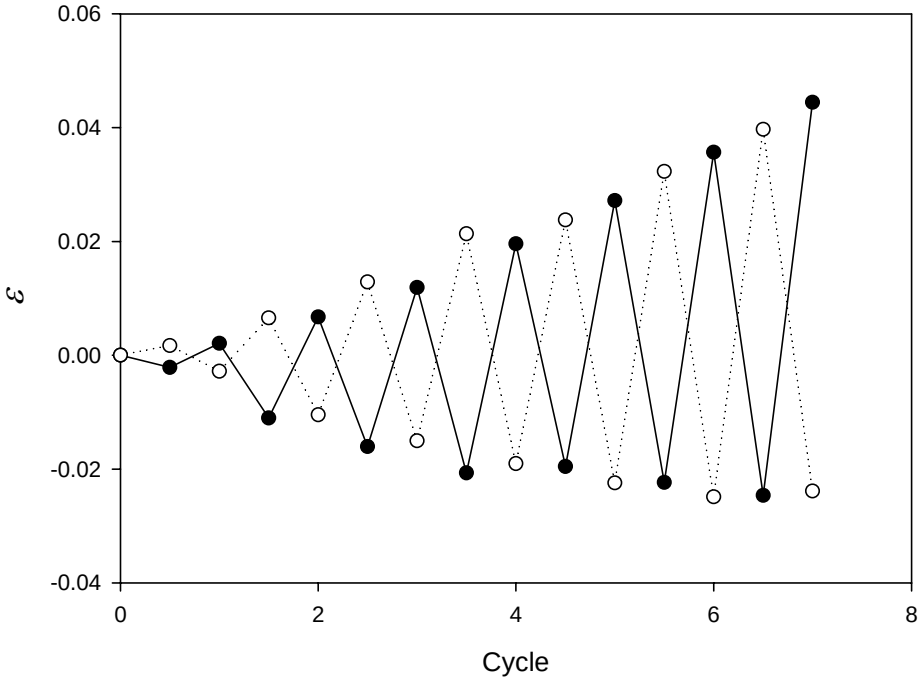

a) U6-I

Fig. 5.8 Strain history near corner

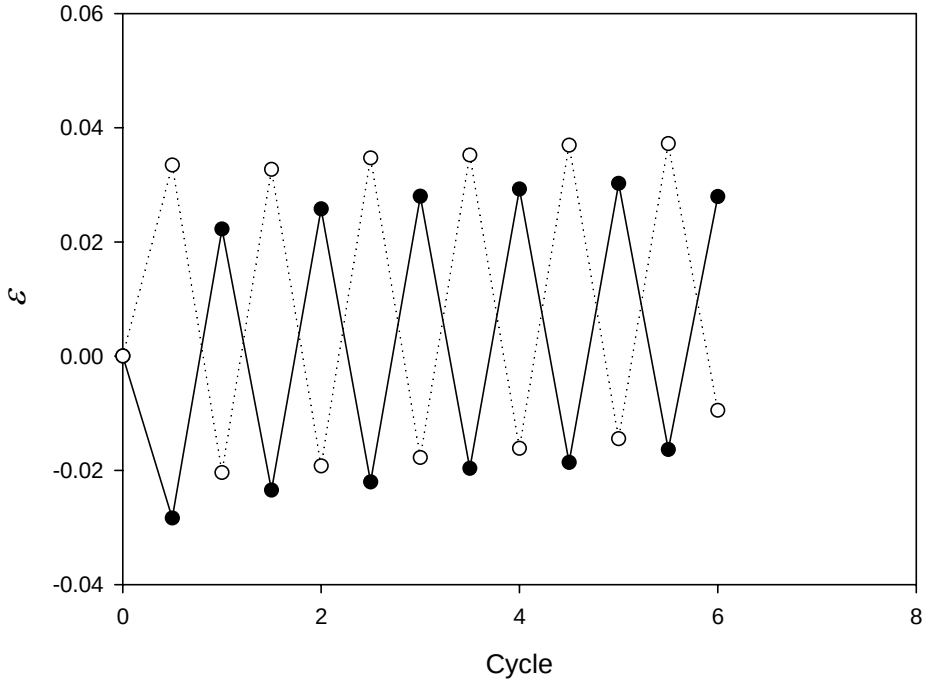

b) U6-C6

Fig. 5.8 Strain history near corner

5.3.3 Visual observations

Crack observation was performed with magnetic particle testing method (MT) at each half cycle.

During all of the tests, cracks initiated at corners of the specimens where strain concentration was large. For specimen U6-I, corner C and D were found with crack at same time. And the crack length was approximately 2.5mm. A 3.0mm length crack was firstly identified at corner C for U6-C6. For U6-C3, crack initiation corner was D and its length was 2.0mm. For specimen U5-C6, the crack was observed with 3.0mm length at corner A. Taking specimen U6-C6 as an example, **Fig. 5.9 a)** provides a typical crack initiation at corner, which is denoted by an arrow. It is also noted that crack initiated from weld deposit at weld toe. The initial cracks occurred at corners and propagated along the weld toe. With the propagation of crack length, oblique cracks formed in flange and web plate before major strength degradation took place, as shown in **Fig. 5.9 b)**. **Fig. 5.9 c)** illustrates the final failure mode when crack formed through flanges.

Fig. 5.10 summarizes all crack lengths of flanges around corner. Meanwhile, horizontal loading is also plotted with cycles. Horizontal axis is number of cycles, whereas left vertical

axis indicates crack length of flange near corner L_P normalized by half width of flange *b/2* and right vertical axis represents horizontal loading H normalized by yield loading H_y. At the beginning of test, MT observation was executed. Whereas crack length was measured without MT after the crack grew to a certain length. They are distinguished by a vertical dash line in the figure. Fatigue crack initiation points are also marked in the figure.

During the test, it was found that crack growth did not cause evident deterioration of the loading capacity and stiffness until the crack has grown up to approximately 0.6 times of half flange width. Once deterioration took place, it occurred at a very high rate leading to failure.

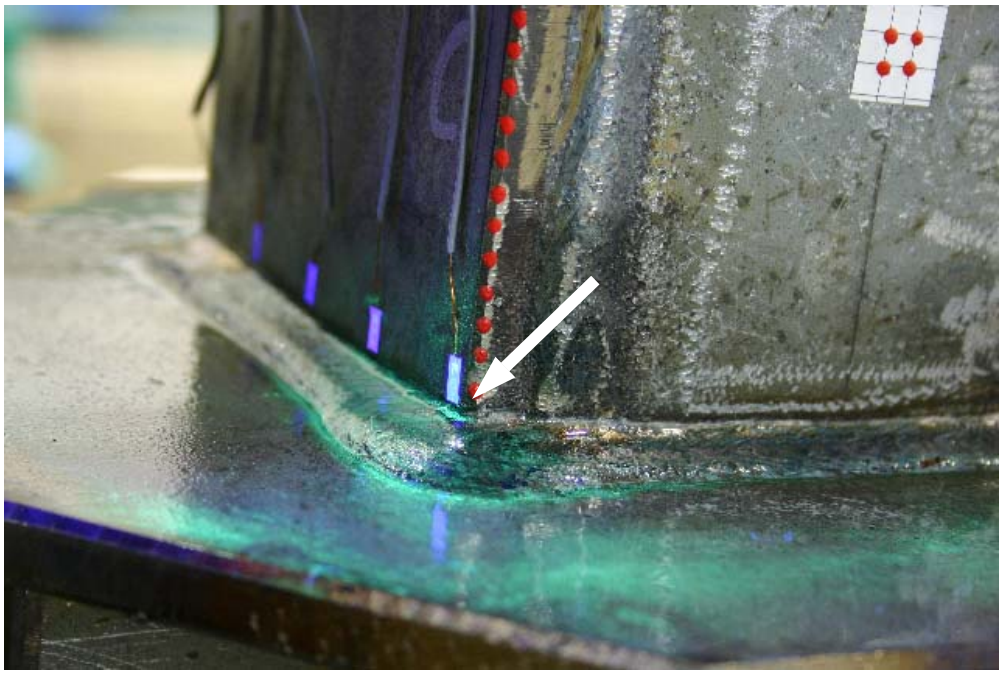

a) Crack initiation at corner (N=4.5)

Fig. 5.9 Crack observation of pier (U6-C6)

b) Oblique crack at flange (N=18)

c) Crack through flange (N=18.5)

Fig. 5.9 Crack observation of pier (U6-C6)

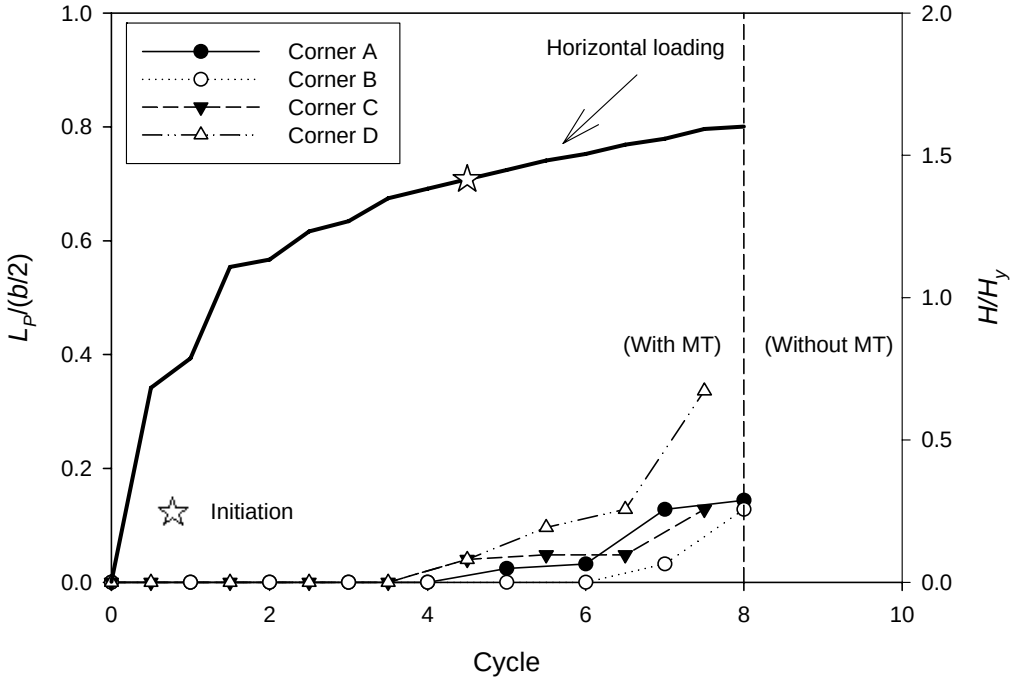

a) Crack propagation of U6-I

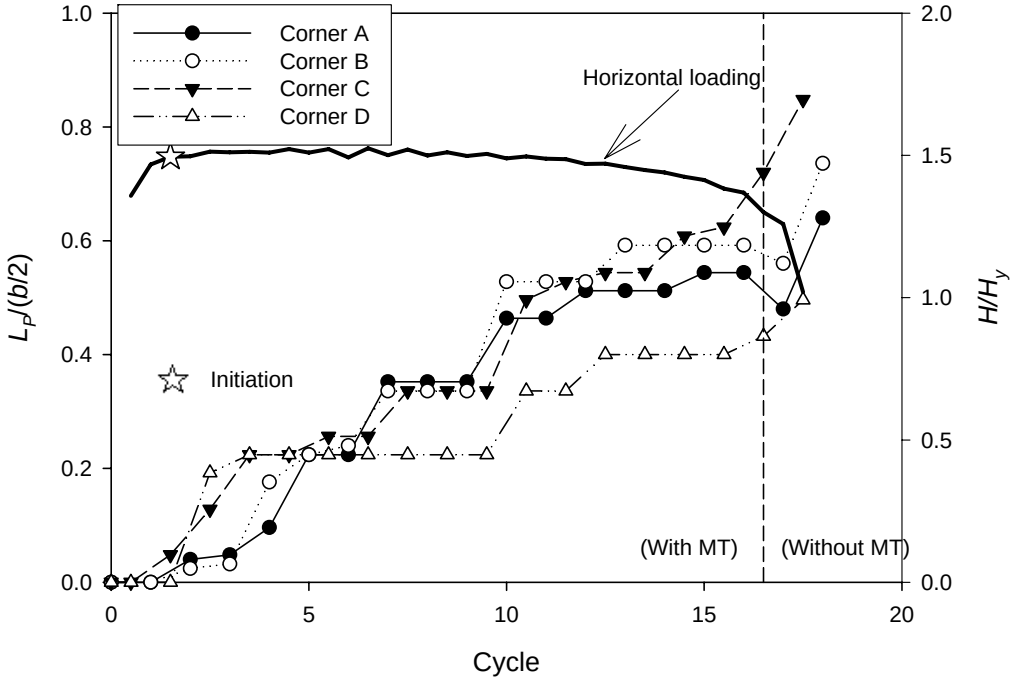

b) Crack propagation of U6-C6

Fig. 5.10 Crack length of flange near corner

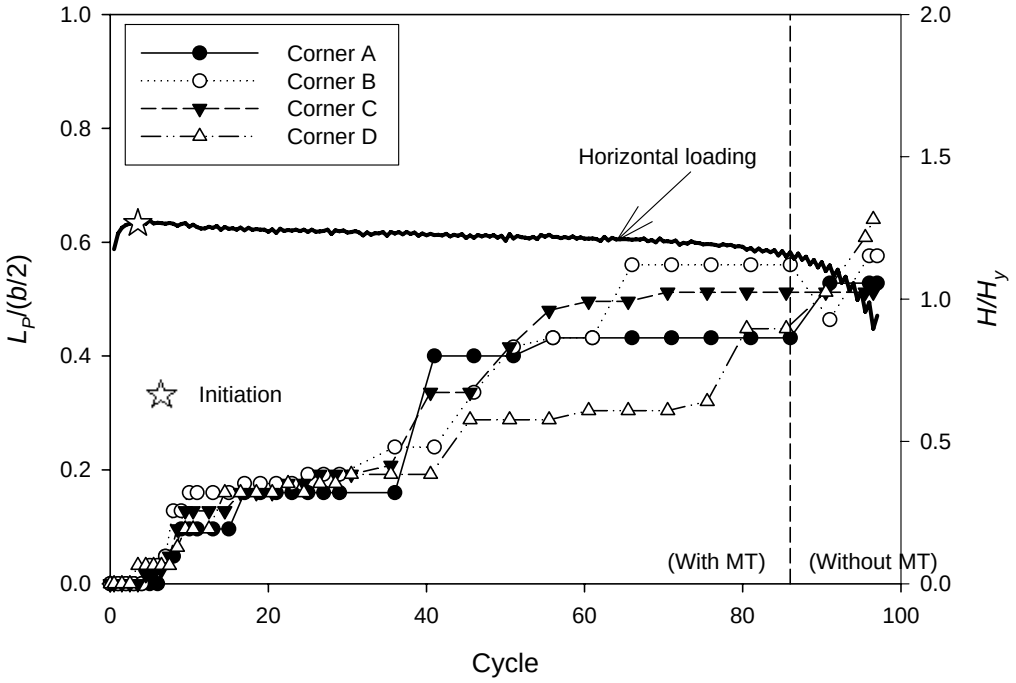

c) Crack propagation of U6-C3

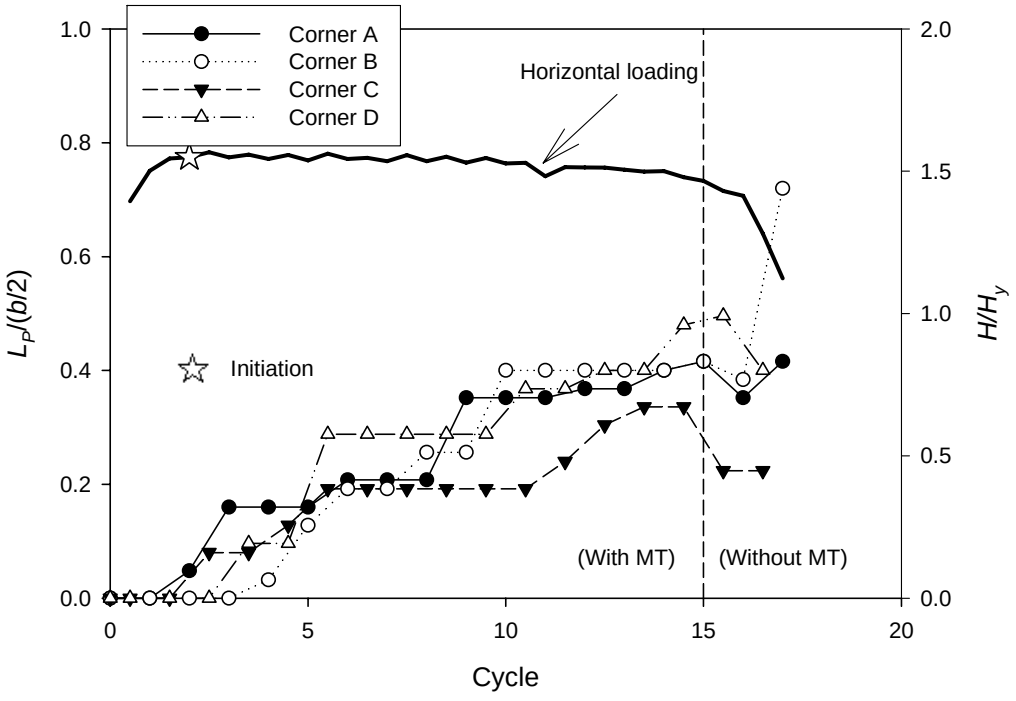

d) Crack propagation of U5-C6

Fig. 5.10 Crack length of flange near corner

5.4 Extremely low cycle fatigue assessment of steel pier

5.4.1 Analytical model

To apply the proposed approach presented in Chapter 4, beam element model of steel pier was created, as shown in **Fig. 5.11**. It was realized by two-node 3D type beam element incorporated in MSC.Marc. For box section, 28 integration points are specified. In the figure, l_e denotes the effective failure length of steel pier, which is the smaller value of 0.7b and diaphragm space (Zheng et al. 2000). Here, five elements are assigned along l_e. It was determined after comparing the results of models with 5, 10,15 and 20 partitions along l_e.

A bilinear constitutive model, which had yield stress of 380MPa and young's modulus of 2×10^5MPa, was adopted. Poisson's ratio was 0.3 and strain-hardening ratio, which is the ratio between post-yield tangent and initial elastic tangent, was assumed as 1/100. The kinematic hardening was used with von Mises yield criterion.

5.4.2 Analytical results

After numerical analysis, nominal strain history along effective failure length was acquired and processed into strain range histogram by rainflow counting method. They were converted to local strain range histogram by equation obtained in Chapter 4. Parameters a and b were obtained by interpolation according to **Table 4.2** according to weld toe radius. In this study, the weld toe radius was obtained by statistical analysis of measured results as shown in **Fig. 5.2**. Lower bound of a 95% confidence interval was taken. So the weld toe radius was 0.60mm. Flank angle was set as 45^o since its influence on local strain distribution is negligible (Hanji et al. 2006). Then parameters a and b in equation were obtained by interpolation form **Table 4.2**.

The number of cycles to crack initiation versus equivalent strain amplitude is plotted in **Fig. 5.12**. Extremely low cycle fatigue strength curves obtained in the former researches are also graphed (Tateishi et al. 2004; 2007). Solid line represents fatigue strength of plain material. Dotted line and dashed line are reflections of weld deposit and HAZ respectively. Data points should be compared with the strength curve for weld deposit, because crack initiations were in the weld deposit at weld toe. All data denoted by solid points are slightly above the fatigue strength curve for weld deposit. This maybe partly owe to inconsistency between the crack initiation lengths, which were 2.0~3.0mm in the tests, while the strength curves were based on the 0.5mm crack initiation length. Except this discrepancy, the proposed approach can predict the crack initiation life in extremely low cycle fatigue region with enough accuracy regardless of loading patterns and specimen geometries.

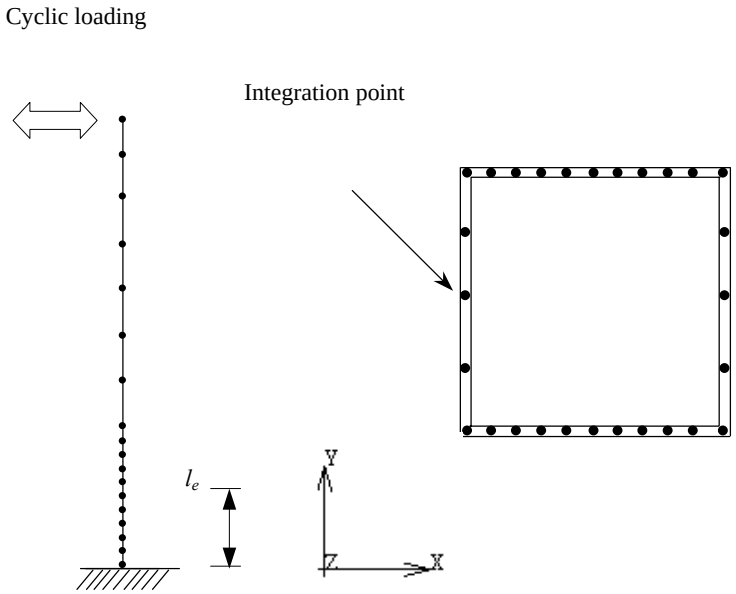

Fig. 5.11 Illustrations of FE model

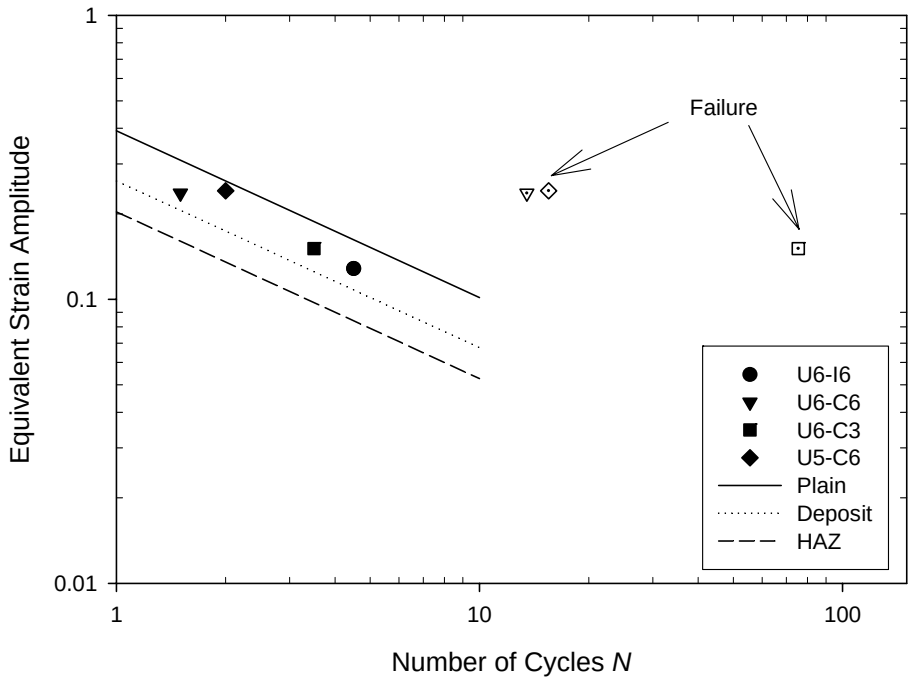

Fig. 5.12 Local strain amplitude versus cycles to crack initiation

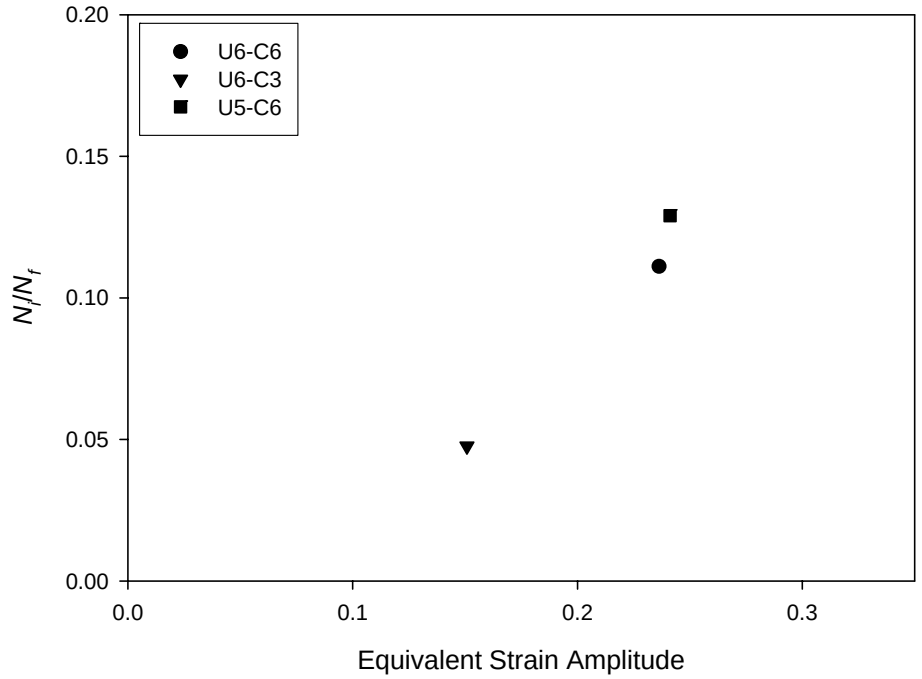

Fig. 5.13 Ratio between crack initiation and failure life

Failure lives, which are the number of cycles when the loading capacity decreased to 95% of the maximum load, were also plotted and pointed out with arrows. They were longer than initiation lives. Ratios between crack initiation and failure life were plotted in **Fig. 5.13**. The ratios are approximately around 0.10 for large strain amplitude. The results indicate the crack propagation stage occupied the most of life of steel pier. In other words, it may be too conservative to neglect the crack propagation life in fatigue design, because much longer life after the crack initiation can be expected. Although crack propagation life in ELCF region should be investigated in future researches in order to establish more rational designing method, the proposed method is well applicable to assess the initiation life of low cycle fatigue.

5.5 Summary and conclusions

This chapter describes an experimental investigation on extremely low cycle fatigue tests on thick-walled steel piers with box section. In particular, this experimental study focused on crack initiation and propagation at weld toe. Test results are used to validate the strain approach proposed in previous research. And the analysis results indicated the validity of proposed approach.

The following main conclusions can be stated as follows:

1) Extremely low cycle fatigue crack initiated from weld toe at corners of thick-walled steel pier. Number of cycles to crack initiation is few comparing to propagation life.

2) The loading capacity didn’t deteriorate until crack length formed significantly. That means fracture failure life is much longer than crack initiation life.

3) Proposed simple strain approach can be used to determine the number of cycles to extremely low cycle fatigue crack initiation.

However, the failure life is still need supplementary tests owing to the complexity of crack propagation.

Chapter 6

SEISMIC INDUCED EXTREMELY LOW CYCLE FATIGUE FOR STEEL PIER

6.1 General remarks

In seismic engineering design practice, the performance of a structure during earthquake excitation is primarily concerned with the largest-excursion failure mechanism, such as ductility ratio and maximum strain. This criterion has been incorporated into existing codes and risk assessments (JRA 2002; Usami 2006), not taking into account the cyclic effect of the earthquake loads. In recent years, researchers and engineers have been paying more attention to damage accumulation of low cycle fatigue. Researches by Cosenza et al. (1993) have indicated that the use of cumulative fatigue as an index for measuring seismic performance of steel structures is more appropriate than the single-excursion ductility factor.

In the previous chapters, a simple strain based approach has been proposed, which presents a realistic means of seismic risk evaluation in prevent of low cycle fatigue and will provide a basis for establishing safer and more reliable steel piers.

In this investigation, nonlinear dynamic analysis has been used to study the local behavior of steel piers under strong ground motions recorded at different sites from real earthquake. The purpose of the FE analyses was to assess the low cycle fatigue life of steel pier by identifying the local strain at weld toe. Local strain is employed to calculate cumulative damage index with material strength curves. Then damage index is plotted with maximum nominal strain and ductility ratio. Subsequently, threshold values of some parameters that are convenient to use in engineering design were obtained.

6.2 Extremely low cycle fatigue assessment methodology

In this section, a brief review of extremely low cycle fatigue assessment methodology is presented before carrying out dynamic analysis.

Extremely low cycle fatigue strength curves were obtained by newly developed image-based testing system (Tateishi 2004; 2007). The results were supplied in Chapter 3.

Crack usually initiates from weld toe in welded joints. In this study, the strain at weld toe, i.e. cracking point, is called local strain. One possible way to assess the extremely low cycle

fatigue strength of welded joint can be proposed based on the local strain, so called local strain approach. Namely, after quantifying the local strain at weld toe, the fatigue life can be predicted by referring to the strength curves. We have already applied this concept to T-shaped weld joint and obtained a successful result (Hanji et al. 2006). In this trial, local strain at weld toe was obtained by finite element analysis with fine mesh.

It's not practicable, however, to use very fine mesh in engineering practice. Therefore, we tried to correlate the local strain range at weld toe to the nominal strain range that can be obtained by averaging strain along effective failure length by beam element model. After extensive finite element analysis carried out on thick-walled steel piers, we finally established the correlation between the local strain range and the nominal strain range in Chapter 4. The results are summarized in **Table 4.2**.

Based on these results, we proposed a simple fatigue assessment method in extremely low cycle fatigue region. **Fig. 6.1** illustrates the conceptual overview of extremely low cycle fatigue assessment for thick-walled steel pier. The nominal strain history is obtained by beam analysis and processed to nominal strain range histogram by rainflow counting method. Nominal strain range histogram can be converted to local strain range histogram by **Table 4.2**. To evaluate the cumulative damage, a linear cumulative damage rule is employed.

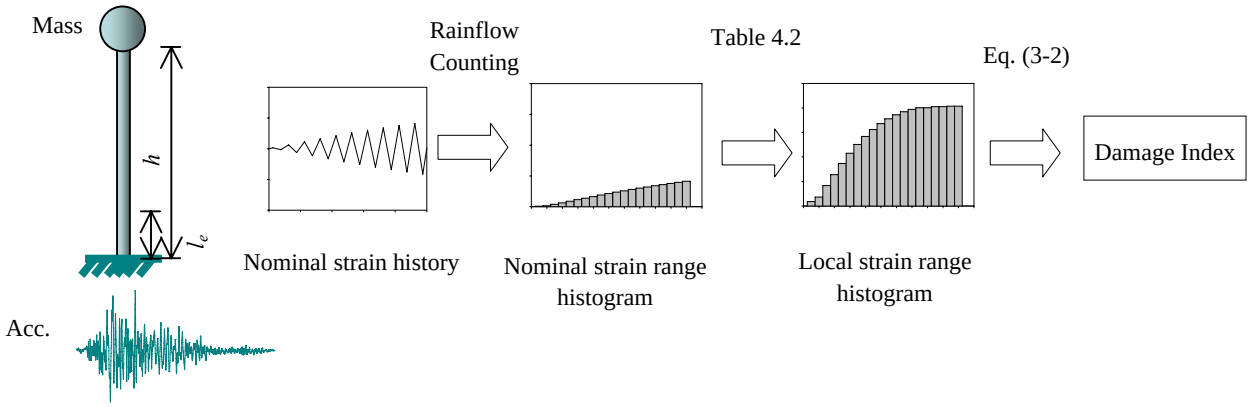

Fig. 6.1 Extremely low cycle fatigue assessment for steel pier—conceptual overview

6.3 Dynamic analysis

Dynamic nonlinear time-history analyses are performed using the general-purpose finite element program MSC. Marc.

6.3.1 Ground motion descriptions

A total of nine modified earthquake acceleration time histories recorded in the Great Hanshin-Awaji Earthquake, which are Level-II design accelerograms representing major earthquake excitations recommended by Japanese code (JRA 2002), are used in this study. The earthquake ground motions are divided into three groups according to the local site conditions at the recording stations. They consist of three records of ground class I (rock ground): JMA-NS-M, JMA-EW-M and INA-NS-M; three of ground class II (stiff soil ground): JRT-NS-M, JRT-EW-M and FUKIAI-M; and three of ground class III (soft soil ground): HKB-NS-M, PIS-NS-M and PIS-EW-M. A complete list of all ground motions including peak ground accelerations (PGA) and site class at the recording station is reported in **Table 6.1**. For the selected records, the peak ground acceleration varied from 557 gal to 812 gal in the horizontal direction.

Table 6.1 Description of input accelerograms

Level II		PGA (gal)	Duration (seconds)
Class I	JMA-NS-M	812	30
	JMA-EW-M	766	
	INA-NS-M	780	
Class II	JRT-NS-M	687	40
	JRT-EW-M	673	
	FUKIAI-M	736	
Class III	HKB-NS-M	591	50
	PIS-NS-M	557	
	PIS-EW-M	619	

6.3.2 Analytical models

Steel pier is fixed at base end with mass lumped at the top, as shown in **Fig. 6.2**. The dimensions of analyzed models are listed in **Table 6.2**, which were originated from Chapter 4.

A bilinear constitutive model with 400MPa yield stress and 2×10^5MPa Young's modulus was used with a density of 7.86×10^3kg/m^3. Poisson's ratio was 0.3 and strain-hardening ratio, which is the ratio between post-yield tangent and initial elastic tangent, was assumed as 1/100. The kinematic hardening was used with von Mises yield criterion. By default, the gravity acceleration, g, is set to 9.8m/s^2.

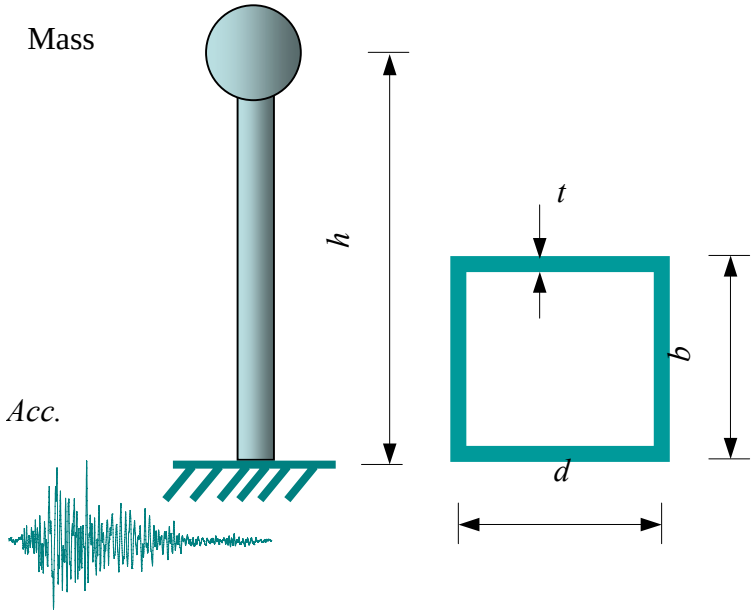

Fig. 6.2 Steel pier model

Table 6.2 Parameters of pier models

No.	R_f	$\bar{\lambda}$	h *	b*	D*	t*	P/P_y
U3	0.2118	0.3068	400	108	88	12	0.1406
U5	0.2451	0.4306	775	125	125	12	0.1103
U6	0.2451	0.3056	550	125	125	12	0.1429
U9	0.3268	0.3062	550	125	125	9	0.1470

*Unit: mm

The beam element model was created and analyzed. It was fulfilled by two-node 3D type beam element incorporated in MSC.Marc. For box section, 28 integration points are specified. Self-weight and P-δ effect was considered during analysis. The seismic analysis is performed supposing the acceleration direction parallel to the axis for simplicity. For all the dynamic analyses in this study, 1% mass damping ratio was assumed and Newmark β method incorporated in Marc was resorted to for solution.

6.3.3 Analysis results and damage evaluation

Fig. 6.3 shows one example of nominal strain history, which is obtained by averaging strain along effective failure length of pier U5 excited by JMA-EW-M accelerogram. The maximum absolute strain occurred around on 9 second and the absolute value was smaller than 0.04. Since oscillation of strain was trivial after 20 seconds, only initial 20 seconds strain history was investigated and the same hereafter.

The rain flow counting method was implemented to convert the strain history to a series of strain ranges. Then they were transformed to local strain range according to **Table 4.2**. Referring to the measurement of weld toe radius (Tagaki et al.1982; Radaj 1996), 0.2, 0.5, 1 and 2mm weld toe radii were assumed during analysis. During extremely low cycle fatigue assessment, only the large strain range is of interest. In other words, strain range of local strain will be neglected if it is less than two times of yield strain. Then Miner's rule was adopted to compute cumulative damage with the strain life curve.

Since crack initiated from weld deposit (Hanji et al. 2006), parameters of deposited metal in **Table 2.2** was selected to calculate cycles under certain amplitude by relationship shown in **Table 4.2**. After that damage index D can be obtained by Miner's rule. A program was coded to calculate the damage index and find failure points with respect to radius.

Damage index D, corresponding time and strain are shown from **Table 6.3** to **Table 6.6** when weld toe radius is 1mm. In the tables, the maximum nominal strain and displacement are also provided as references. Time underlined denotes the moment when damage index attained 1.0 within 20 seconds, and steel pier is assumed failed due to low cycle fatigue. Otherwise the time is 20 seconds and the cumulative fatigue damage didn't reach 1.0. Same procedure was applied for other radiuses. The circles in **Fig. 6.3** show the locations, where D is firstly large than 1.0 at peak or trough with different radiuses.

From the nine analyses shown in the **Table 6.3**, records of ground class I resulted in failure. Strains, which are corresponding to damage indexes surpassing 1.0, varied from the maximum value owing to cumulative effect. Results similar to those of pier U3 are observed for pier U6 and U9, which are shown in **Table 6.5** and **Table 6.6**. Pier U5 with a large

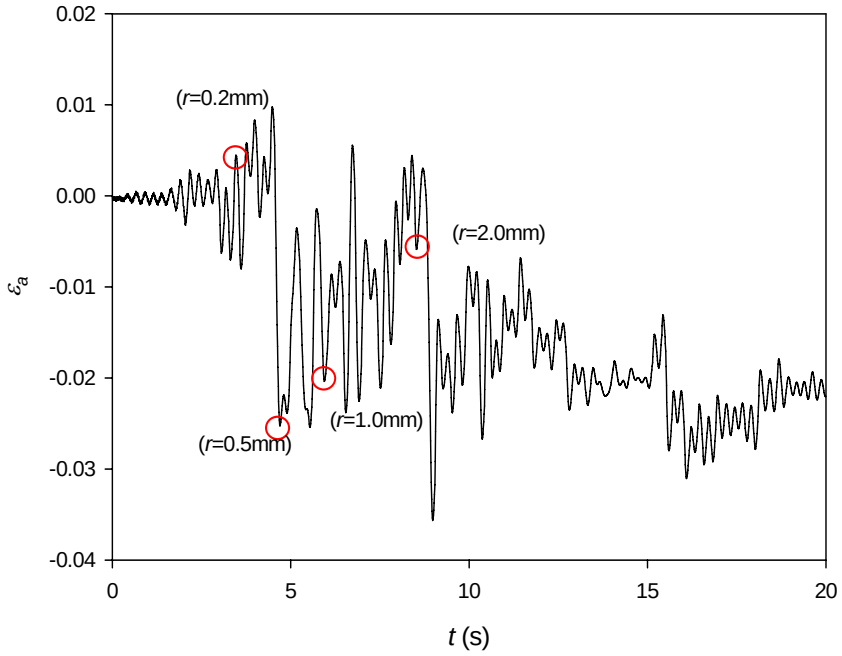

Fig. 6.3 Nominal strain response

Table 6.3 Summary of damage indexes for pier U3 (r=1mm)

Acc.	Time (seconds)	$\frac{\lvert\varepsilon_{D=1}\rvert}{\varepsilon_y}$	$\frac{\lvert\varepsilon_a\rvert_{\max}}{\varepsilon_y}$	$\frac{\lvert\delta\rvert_{\max}}{\delta_y}$	D
JMA-NS-M	10.13	5.85	16.65	9.80	1.0116
JMA-EW-M	9.89	6.50	8.19	4.49	1.0180
INA-NS-M	14.84	3.95	11.03	5.92	1.0049
JRT-NS-M	20	NA	10.33	6.18	0.5689
JRT-EW-M	20	NA	9.65	5.15	0.8033
FUKIAI-M	20	NA	16.40	10.02	0.7036
HKB-NS-M	20	NA	6.15	3.95	0.2209
PIS-NS-M	20	NA	5.37	3.55	0.6504
PIS-EW-M	20	NA	7.71	4.79	0.4106

Table 6.4 Summary of damage indexes for pier U5 (r=1mm)

Acc.	Time (seconds)	$\frac{\lvert\varepsilon_{D=1}\rvert}{\varepsilon_y}$	$\frac{\lvert\varepsilon_a\rvert_{\max}}{\varepsilon_y}$	$\frac{\lvert\delta\rvert_{\max}}{\delta_y}$	D
JMA-NS-M	8.22	21.70	25.80	12.02	1.0136
JMA-EW-M	5.94	10.20	17.82	7.31	1.0087
INA-NS-M	9.35	5.50	20.65	9.12	1.0697
JRT-NS-M	5.71	22.60	22.59	10.04	1.0191
JRT-EW-M	9.78	1.05	15.11	6.50	1.0026
FUKIAI-M	9.89	26.60	35.08	18.51	1.0092
HKB-NS-M	20	NA	13.38	5.34	0.9852
PIS-NS-M	20	NA	15.83	6.54	0.7564
PIS-EW-M	13.87	6.20	16.95	7.11	1.0079

Table 6.5 Summary of damage indexes for pier U6 (r=1mm)

Acc.	Time (seconds)	$\frac{\lvert\varepsilon_{D=1}\rvert}{\varepsilon_y}$	$\frac{\lvert\varepsilon_a\rvert_{\max}}{\varepsilon_y}$	$\frac{\lvert\delta\rvert_{\max}}{\delta_y}$	D
JMA-NS-M	9.17	10.75	20.28	9.92	1.0011
JMA-EW-M	9.93	9.90	12.17	5.73	1.0216
INA-NS-M	10.85	2.40	11.11	5.03	1.0042
JRT-NS-M	20	NA	8.81	4.45	0.8552
JRT-EW-M	20	NA	11.90	5.81	0.9785
FUKIAI-M	10.37	19.95	29.58	16.76	1.0025
HKB-NS-M	20	NA	8.26	4.71	0.4369
PIS-NS-M	20	NA	6.13	3.11	0.5514
PIS-EW-M	20	NA	12.97	6.98	0.6466

Table 6.6 Summary of damage indexes for pier U9 (r=1mm)

Acc.	Time (seconds)	$\frac{\lvert\varepsilon_{D=1}\rvert}{\varepsilon_y}$	$\frac{\lvert\varepsilon_a\rvert_{\max}}{\varepsilon_y}$	$\frac{\lvert\delta\rvert_{\max}}{\delta_y}$	D
JMA-NS-M	9.04	18.25	19.34	9.02	1.0038
JMA-EW-M	9.60	10.10	14.19	6.69	1.0156
INA-NS-M	10.63	8.85	13.36	6.21	1.0536
JRT-NS-M	20	NA	11.28	5.08	0.8954
JRT-EW-M	20	NA	12.90	5.81	0.7800
FUKIAI-M	9.99	25.70	33.15	18.86	1.0254
HKB-NS-M	20	NA	10.69	5.24	0.6426
PIS-NS-M	20	NA	7.28	3.87	0.6948
PIS-EW-M	20	NA	14.86	7.73	0.7169

slenderness ratio failed most of the accelerograms. It seems it is easier to fail than pier U6 with a small slenderness ratio. However it cannot be generalized since the behavior depends on the accelerograms being used, although they are from the same Hanshin earthquake.

When it comes to maximum displacement listed in the fifth column, it is observed that pier excited by FUKIAI-M accelerogram of ground class II gives the largest value. The observation made for pier U3 is also valid for other piers. This maybe owes to characteristic of waveform.

6.3.4 Discussions

From an engineering point of view, it is not practicable to apply the cumulative damage analysis presented in the above. So endeavor was exerted to find some parameters that can define the threshold of low cycle fatigue, it should be convenient to use. In performance-based design of thin walled steel pier (Usami 2006), displacement-based index and strain-based index are employed. Here we also considered them as main parameters with cumulative damage index. Then maximum nominal strain normalized by yield strain versus damage index

was plotted in **Fig. 6.4**. Judging from the graphs, it is evident that steel piers are prone to fail for small weld toe radius. All damage indexes are larger than 1.0 when weld toe radius is 0.2mm. Whereas, only four damage indexes exceed 1.0 when weld toe radius is 2.0mm.

Further investigation on **Fig. 6.4 c)**, which is the results of 1.0mm weld toe radius, demonstrated that normalized maximum nominal strain vary from 8.8 to 35.1. For the damage indexes less than 1.0, normalized maximum nominal strain vary in the range with an upper bound of 16.40. Various results exist for different excitations. When it comes to ground classifications, following observations can be obtained. Results excited by accelerograms of class I, all damage indexes exceed 1.0 and corresponding normalized strain locate in a small range; excited by class II accelerograms, normalized strains scattered; excited by class III, normalized strains locate in left side and most of damage indexes are less than 1.0. For safety consideration, it is probably applicable to take the lower bound of normalized strain of failure as the threshold of low cycle fatigue.

Ductility is another important indicator to assess seismic resistance. And it is defined as $\mu=\delta/\delta_y$, where δ is the current displacement and δ_y is the yield displacement. We also plotted the damage indexes with ductility ratio. Similar phenomena were observed, as graphed in **Fig. 6. 5**.

Table 6.7 provides the lower bound estimates of threshold values of the normalized maximum nominal strain and displacement when damage indexes are larger than one. These values provide conservative estimates of low cycle fatigue of crack initiation life. Another factor contributing to the conservative estimation is owing to upper bound of relationships adopted during conversion from average strain range to local strain range.

But according to the observations from Chapter 5, number of cycles to fracture failure of steel pier is much longer than the crack initiation predicted in this chapter. This problem still needs further research.

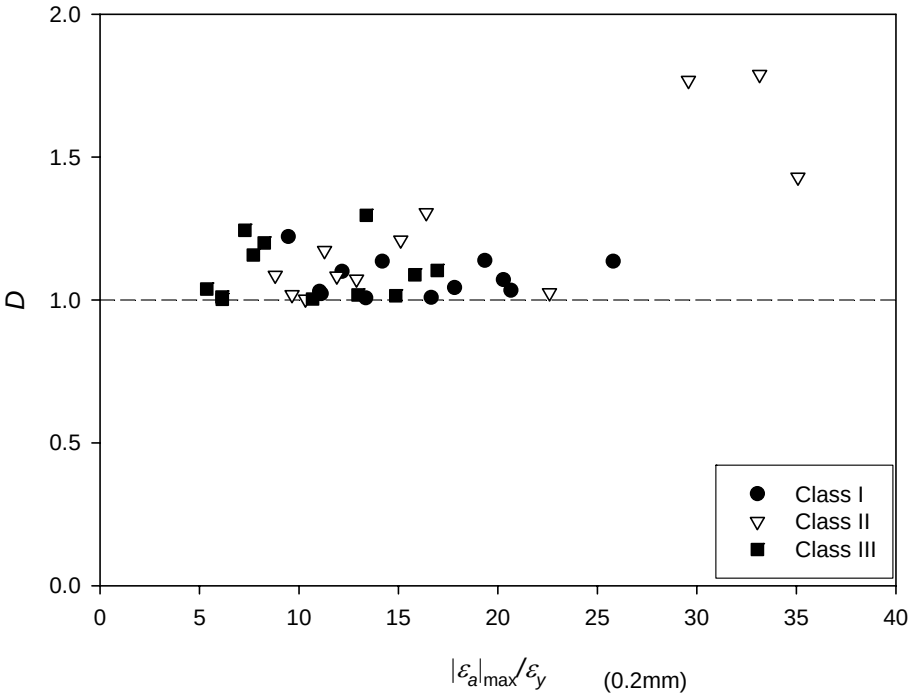

a) r=0.2mm

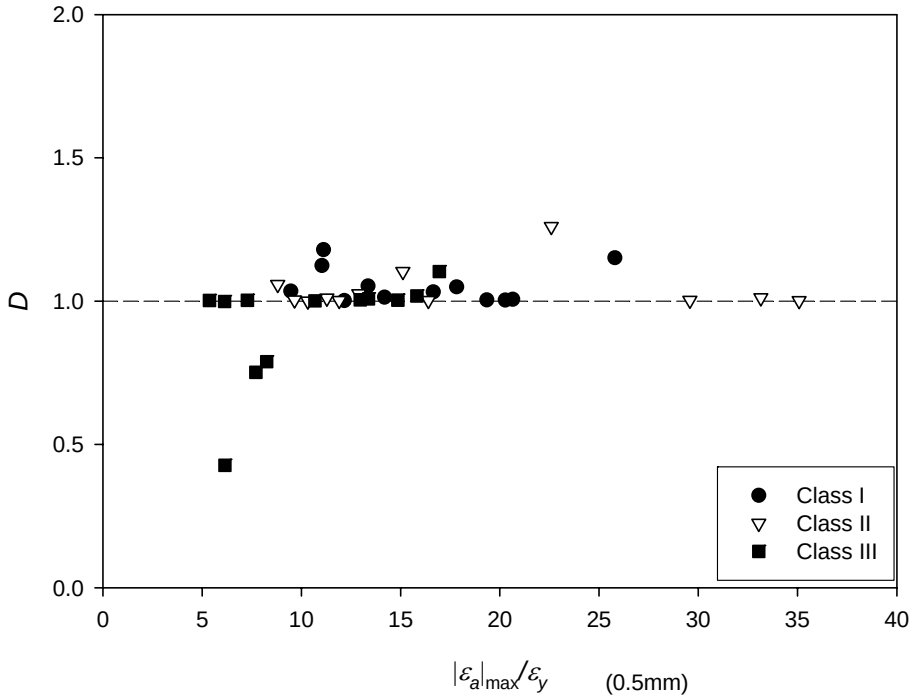

b) r=0.5mm

Fig. 6.4 Damage indexes versus average strain ratio

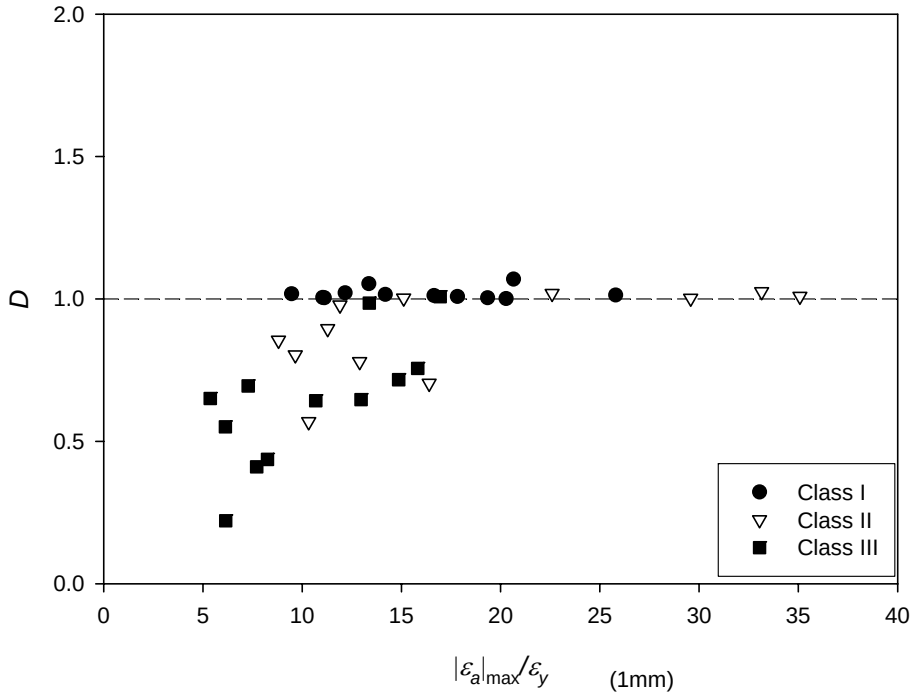

c) r=1.0mm

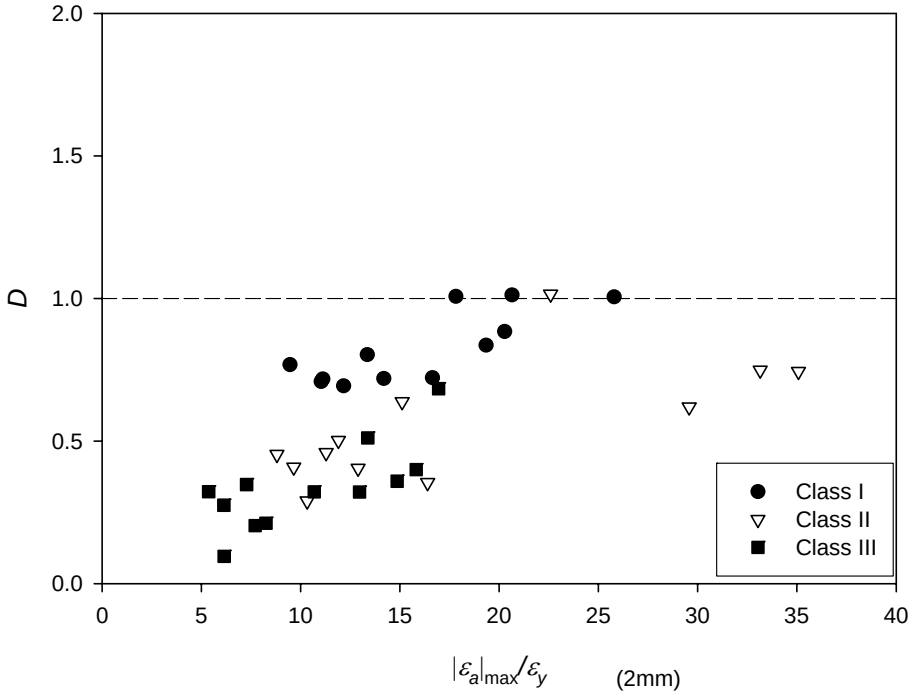

d) r=2.0mm

Fig. 6.4 Damage indexes versus average strain ratio

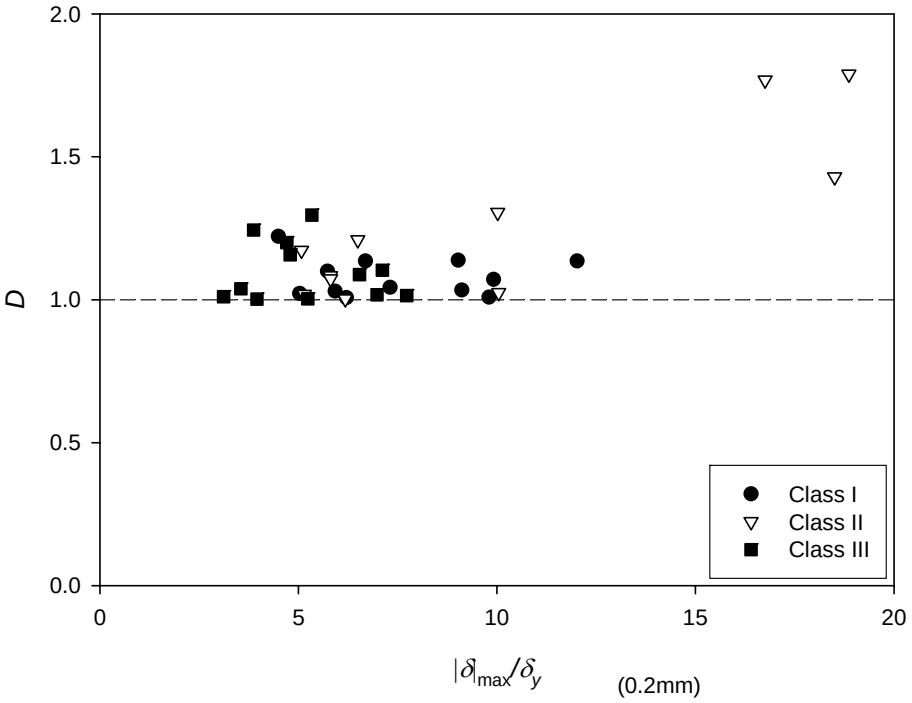

a) r=0.2mm

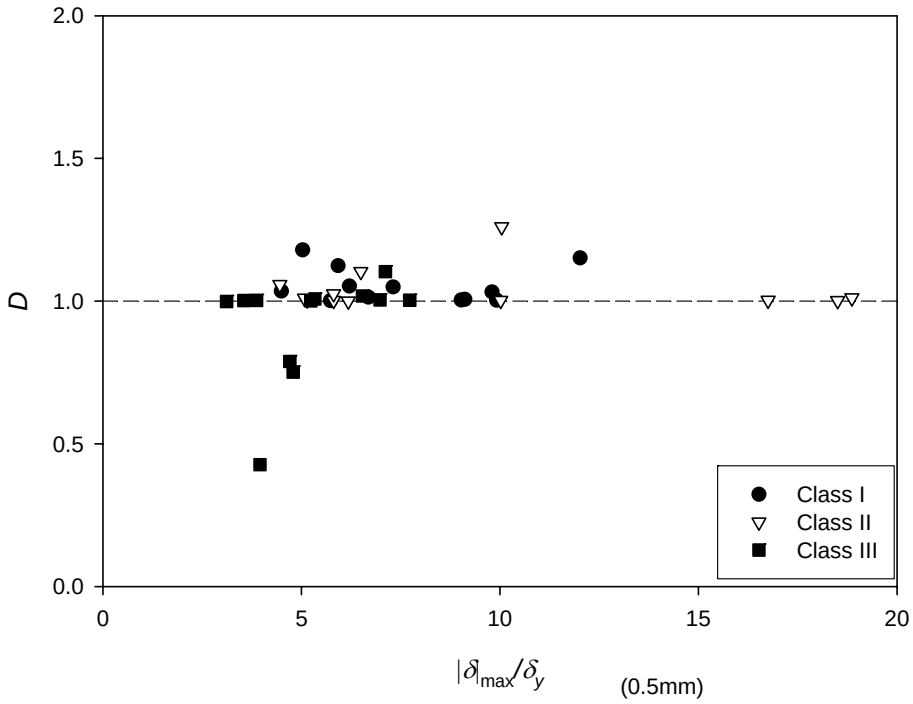

b) r=0.5mm

Fig. 6.5 Damage indexes versus displacement ductility ratio

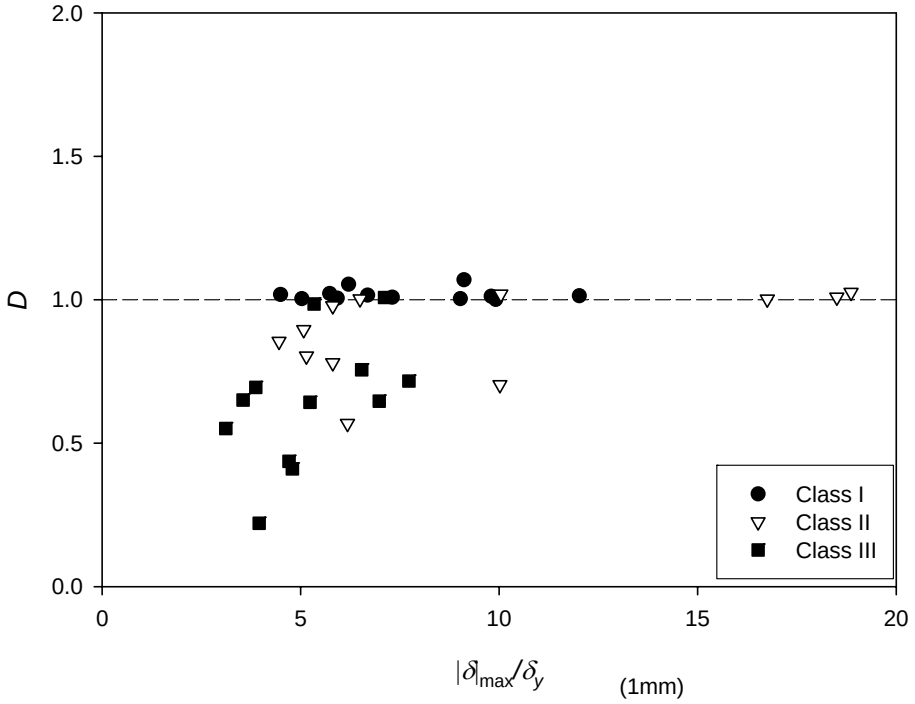

c) r=1.0mm

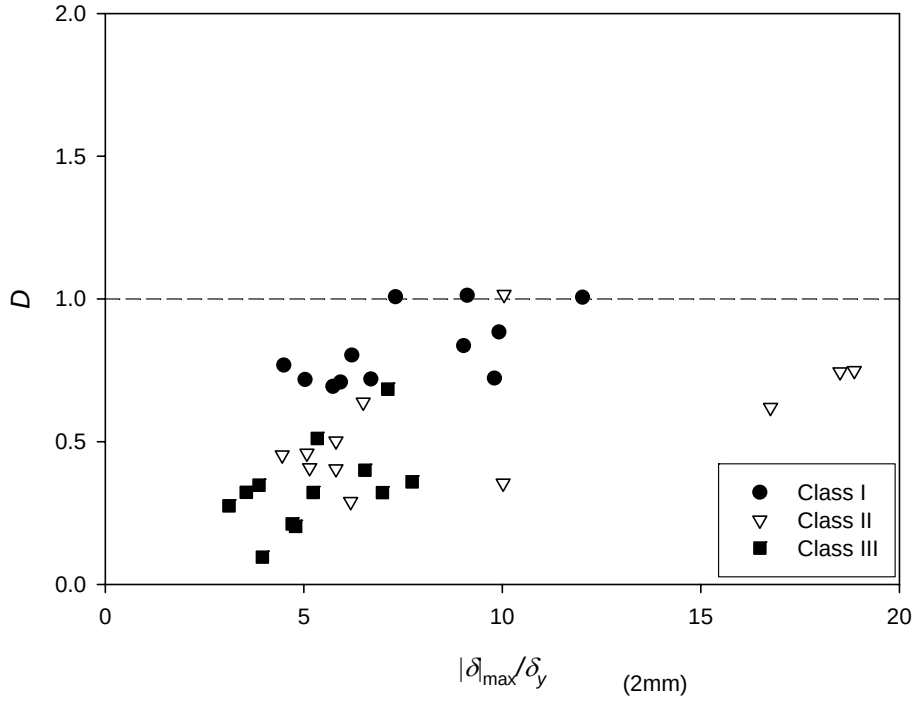

d) r=2.0mm

Fig. 6.5 Damage indexes versus displacement ductility ratio

Table 6.7 Estimated threshold values of maximum nominal strain and ductility ratio

Weld toe radius r (mm)	$\frac{\lvert\varepsilon_a\rvert_{\max}}{\varepsilon_y}$	$\frac{\lvert\delta\rvert_{\max}}{\delta_y}$
0.2	NA	NA
0.5	5.4	3.6
1.0	9.5	4.5
2.0	17.8	7.3

* $0.2 \le R_f \le 0.35$, $0.3 \le \bar{\lambda} \le 0.45$, $0 \le P/P_y \le 0.15$

6.4 Summary and conclusions

This chapter is concerned with the development of a simple method to guide the design practice. It presented an analytical study of evaluation of seismic behavior of thick-walled steel piers during future earthquakes in prevent of extremely low cycle fatigue failure. Piers were subjected to strong ground motions and endeavor has focused on local strain where cracks emanate from. A linear damage accumulation law and the rainflow counting method were applied. Then extremely low cycle fatigue failure was correlated to the normalized maximum nominal strain and displacement. It is believed that this study provides further information towards the evaluation of low cycle fatigue failure.

Following conclusions can be drawn:

1) Inelastic dynamic analyses with the Great Hanshin accelerograms showed that steel piers might fail due to extremely low cycle fatigue. Through several case analyses, cumulative damage indexes were calculated by local strain based on the relationship between nominal strain and local strain at weld toe.

2) Piers with smaller weld toe radius are prone to fail. For straightforward evaluation, the normalized maximum nominal strain and displacement were graphed versus damage indexes with respect to weld toe radius.

3) Different classes of accelerograms yielded out various results. For safety consideration, the lower bound of the normalized maximum nominal strain and displacement probably can be assumed as the threshold values to prevent crack initiation due to extremely low cycle fatigue.

This chapter presents a comprehensive quantification of the low cycle fatigue evaluation in earthquakes. However, the results are only applicable to the crack initiation life. For fracture failure life relating to crack propagation, further experimental and numerical researches are necessary.

Chapter 7

SUMMARY AND CONCLUSIONS

Extremely low cycle fatigue is assumed as one possible failure mode after strong ground motion for steel piers. Unfortunately, specification guidance on this related case hasn't been quantified. This dissertation research was to examine this problem through strain approach, efforts were exerted to found possible way. The following is a summary of the research findings.

7.1 Conclusions

In Chapter 2, a new local strain based approach has been developed as a solution to eliminate cumbersome modeling weld toe profile. Several two-dimensional FE models of T-shaped joints with various weld toe radius were built and analyzed when they were subjected to random loading blocks. Parameters such as main plate thickness, weld leg length, constitutive model, yield stress and weld toe radius were discussed in this paper. Besides these, bending and axial loading pattern's effects were also studied. It turns out that weld toe radius is the most influential parameter while others are trivial. Then an approach based on strain range relationship was established for low cycle fatigue assessment from the engineering viewpoint. The strain range relationships between coarse model and fine model were obtained by regression.

In Chapter 3, random amplitude loading test on T-shaped weld joint was conducted. The test was conducted to verify the simple local strain approach proposed in the chapter 2. Test results, together with the results of constant amplitude in former research, show that the proposed approach is applicable and easy to use in low cycle fatigue assessment.

In Chapter 4, a strain approach was proposed based on beam model, which relate the nominal strain range to local strain range at weld toe. It was obtained after extensive FE analysis of thick-walled steel piers subjected to incremental cyclic loading. The numerical investigation on both solid-shell element model and beam element model were carried out. Based on the analytical results, the following conclusions are reached.

1) The relationships between strain range ratio and nominal strain range are not influenced by axial loading and width-thickness ratio. Whereas slenderness ratio and weld toe radius are dominant parameters.

2) A simple approach to assess ELCF of steel piers based on beam model analysis was proposed.

The strain based damage assessment method will provide the researchers and structural engineers with valuable tool for the design; retrofit and post-earthquake damage evaluation of steel piers.

In Chapter 5, it describes an experimental investigation on extremely low cycle fatigue tests on thick-walled steel piers with box section. In particular, this experimental study focused on crack initiation and propagation at weld toe. Test results are used to validate the strain approach proposed in previous chapters. And the analysis results indicated the validity of proposed approach. It was demonstrated that

1) Extremely low cycle fatigue crack initiated from weld toe at corners of thick-walled steel pier. Number of cycles to crack initiation is very few comparing to propagation life.

2) The loading capacity didn't deteriorate until crack length formed significantly. That means fracture failure life is much longer than crack initiation life.

3) Proposed simple strain approach can be used to determine the number of cycles to extremely low cycle fatigue crack initiation.

However, the failure life is still need supplementary tests owing to the complexity of crack propagation.

In Chapter 6, it is concerned with the development of a simple method to guide the design practice. It presented an analytical study of evaluation of seismic behavior of thick-walled steel piers during future earthquakes in prevent of extremely low cycle fatigue failure. Piers were subjected to strong ground motions and endeavor has focused on local strain where cracks emanate from. A linear damage accumulation law and the rainflow counting method were applied. Then extremely low cycle fatigue failure was correlated to the normalized maximum average strain and displacement. It is believed that this study provides further information towards the evaluation of low cycle fatigue failure. Following conclusions can be drawn:

1) Inelastic dynamic analyses with the Great Hanshin accelerograms showed that steel piers might fail due to extremely low cycle fatigue. Through several case analyses, cumulative

damage indices were calculated by local strain based on the relationship between nominal strain and local strain.

2) Piers with smaller weld toe radius are prone to fail. For straightforward evaluation, the normalized maximum nominal strain and displacement were graphed versus damage indexes with respect to weld toe radius.

3) Different classes of accelerograms yielded out various results. For safety consideration, the lower bound the normalized maximum nominal strain and displacement probably can be assumed as the threshold values to prevent crack initiation due to extremely low cycle fatigue.

This chapter presents a comprehensive quantification of the low cycle fatigue evaluation in earthquakes. However, the results are only applicable to the crack initiation life. For fracture failure life relating to crack propagation, further experimental and numerical researches are necessary.

7.2 Recommendations for future research

Throughout this study, the following recommendations for further study are suggested as follows:

1) Additional tests need to be conducted to further validate the proposed low cycle fatigue assessment methodology.

2) As discussed in Chapter 5 and 6, supplementary parameters to guidance of design should be found based on the crack propagation life and they should be verified in the future test.

3) This research is focused on the low cycle fatigue induced by seismic action and is not applicable to mixed failure mode of local buckling and low cycle fatigue. However, the potential for the combined failure problems should be investigated.

4) Besides as welded specimen, other welding methods should be designed and tested, especially for treatment of weld toe, such as TIG.

BIBLIOGRAPHY

Albert, W. A. J.: Über treibseile am Harz, *Archive für Mineralogie Geognosie Bergbau und Hüttenkunde*, Vol. 10, pp 215-234, 1838.

Anderson, T.L.: Fracture Mechanics: Fundamentals and applications (Third edition), *CRC Press*, 2005.

Ballio, G. and Castiglioni, C.A.: A Unified approach for the design of steel structures under low and/or high cycle fatigue, *J. Construct. Steel Research*, Vol.34, pp.75-101, 1995.

Ballio G., Calado L., Castiglioni C.A.: Low cycle fatigue behaviour of structural steel members and connections, *Fatigue & Fracture of Engineering Materials & Structures*, Vol.20, No. 8, pp.1129-1146, 1997.

Calado, L. and Azevedo, J.: A Model for predicting the failure of structural steel elements, *Journal of Constructional Steel Research*, Vol.14, pp.41-64, 1989.

Chi, W.M., Kanvinde, A.M. and Deierlein, G.G.: Prediction of ductile fracture in steel connections using SMCS criterion, *Journal of Structural Engineering*, ASCE, Vol.132, No.2, pp.171-181, 2006.

Clough, R. and Penzien, J.: Dynamics of Structures, second edition (revised), *Computer and Structures*, Inc., 2003.

Coffin, L.F.: A study of the effects of cyclic thermal stresses on a ductile metal, *Transactions of the ASME*, Vol.76, pp.931-950, 1954.

Cosenza, E., Manfredi, G. and Ramasco, R.: The Use of Damage Functionals in Earthquake Engineering: A Comparison between Different Methods, *Earthquake Engineering and Structural Dynamics*, Vol. 22, No10, pp. 855-868, 1993.

Dong, P.: A robust structural stress method for fatigue analysis of offshore/marine structures, *Transactions of the ASME*, Vol.127, No.2, pp.68-74, 2005.

Dufailly, J. and Lemaitre, J.: Modeling very low cycle fatigue, *International Journal of Damage Mechanics*, Vol.4, pp.153-170, 1995.

Ferreiraa, J., Castiglionib, C.A., Caladoa, L. and Agatino, M. R.: Low cycle fatigue strength assessment of cruciform welded joints, *Journal of Constructional Steel Research*, Vol.47, pp.223–244, 1998.

Ge, H.B., Gao, S.B., and Usami, T.: Stiffened steel box columns Part 1: Cyclic behaviour, *Earthquake engineering and structural dynamics*, Vol.29, pp.1691-1706, 2000.

Ge, H.B., Kawahito, M. and Ohashi, M.: Fundamental study on ductile crack initiation condition in structural steels considering mirco-void growth, *Journal of Earthquake Engineering*, JSCE, No.28, Paper No.190, 2005. (in Japanese)

Ge, H.B., Ohashi, M. and Tajima, R.: Experimental study on ductile crack initiation and its propagation in steel bridge piers of thick-walled box section, *Journal of Structural Engineering*, JSCE, Vol.53A, pp.493-502, March 2007. (in Japanese)

Ge, H.B. and Usami, T.: Cyclic tests of concrete-filled steel box columns, *Journal of structural engineering*, ASCE, Vol.122, No.10, pp.1169-1177, 1996

Goto, Y., Wang, Q. Y. and Obata, M.: FEM analysis for hysteretic behavior of thin-walled columns, *Journal of structural engineering*, Vol.124, No.11, pp.1290-1301, 1998.

Hanji, T., Tateishi, K., Minami K., and Kitoh, K.: Extremely low cycle fatigue assessment for welded joints based on peak strain approach, *Journal of Structural Mechanics and Earthquake Engineering*, JSCE, Vol.I-74, No.808, pp.137-145, 2006. (in Japanese)

Hobbacher, A.: Recommendations on fatigue of welded joints and components, *International Institute of Welding*, Paris, IIW-XIII-1965 – 03 / XV-1127 – 03, 2003.

Jankovie, M.: The application of some approximate solutions of stress and strain concentration for life estimation in the low cycle fatigue region, T*he Scientific Journal FACTA UNIVERSITATIS*, Series Mechanical Engineering, Vol.1 No. 8, 1205-1032, 2001.

Japan Road Association (JRA): *Specifications for Highway Bridges, Part V. Seismic design*. JRA, Tokyo, Japan, 2002. (in Japanese)

Japan Society of Steel Construction (JSSC): *Fatigue Design Recommendation for Steel Structures*, Dec.1995.

Jonge, J.B.: The Analysis of Load-Time Histories by Means of Counting Methods, *National Aerospace Laboratory (NLR)*, Amsterdam, The Netherlands, 1982.

Kanvinde, A.M. and Deierlein, G.G.: Micromechanical simulation of earthquake-induced fracture in steel structures, *The John A. Blume Earthquake Engineering Center*, Stanford University, Report No. 145, July 2004.

Komotori, J. and Shimizu, M.: Mircostructural effect controlling exhaustion of ductility in extremely low cycle fatigue, *Journal of the Japan Society of Mechanical Engineers*, Vol.57, No.544, pp.2879-2883, 1991. (in Japanese)

Krawinkler, H. and Zohrei, M.: Cumulative damage in steel structures subjected to earthquake ground motions, *Computers & Structures*, Vol.16, No. 1-4, pp.531-541, 1983.

Kuwamura, H.: Transition between fatigue and ductile fracture in steel, *Journal of structural Engineering*, ASCE, Vol.123, No.7, pp.864-870, 1997.

Kuwamura, H. and Takagi, N.: Similitude law of prefracture hysteresis of steel members, *Journal of Structural Engineering*, Vol.130, No.5, pp.752-761, 2004.

Kuwamura, H. and Yamamoto, K.: Ductile crack as trigger of brittle fractures in steel, *Journal of structural Engineering*, ASCE, Vol.123, No.6, pp.729-735, 1997.

Liu, W.C., Liang, Z. and Lee, G.C.: Low-cycle Bending-Fatigue strength of steel bars under random excitation. Part I: Behavior, *Journal of Structural Engineering*, ASCE, Vol.131, No. 6, pp.913-918, 2005.

Liu, W.C., Liang, Z. and Lee, G.C.: Low-cycle Bending-Fatigue strength of steel bars under random excitation. Part II: Design Considerations, *Journal of Structural Engineering*, ASCE, Vol.131, No. 6, pp.919-923, 2005.

Maddox, S. J., Fatigue strength of welded structures, *Abington Publishing*, Cambridge, 1991.

Madi, Y., Matheron, P. Recho, N. and Mongabure, P.: Low cycle fatigue of welded joints: new experimental approach, *Nuclear Engineering and Design*, Vol.228, pp.161-177, 2004.

Mander J.B., Panthaki, F.D. and Kasalanati A.: Low-Cycle fatigue behavior of reinforcing steel, *Journal of Materials in Civil Engineering*, ASCE, Vol. 6, No.4, pp.453-468, 1994.

Manson, S.S.: Behavior of materials under conditions of thermal stress, *NACA technical note*, 2933, 1953.

Marquis, G. and Samuelsson, J.: Modeling and fatigue life assessment of complex structures. *Mat.-wiss. u. Werkstofftech*, Vol.36, No. 11, pp.678-684, 2005.

Masatoshi K.: Extremely low cycle fatigue life prediction based on a new cumulative fatigue damage model, *International Journal of Fatigue*, Vol.24, pp.699-703, 2001.

Matsui, N. and Ge, H.B.: Evaluation of Strain Concentration for Prediction of Ductile Crack Initiation in Steel Bridge Piers, *Proceedings of the Eighth International Summer Symposium*, Nagoya, Japan, pp.31-34, July 29, 2006.

Miner, M.A.: Cumulative damage in fatigue, *Transactions, American Society of Mechanical Engineers*, Vol.67, pp. A159-A164, 1945.

MSC.Marc, Volume A: Theory and User Information, *MSC.Software Corporation*, Santa Ana, CA, 2005.

Nakajima, N. and Yamada, M.: Research on the extremely low cycle fatigue fracture limit of structural steel from the view point of damage energy, *Journal of Structural Construction Engineering*, AIJ, No.534, 2000. (in Japanese)

Nihei, K., Inamura, F. and Koe, S.: Study on unified fatigue strength assessment method for welded structure, *Journal of the Society of Naval Architects of Japan*, Vo.l.179, pp.425-432, 1996. (in Japanese)

Nishimura, T. and Miki, C.: Strain controlled low cycle fatigue behavior of structural steels, *Proceedings of the Japan society of civil engineers*, No.279, pp.29-44, 1978. (in Japanese)

Okashita, K., Ohaminami, R., Michiba, K., Yamamoto, A., Tomimatsu, M., Tanji, Y. and Miki, C., Investigation of the brittle fracture at the corner of P75 rigid-frame pier in Kobe harbor highway during the Hyogoken-nanbu earthquake, *Journal of Structural Mechanics and Earthquake Engineering*, JSCE, Vol.I-43, No.591, pp.243-261, 1998. (in Japanese)

Radaj, D.: Review of fatigue strength assessment of nonwelded and welded structures based on local parameters, *International Journal of Fatigue*, Vol.18, No.3, pp.153-170, 1996.

Radai, D. and Sonsino,C.M: Fatigue Assessment of Welded Joints by Local Approaches, *Abington Publishers*, Cambridge, 1998.

Rudolph, J., Weib, E., and Forster, M.: Modeling of welded joints for design against fatigue, *Engineering with Computers*, Vol.19, pp.142-151, 2003.

Sakano, M., Kishigami, N., ONO, T. and Mikami, I.: Super-low-cycle fatigue behavior of steel pier base joint with triangular ribs, *Journal of Structural Engineering*, JSCE, Vol.44A, pp.1281-1288, 1998. (in Japanese)

Sakano, M., Kishigami, N., ONO, T. and Mikami, I.: Super-low-cycle fatigue behavior of steel rigid frame pier beam-column joint, *Steel Construction Engineering*, JSSC, Vol.4, No.16, pp.17-26, 1997. (in Japanese)

Sakano, M., Mikami, I., Murayama, H. and Misumi, Y.: Super-low-cycle fatigue behavior of steel pier base Joint, *Steel Construction Engineering*, Vol.2, No.8, pp.73-82, 1995. (in Japanese)

Sakano, M., Mikami, I. and Takaba, S.: Low cycle fatigue behavior of steel pier beam-column joint, *Journal of Structural Mechanics and Earthquake Engineering*, JSCE, Vol.I-39, No. 563, pp.49-60, 1997. (in Japanese)

Sakano, M. and Wahab M.A.: Extremely low cycle (ELC) fatigue cracking behaviour in steel bridge rigid frame piers, *Journal of Materials Processing Technology*, Vol.118, pp.36-39, 2001.

Schütz, W.: A History of Fatigue, *Engineering Fracture Mechanics*, Vol.54 No.2, pp.263-300, 1996.

Seto, A., Masuda, T., Machida, S. and Miki, C.: Very low cyclic fatigue properties of butt welded joints containing weld defects, *Quarterly Journal of the Japan Welding Society*, Vol. 17, No.1, pp.130-138, 1999. (in Japanese)

Shimada, K., Komotori, J. and Shimizu, M.: The applicability of the Manson-Coffin law and Miner's law to extremely low cycle fatigue, *Journal of the Japan Society of Mechanical Engineers*, Vol.53, No.491, pp.1178-1185, 1987.

Tagaki, N., Kondo, A., Yamada, K. and Kikuchi, Y.: Effect of weld toe profiles on fatigue strength of fillet welded specimens, *Proceedings of the Japan Society of Civil Engineers*, No.324, pp151-159, 1982. (in Japanese)

Tateishi, K. and Hanji, T.: Low cycle fatigue strength of butt welded steel joint by means of new testing system with image technique, *International Journal of Fatigue*, Vol.26, No.12, pp.1349-1356, 2004.

Tateishi, K., Hanji, T., Kitoh, K. and Minami, K.: A prediction model for extremely low cycle fatigue strength of welded materials, *Journal of Structural Engineering*, JSCE, Vol.51A, pp.1275-1282, 2005. (in Japanese)

Tateishi, K., Hanji, T. and Minami, K.: A prediction model for extremely low cycle fatigue strength of structural steel, *International Journal of Fatigue*, Vol.29, pp.887-896, 2007.

Tominaga T. and Yasunami H.: An experimental study on ductility of steel bridge piers with thick walled cross section and small number of stiffeners, *Journal of Structural Engineering*, Vol.40A, pp.189-200, 1994. (in Japanese)

Usami, T., Gao, S.B. and Ge, H. B.: Stiffened steel box columns Part 2: Ductility evaluation, *Earthquake engineering and structural dynamics*, Vol.29, pp.1707-1722, 2000.

Usami, T.: Guidelines for stability design of steel structures (2nd edition), *Japan Society of Civil Engineers*, Sep. 2005. (in Japanese)

Usami, T.: Guidelines for seismic and damage control design of steel bridges, *Japan Society of Steel Construction*, Sep. 2006. (in Japanese)

Xiao, Z.G. and Yamada, K.: A method of determining geometric stress for fatigue strength evaluation of steel welded joints, *International Journal of Fatigue*, Vol.26, pp.1277-1293, 2004.

Yamashita, Y., Torigoe, M. and Ibata T.: Simplified crack growth analysis method at shell-annular welded joints in cylindrical storage tank under cyclic large deformation, *Journal of the Society of Naval Architects of Japan*, Vo.l.194, pp.201-209, 2003. (in Japanese)

Zheng, Y., Usami, T., and Ge, H. B.: Ductility evaluation procedure for thin-walled steel structures, *Journal of Structural Engineering*, ASCE, Vol.126, No.11, pp.1312–1319, 2000.

APPENDIX

Following figures are numerical results of thick-walled steel piers of Chapter 4.

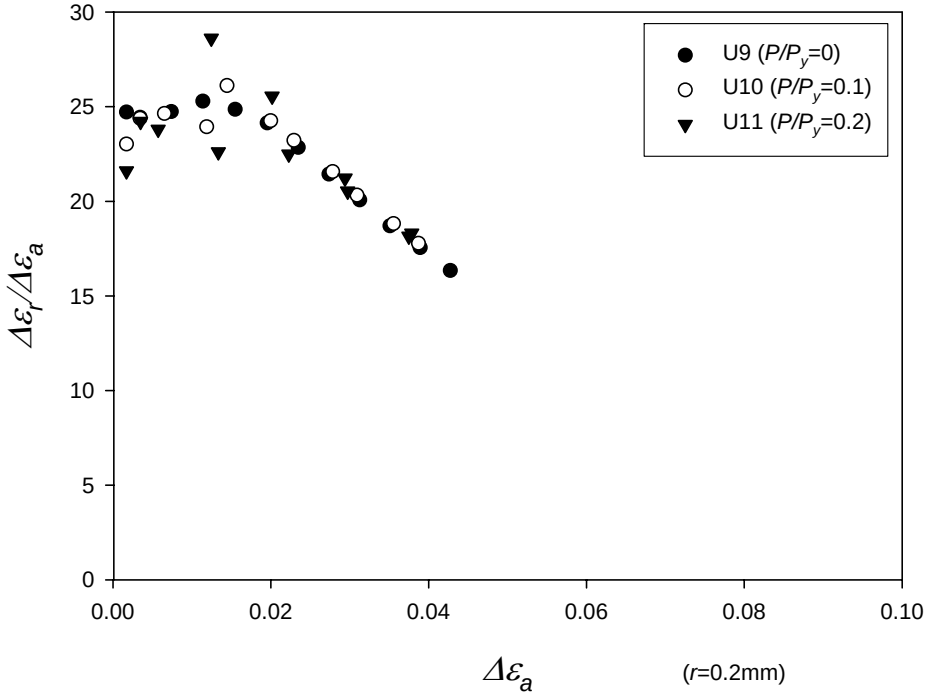

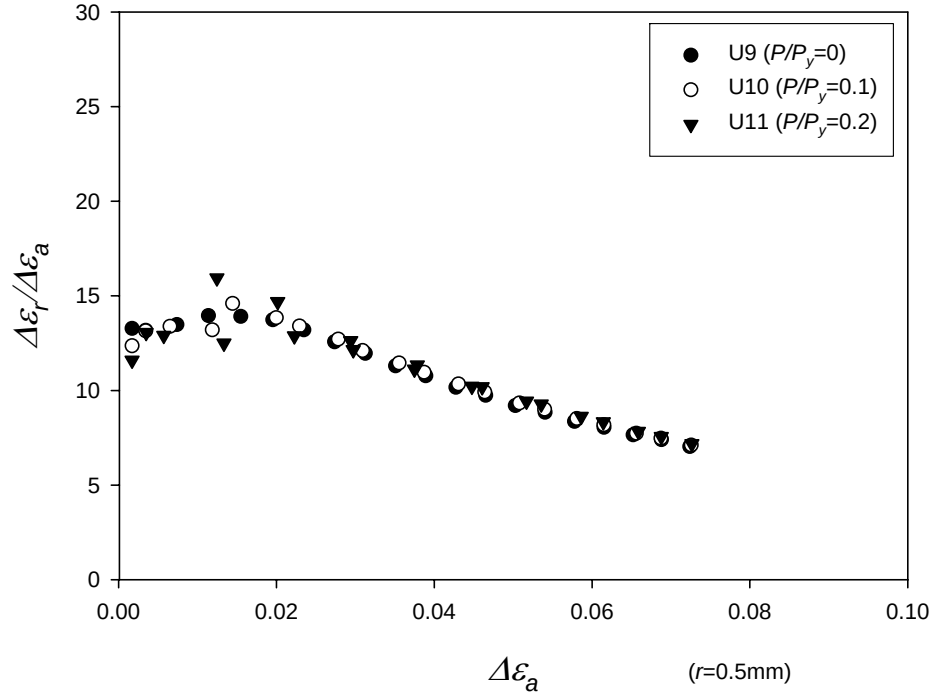

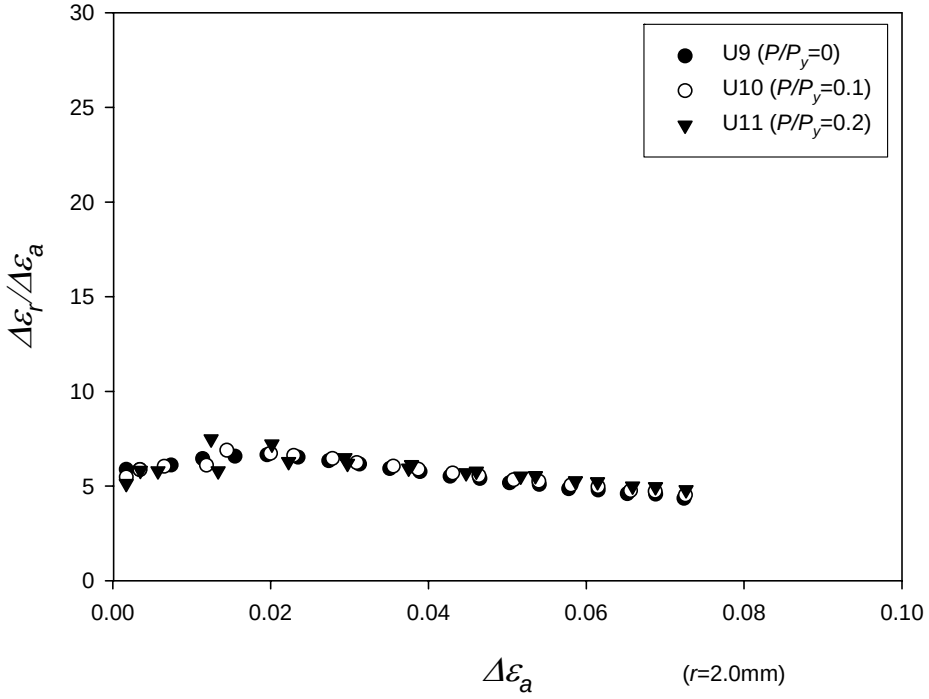

Fig. A1 Relationship with respect to axial loading

(R_f=0.3268, $\bar{\lambda}$ =0.3062)

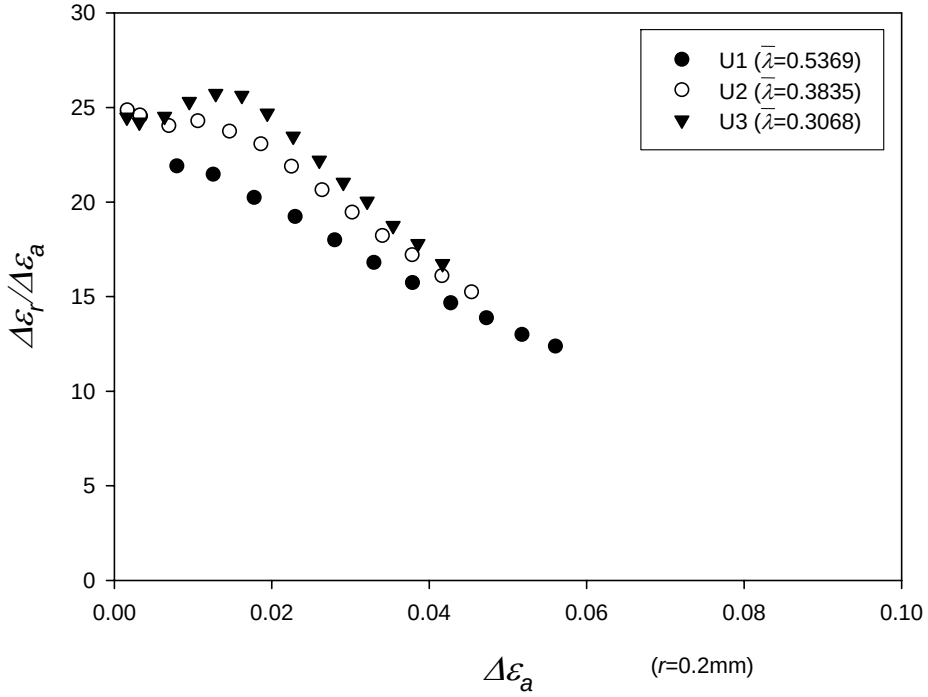

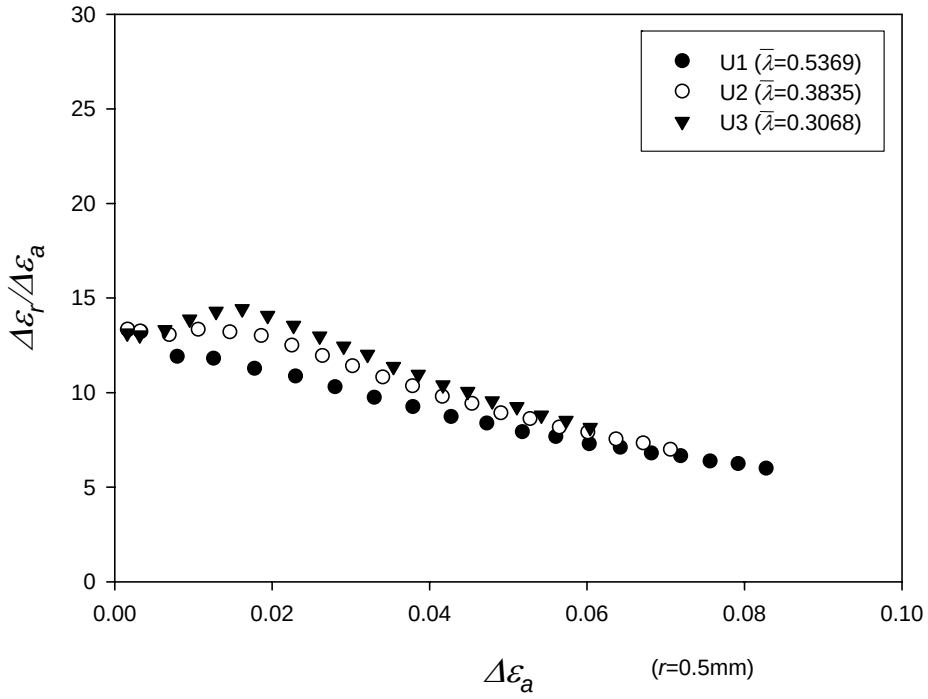

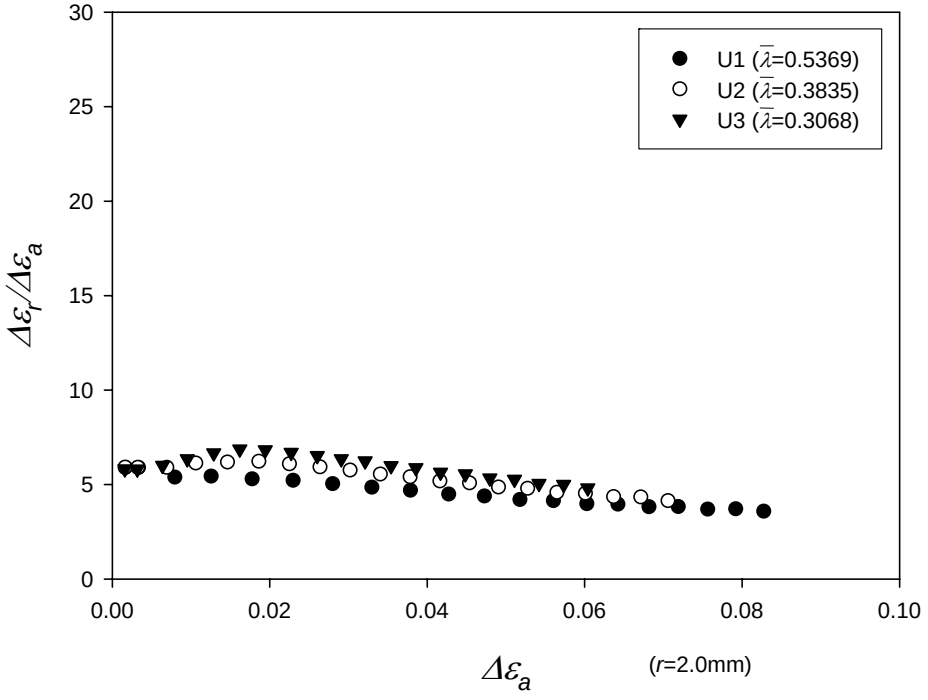

a) R_f=0.2118, P/P_y=0

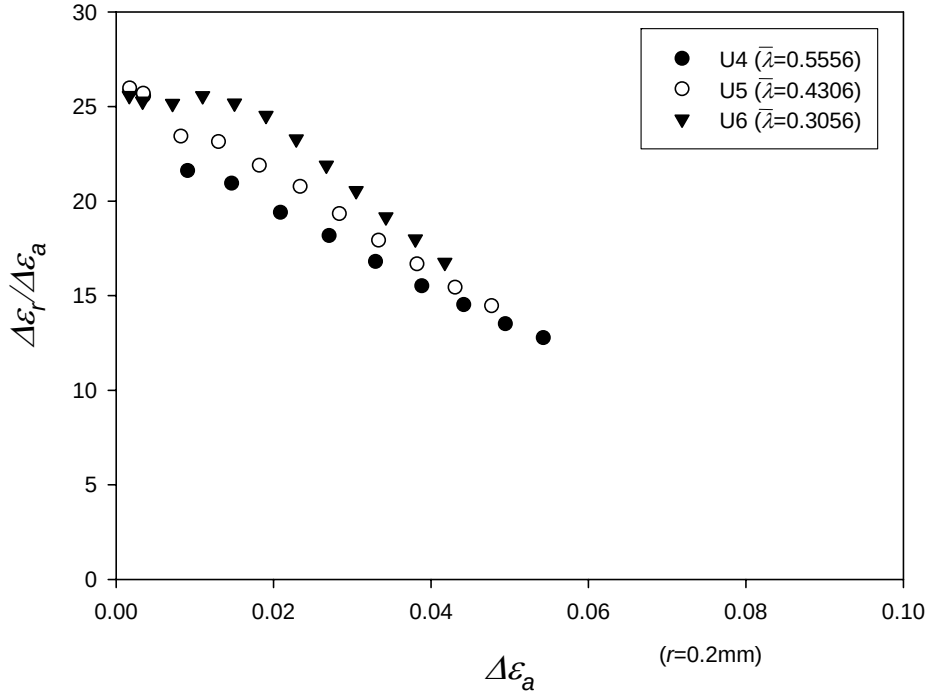
U4 ($\bar{\lambda}$=0.5556)
U5 ($\bar{\lambda}$=0.4306)
U6 ($\bar{\lambda}$=0.3056)
$\Delta\varepsilon_r/\Delta\varepsilon_a$
$\Delta\varepsilon_a$
(r=0.2mm)

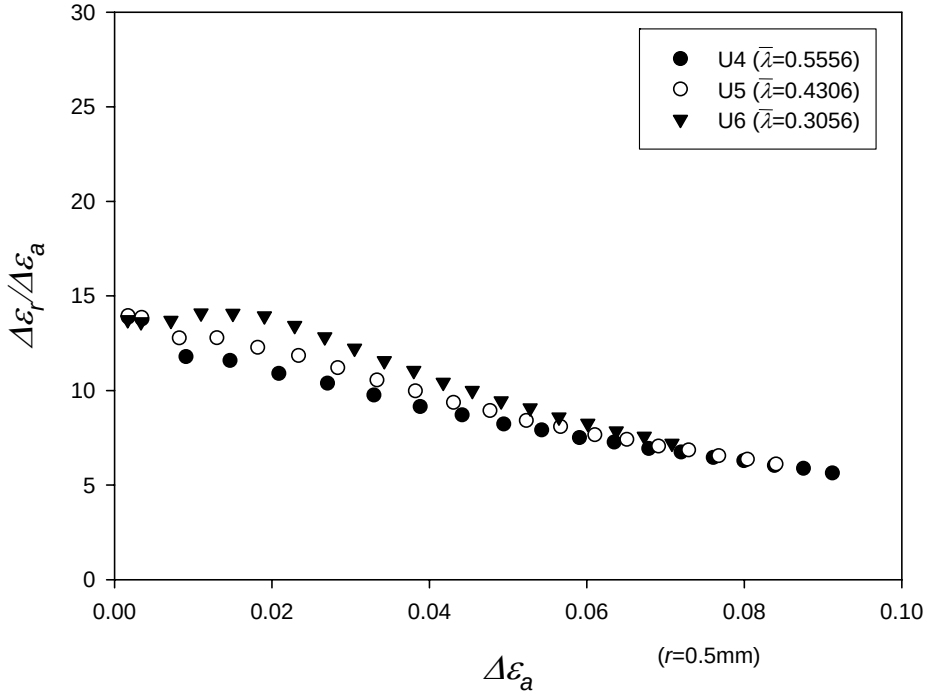
U4 ($\bar{\lambda}$=0.5556)
U5 ($\bar{\lambda}$=0.4306)
U6 ($\bar{\lambda}$=0.3056)
$\Delta\varepsilon_r/\Delta\varepsilon_a$
$\Delta\varepsilon_a$
(r=0.5mm)

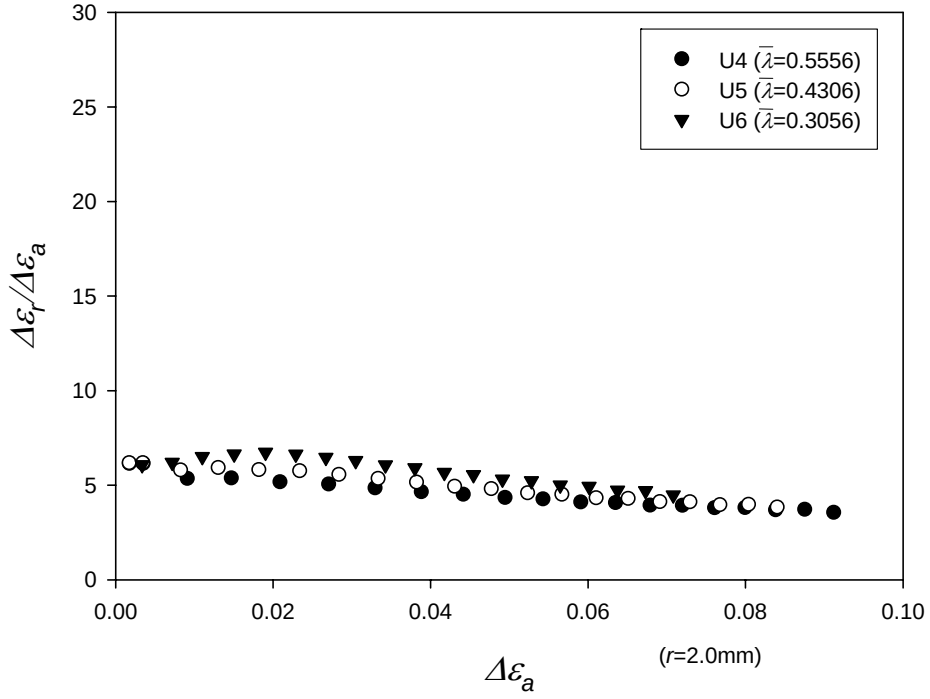

b) R_f=0.2451, P/P_y =0

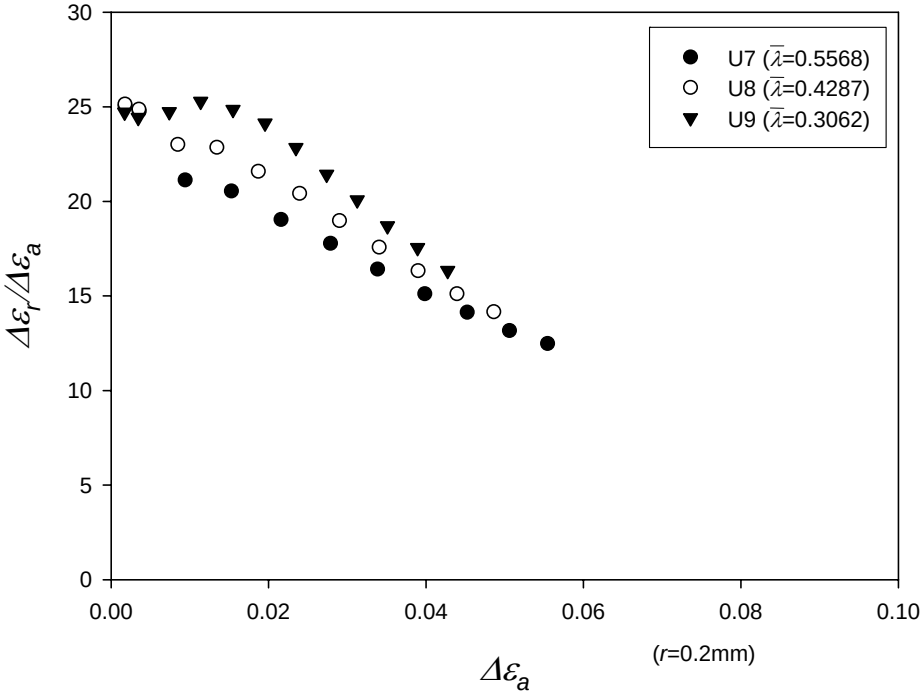

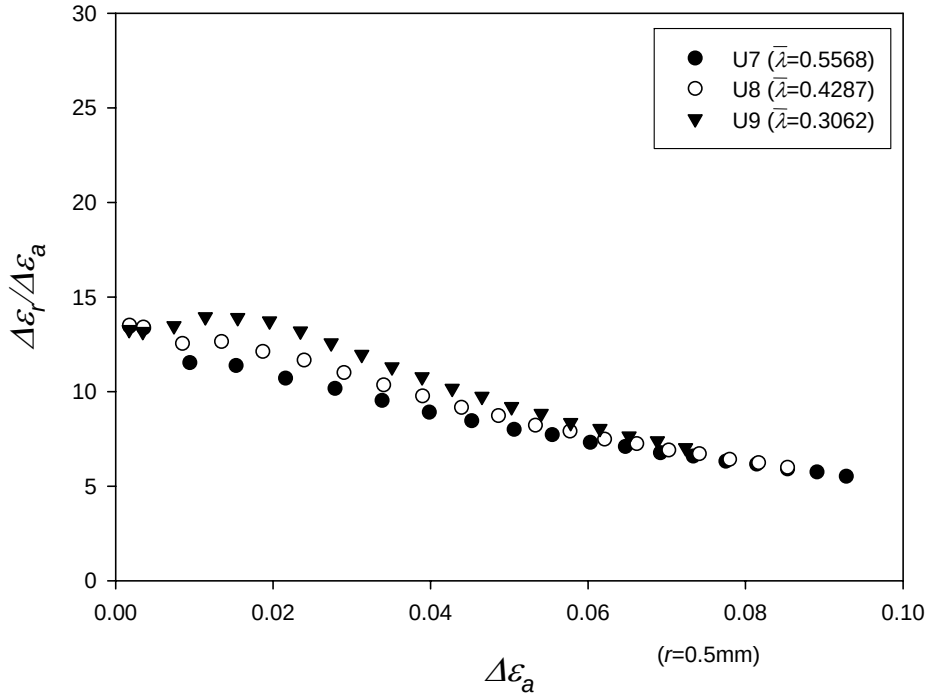

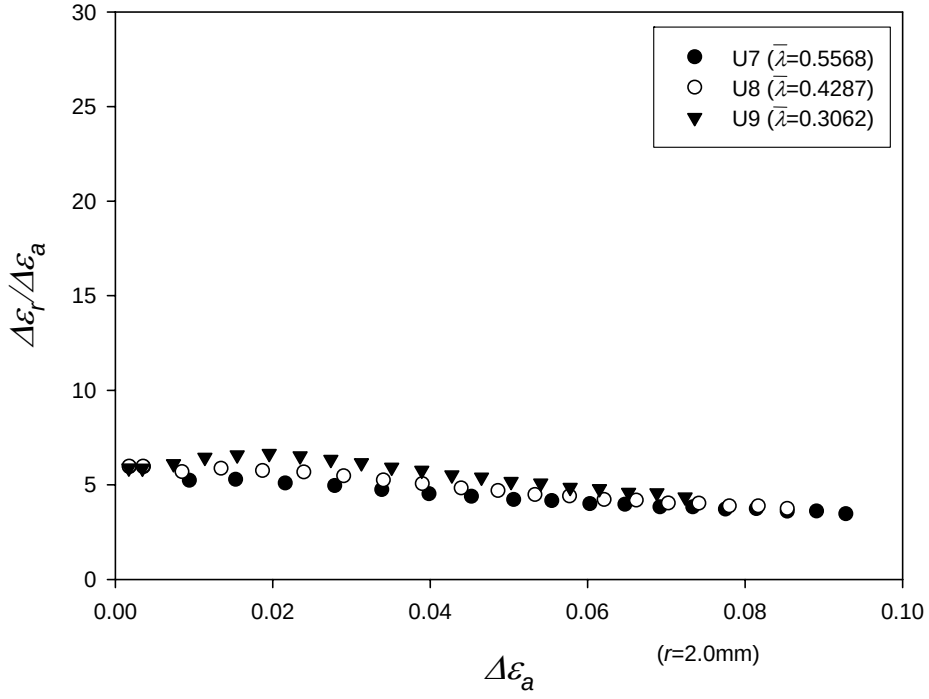

c) R_f=0.3268, P/P_y =0

Fig. A2 Relationship with respect to slenderness ratio

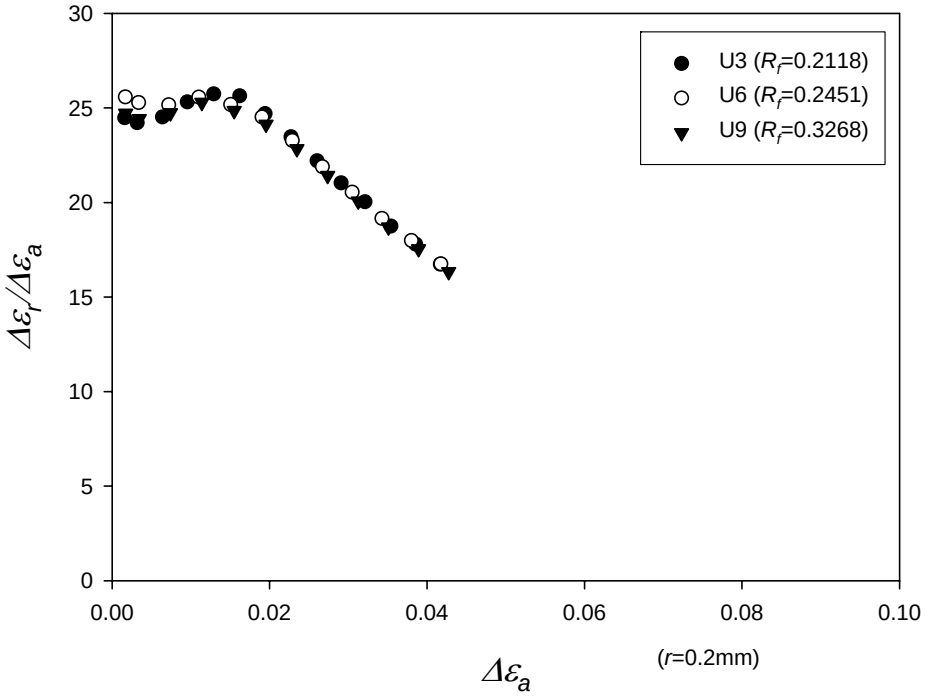
U3 (R_f=0.2118)
U6 (R_f=0.2451)
U9 (R_f=0.3268)
$\Delta\varepsilon_r/\Delta\varepsilon_a$
$\Delta\varepsilon_a$
(r=0.2mm)

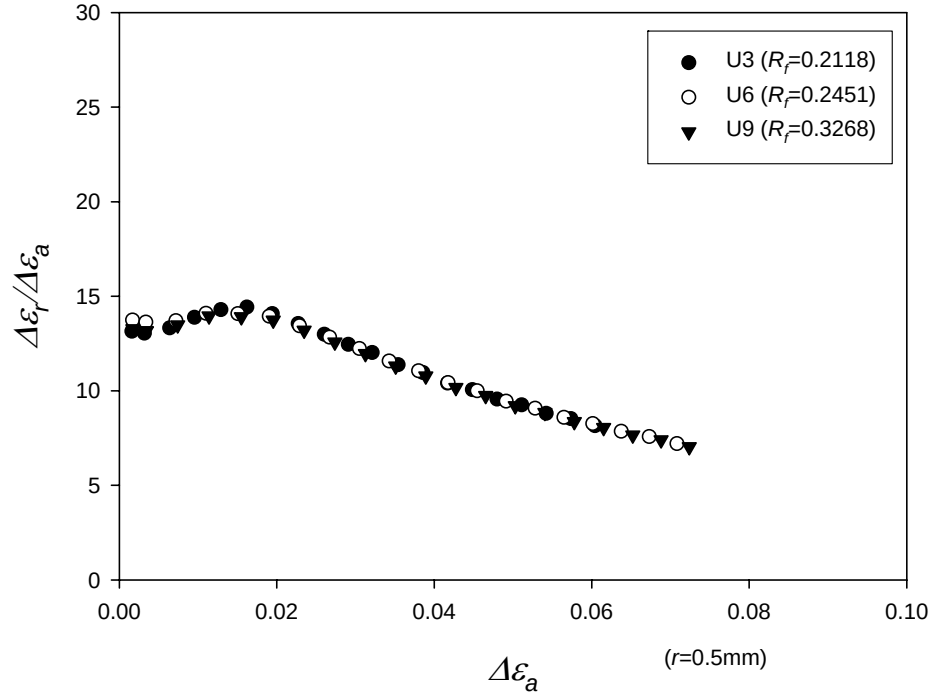
U3 (R_f=0.2118)
U6 (R_f=0.2451)
U9 (R_f=0.3268)
$\Delta\varepsilon_r/\Delta\varepsilon_a$
$\Delta\varepsilon_a$
(r=0.5mm)

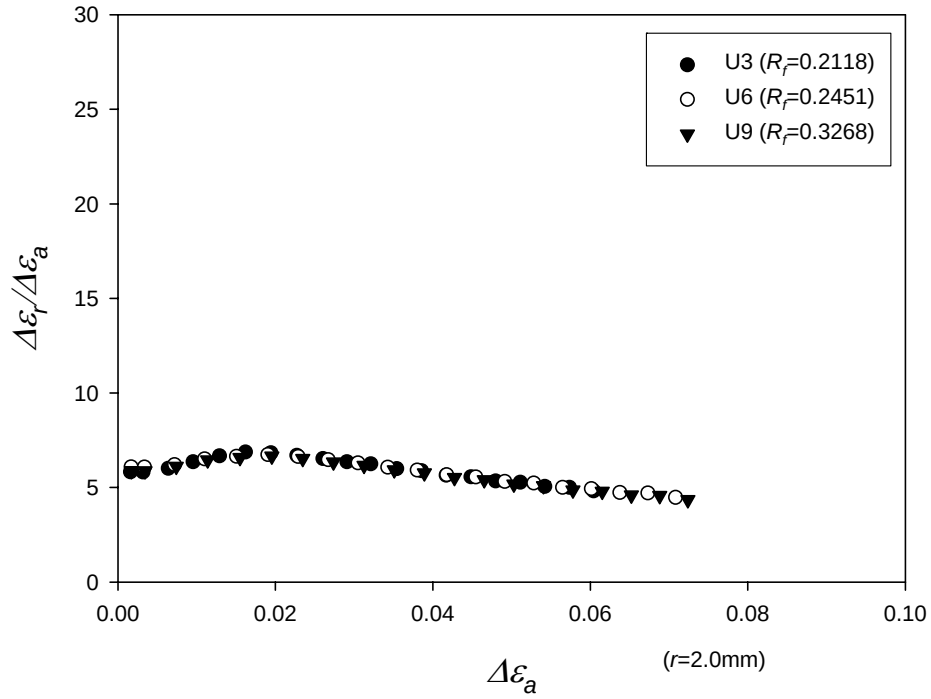

Fig. A3 Relationship with respect to width thickness ratio

($\bar{\lambda}$ ≈0.3062, P/P_y =0)